STUDIES OF ION ELECTROADSORPTION IN SUPERCAPACITOR ELECTRODES

A Dissertation
Presented to
The Academic Faculty

by

Sofiane Boukhalfa

In Partial Fulfillment
of the Requirements for the Degree
Doctor of Philosophy in the
School of Materials Science and Engineering

Georgia Institute of Technology
December 2013

STUDIES OF ION ELECTROADSORPTION IN SUPERCAPACITOR ELECTRODES

Approved by:

Dr. Gleb Yushin, Advisor
School of Materials Science and Engineering
Georgia Institute of Technology

Dr. Hamid Garmestani
School of Materials Science and Engineering
Georgia Institute of Technology

Dr. Preet Singh
School of Materials Science and Engineering
Georgia Institute of Technology

Dr. Alexander Alexeev
School of Mechanical Engineering
Georgia Institute of Technology

Dr. Bogdan Zdyrko
Sila Nanotechnologies, Inc.

Date Approved: November 5th, 2013

ACKNOWLEDGEMENTS

I wish to thank all of those that have helped me throughout my graduate studies to accomplish the work that can be found in this dissertation. First and foremost, I would like to thank my advisor, Dr. Gleb Yushin, for his mentorship and guidance, and for helping me develop into the scientist I am today. Dr. Yushin is one of many wonderful mentors who have guided me and inspired me through their excellent insight and work during my career in science thus far; they include most notably Dr. Sahraoui Chaieb, Dr. Stephen K. Doorn, and Dr. Moonsub Shim. I would also like to thank our research group's post-doctoral research associates, Dr. Igor Kovalenko, Dr. Alexandre Sasha Magasinski, and Dr. Hyea Kim, for their help through these past 4 years. I possess much gratitude for the camaraderie and the help I have gotten from the other graduate students who have been alongside me since the beginning of my graduate studies: Dr. Benjamin Hertzberg, Dr. Lu Wei, Kara Evanoff, Jim Benson, Wentian Gu, Daniel Gordon, Jung-Tae Lee, Naoki Nitta, Feixang Wu, and Dong-Chan Lee. I would also like to express my thanks to the many undergraduate students without whose help I would not have been to accomplish all I have done. They include Joseph and Andrew Foote, Tim Lin, and Kyle Beatty. It is by being surrounded by so many of these talented and intelligent individuals that I was able to keep learning and growing. Finally, I would like to express my sincere thanks to my friends and family, those that were always there for me during my time at Georgia Tech. They include my parents, who always supported me and inspired me through their actions to become a better man and to continue my academic pursuits as far as they would take me; my little brother, who has never doubted me and who inspired me

to keep achieving my goals and accomplish my dreams; and Gaelle Guse, who has helped me in these stressful last months to keep working diligently, and to never give up.

TABLE OF CONTENTS

LIST OF TABLES

LIST OF FIGURES

LIST OF SYMBOLS AND ABBREVIATIONS

ACF	activated carbon fiber
ALD	atomic layer deposition
CE	counter electrode
CNT	carbon nanotube(s)
CV	cyclic voltammogram
CVD	chemical vapor deposition
C-D	charge-discharge
EIS	electrochemical impedance spectroscopy
ESR	equivalent series resistance
EDLC	electric double-layer capacitor
NW	nanowire
MWNT	multi-walled nanotube(s)
SANS	small angle neutron scattering
SEM	scanning electron microscopy
TEATFB	tetraethylammonium tetrafluoroborate
VO_x	vanadium oxide(s)
WE	working electrode
XRD	x-ray diffraction

SUMMARY

Electrochemical capacitors, now often termed supercapacitors, are high power electrochemical energy storage devices that complement or replace high power batteries in applications ranging from wind turbines to hybrid engines to uninterruptable power supplies to electronic devices. My dissertation explores the applications of relatively uncommon techniques for both supercapacitor material syntheses and gaining better mechanistic understanding of factors impacting electrochemical performance of supercapacitors. From fundamental ion electroadsorption studies made possible by using small angle neutron scattering (SANS), to the systematic investigations of coating thickness and microstructure in metal oxide / carbon nanocomposite electrodes realized through the novel use of the atomic layer deposition (ALD) technique, new avenues of material characterization and fabrication have been studied.

In this dissertation I first present the motivation to expand the knowledge of supercapacitor science and technology, and follow with an in-depth literature review of the state of the art. The literature review covers different types of supercapacitors, the materials used in the construction of commercial and exploratory devices, an exploration of the numerous factors which affect supercapacitor performance, and an overview of relevant materials synthesis and characterization techniques The technical objectives for the work performed in this dissertation are then presented, followed by the contributions that I made in this field in my two primary research thrusts: advances to the understanding of ion electroadsorption theory in both aqueous and organic electrolytes

through the development of a SANS-based methodology, and advances to metal-oxide carbon nanocomposites as electrodes through the use of ALD.

The understanding of ion electro-adsorption on the surface of microporous (pores < 2 nm) solids is largely hindered by the lack of experimental techniques capable of identifying the sites of ion adsorption and the concentration of ions at the nanoscale. In the first research thrust of my dissertation, I harness the high penetrating power and sensitivity of neutron scattering to isotope substitution to directly observe changes in the ion concentration as a function of the applied potential and the pore size. I have conducted initial studies in selected aqueous and organic electrolytes and outlined the guidelines for conducting such experiments for the broad range of electrode-ions-solvent combinations. I unambiguously demonstrate that depending on the solvent properties and the solvent-pore wall interactions, either enhanced or reduced ion electro-adsorption may take place in sub-nanometer pores. More importantly, for the first time I demonstrate the route to identify the critical pore size below which either enhanced or reduced electrosorption of ions takes place. My studies experimentally demonstrate that poor electrolyte wetting in the smallest pores may indeed limit device performance. The proposed methodology opens new avenues for systematic *in-situ* studies of complex structure-property relationships governing adsorption of ions under applied potential, critical for rational optimization of device performance.

In addition to enhancing our understanding of ion sorption, there is a critical need to develop novel supercapacitor electrode materials with improved high-energy and high-power characteristics. The formation of carbon-transition metal oxide nanocomposites may offer unique benefits for such applications. Broadly available transition metal

oxides, such as vanadium oxide, offer high ion storage capabilities due to the broad range of their oxidation states, but suffer from high resistivities. Carbon nanomaterials, such as carbon nanotubes (CNT), in contrast are not capable to store high ion content, but offer high and readily accessible surface area and high electrical conductivity. In the second research thrust of my thesis, by exploiting the ability of atomic layer deposition (ALD) to produce uniform coatings of metal oxides on CNT electrodes, I demonstrated an effective way to produce high power supercapacitor electrodes with ultra-high energy capability. The electrodes I developed showed stable performance with excellent capacitance retention at high current densities and sweep rates. Electrochemical performance of the oxide layers were found to strongly depend on the coating thickness. Decreasing the vanadium oxide coating thickness to ~10 nm resulted in some of the highest values of capacitance reported to date (~1550 $F \cdot g^{-1}_{VOx}$ at 1 $A \cdot g^{-1}$ current density). Similar methodology was utilized for the deposition of thin vanadium oxide coatings on other substrates, such as aluminum (Al) nanowires. In this case the VO_x coated Al nanowire electrodes with 30-50% of the pore volume available for electrolyte access show volumetric capacitance of 1390-1950 F cc^{-1}, which exceeds the volumetric capacitance of porous carbons and many carbon-metal oxide composites by more than an order of magnitude. These results indicated the importance of electrode uniformity and precise control over conformity and thickness for the optimization of supercapacitor electrodes.

CHAPTER 1

MOTIVATION AND PROBLEM STATEMENT

Energy storage capabilities have been the subject of much research. Because many electronic devices (such as laptop computers, smart phones, and digital cameras) have become an integral part of an increasingly more mobile man, demands for energy storage and consumption have drastically augmented. Smaller, more efficient energy storage devices are becoming essential in nearly every domain. There is a pressing need to find an economical, long-lasting and ecologically friendly way to store the energy we harness from an increasingly diverse array of sources. The development of supercapacitors has been proposed to address some of these energy storage needs because of their many advantages in these types of applications. These include rapid charging/discharging and longer cycle life.

Supercapacitors are rechargeable electrochemical energy storage devices which offer a higher power density and efficiency, and longer lifetime than traditional batteries at the cost of a lower energy density. Supercapacitors can replace or complement batteries in various high power applications, ranging from hybrid electrical engines for vehicles to pulse-power applications in the aerospace and defense industries.

Two main types of supercapacitors exist: electrical double-layer capacitors (EDLCs) with carbon electrodes and pseudo capacitors with metal-oxide or conducting polymer electrodes. Carbon electrodes offer long cycle life and rapid charging, but suffer from limited volumetric capacitance. Metal-oxide electrodes usually possess much higher capacitance than carbon electrodes at the cost of a dramatically lower electrical

conductivity. The only metal-oxide with an appropriate capacitance and conductivity is ruthenium oxide, but its high cost is prohibitive to most commercial applications. The use of conductive carbon electrodes decorated with low cost metal oxides (such as vanadium oxide) may offer a viable solution for high capacitance / low-cost supercapacitor technology.

In spite of the significant recent efforts in gaining better fundamental understanding on structure-property relationships related to the ion transport and electro-adsorption in both types of electrodes, many open questions remain. For example, in porous carbons the effect of the electrolyte-carbon wall interfacial energy on the ions adsorption within the micropores (< 2 nm) as a function of the electrolyte solvation energy and carbon surface chemistry remains a subject of debate. In various metal oxides, the effects of size, morphology, doping and microstructure of the discussed metal oxides on their electrochemical performance in different electrolytes are still poorly investigated and understood.

Gaining better understanding of key physical processes governing electrolyte ion transport and sorption will contribute to fabrication of more efficient supercapacitor devices. In addition, the knowledge gained could be utilized to advance other important applications, such as electrochemical sensors, water desalination and purification devices, microfluidic devices and even nanorobotics. In this work I aim to partially fill the existing gap in knowledge and systematically examine both types of supercapacitor electrodes. I further aim to contribute to the development of novel fabrication routes for the formation of supercapacitor electrodes with enhanced performance characteristics.

CHAPTER 2

LITERATURE REVIEW

2.1 Introduction

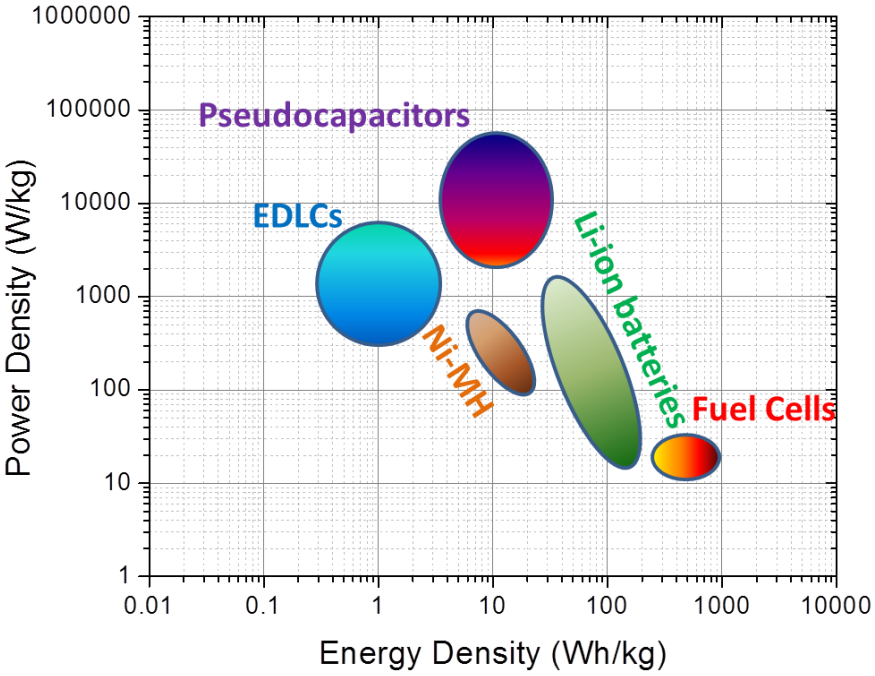

Figure 2.1. Ragone plot showing location of different energy storage devices according to their capabilities.

Supercapacitors fill in a critical position in the Ragone plot[20] (specific energy vs. specific power – see Fig. 2.1). The specific energy axe represents how much energy a particular device stores, while the specific power axe represents how rapidly this energy can be transferred from/to the device and is related to how fast this device can be charged and discharged. Supercapacitors are located between conventional batteries and conventional capacitors in terms of both the energy and power density. While they store less energy than conventional batteries, they can be charged/discharged in mere seconds

(as opposed to hours for batteries)[21]. Because of this and due to their ultra-long cycle-life (50,000-2,000,000 cycles[22]), supercapacitors have been proposed as an alternative to high-power batteries. A supercapacitor can be used on its own as an efficient and long-lasting energy storage device, or coupled with a battery if power requirements are found to be at the border of the battery's capabilities (the supercapacitor's high power density and the battery's energy storage capabilities can then be coupled effectively)[23].

Numerous modern electronics currently make use of supercapacitors (for example in PCMCIA cards or for use with flash devices in cameras[24]), and continued research will only increase the number of applications they will be used in. For example, supercapacitors have been tested as pulse-power sources for fuel cell and hybrid vehicle applications and demonstrated excellent performance characteristics[25]. A pulse-power source provides peak power for acceleration and stores energy during braking. If used together with a battery, supercapacitors can significantly increase the battery lifetime[26]. Because of their fast response time, supercapacitors are especially useful for power-quality applications, where high bursts of power are necessary for very short periods of time (for example for use in data centers in conjunction with batteries or for digital communications systems[27]). A study on the supercapacitor market was performed by iRAP (Innovative research and products, Inc.) in February 2010[28]. It was concluded that the supercapacitor market will continue to rapidly grow in 2009-2014 and that worldwide business (over $275 million in 2009) will grow at an AAGR of 21.4% through 2014. Furthermore, the study identified four major markets for supercapacitors: stationary (short duration applications of energy storage requiring high power for short periods of time), industrial (such as using supercapacitors to handle power surges and short-term

power loss), consumer (for use in consumer electronics that require small high frequency devices), and transport energy storage (mostly automotive applications, this area will show the highest growth rate in 2009-2014) power management.

2.2 Types of Supercapacitors

Electrochemical capacitors (supercapacitors) fall into two categories: (i) Pseudocapacitors (also known as redox supercapacitors) and (ii) Electric Double Layer Capacitors (EDLCs). The difference between the two is in the way charge is being stored at the capacitor. For pseudocapacitors, the charge storage occurs as a result of rapid Faradaic redox reactions occurring at an electrode[29], while EDLCs store charge in a more traditional way, with charge separation taking place across the electrical double layer defined by the charged surface of the electrode and the adsorbed electrolyte ions of the opposite sign (Fig. 2.2).

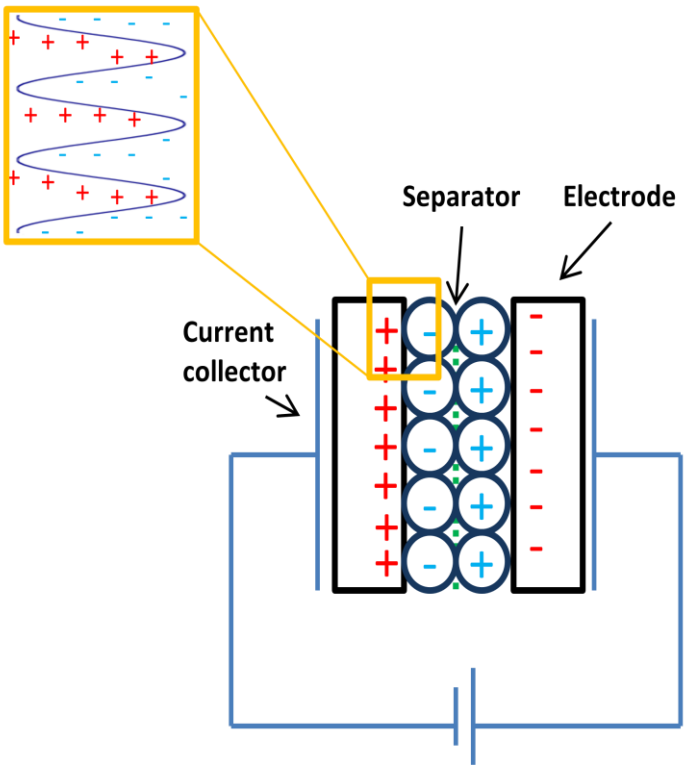

Figure 2.2. Diagram showing operating mechanism of EDLCs

2.2.1 Electric Double Layer Capacitors

Traditional electrostatic capacitors store charge by polarizing the two metal plates (current collectors) separated by a dielectric material. The capacitance of this simple device is determined by the surface area of the plates as well as the thickness and the dielectric constant of a dielectric material:

$$C = \frac{Q}{V} = \varepsilon_0 \varepsilon_r \frac{A}{d},$$

where Q is the amount of charge, V is the potential difference between the two plates, A is the area of the plates, ϵ_r is the relative dielectric constant and ϵ_0 is the permittivity of free space. Several polarization mechanisms may take place in a dielectric, such as electronic, ionic, dipolar, and space charge polarizations. These mechanisms are

frequency dependent[30]. As such, different speeds of charge will involve different polarization mechanisms throughout the involved electrodes.

Symmetric electrochemical capacitors consist of two metal current collector – electrode modules which are separated by an ion-permeable but electrically isolative membrane. The electrode assembly is immersed in a solution of electrolyte ions. Upon application of a potential, positive ions move towards the negative electrode and negative ions move towards the positive electrode, adsorbing on the internal surface of the active material particles (Fig. 2.2).

In contrast to pseudocapacitors and batteries, EDLCs have very long lifecycles, lasting for up to 10^6 charge-discharge cycles[31] in organic electrolytes (repeated redox reactions may degrade the electrode) and possessing faster charge-discharge times (ion movement in the solution can proceed much faster than chemical redox reactions and diffusion of ions within a solid).

2.2.2 Pseudocapacitors

Because pseudocapacitors rely on Faradaic redox reactions for charge storage (Fig 2.3), the electrode materials are limited to materials that possess this capability: transition metal oxides[32-34] and conducting polymers[35-37]. Conducting polymers exhibit large volume changes during the device operation and tend to have lower lifetimes and slower redox kinetics than the transition metal oxides. This is a result of two factors: the repeated volume changes strain the material and degrade the polymer, and the redox sites which are located on the polymer backbone are not strong enough to sustain numerous redox processes (because redox processes involve multiple electron transfer reactions that degrade the fragile polymer bonds)[36, 38].

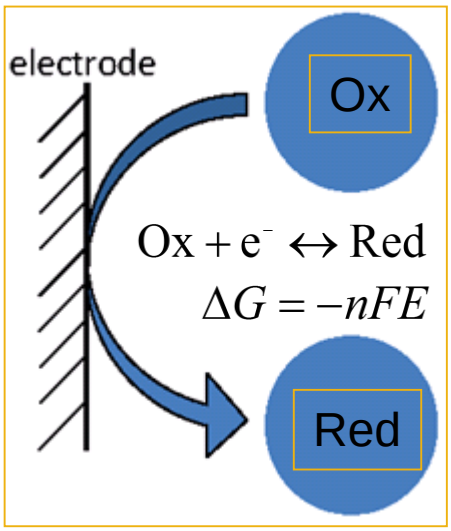

Figure 2.3. Diagram showing operating mechanism of pseudocapacitors

Transition metals have two or more oxidation states. During pseudocapacitor operation, charge storage occurs when electrolyte ions electrochemically react with the oxide surface (or bulk) by injecting the charge into the oxide particles. This charge injection is analogous to the oxidation/reduction (redox) reactions commonly observed in battery electrodes, but occurs within a much broader range of potentials[21]. Possessing a higher number of oxidation states commonly increases the probability of finding a suitable redox reaction to store charge in a supercapacitor. Transition metal oxides are also suitable choices for supercapacitor applications because they are commonly compatible with aqueous electrolytes[39] and organic electrolyte having small ions (e.g., Li^+)[40]. The transition metal oxides have so far demonstrated the highest values of specific capacitance[33]. In order to achieve rapid ion transport to electrochemically active sites, high surface area and well developed porosity are commonly desirable features in metal oxides[41].

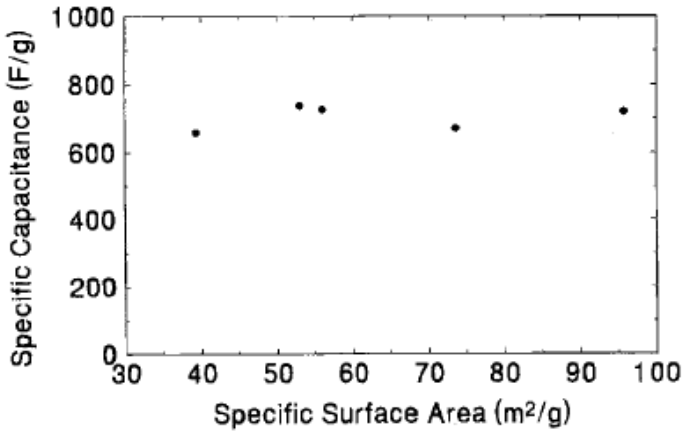

Figure 2.4. Performance of RuOx-based supercapacitors. Taken from[11].

Ruthenium oxide (RuO_x) was studied extensively when research on pseudocapacitors constructed from transition metal oxides first began because of its high electrical conductivity combined with its high capacitance (its ability to reversibly insert a large number of ions). It is important to note that different values for specific capacitance were recorded for crystalline ruthenium oxide (RuO_2) versus amorphous ruthenium oxide ($RuO_2.nH_2O$): 350 $F \cdot g^{-1}$ for RuO_2 vs. 720 $F \cdot g^{-1}$ for $RuO_2.nH_2O$[42] (Fig. 2.4). Ruthenium oxide-based supercapacitors were found to be good devices, earning a maximum specific capacitance as high as 800 $F \cdot g^{-1}$ [43, 44]. However, due to limited worldwide availability of ruthenium and its ultra-high cost (over $10,000/kg), it has found only a few applications in the defense industry.

Manganese oxide (MnO_2) has been considered as a material for pseudocapacitor electrodes because of its experimentally achievable high specific surface area (~132 m^2g^{-1}). Moreover, it is abundant in nature, has a low cost, and is environmentally friendly[45]. However, unlike ruthenium oxide, it has a very low electrical conductivity, and as such it must be used in conjunction with a conductive substrate to produce suitable supercapacitor electrodes. Manganese has three possible oxidation states (Mn_2O_3, Mn_3O_4,

and MnO), and all of its oxides are very complex[32]. Values of capacitance were found to vary according to deposition method and thickness of the MnO_2 film. For example, electrodes made from 20 % carbon black, 5% PVdF-HFF binder, and hydrothermally synthesized MnO_2 was found to have a specific capacitance of 168 $F \cdot g^{-1}$ [45] (Fig. 2.5). MnO_2 thicknesses were found to affect values of specific capacitance in composite electrodes of carbon and binder or in as-deposited thick films: large micrometer-thick deposits resulted in values of ~150-250 $F \cdot g^{-1}$, while ultrathin MnO_2 deposits (~10-100nm) resulted in values ranging from ~700-1380 $F \cdot g^{-1}$ [46].

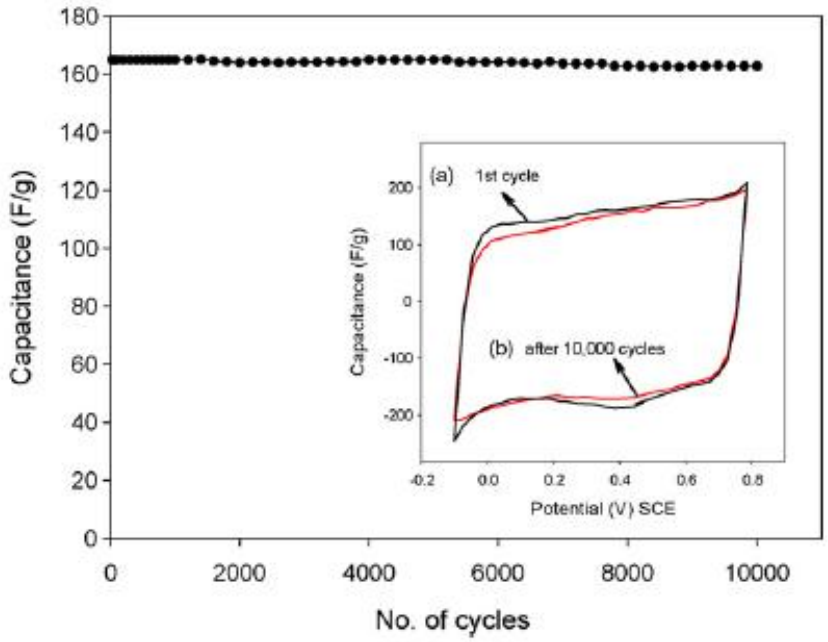

Figure 2.5. Performance of Mn-carbon composite electrodes. Taken from [18]

Various other nanocrystalline metal oxides have been investigated as additives for supercapacitor electrodes because of their large surface area, high conductivity, electrochemical stability and pseudocapacitive behavior. For example, SnO_2 has been used in conjunction with RuO_2 and Fe_3O_4 to create pseudocapacitive electrodes because

of its high electrical conductivity. Fe_3O_4 (magnetite) is an attractive option for electrode materials, since it is one of the cheapest common oxides available, possesses low toxicity (it is naturally found in Fe rust), is environmentally friendly, has one of the highest conductivities of the simple oxides ($\sigma = 2x10^4$ S m^{-1})[47], and a high value of capacitance (~480 $F \cdot g^{-1}$). SnO_2-Fe_3O_4 composite electrodes were found to exhibit a capacitance of 33 $F \cdot g^{-1}$ at a sweep rate of 4mV s^{-1} in 1M KOH. SnO_2-RuO_2 composite electrodes were found to exhibit a capacitance of 16 $F \cdot g^{-1}$ at a sweep rate of 50 $mV \cdot s^{-1}$ in 1M Na_2SO_4[48].

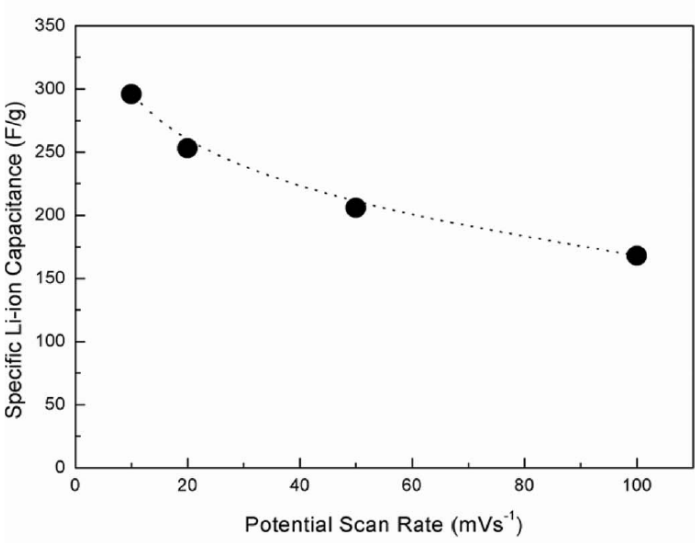

Figure 2.6. Performance of VOx-CNT composite electrodes. Taken from [17].

Vanadium has many different oxidation states and is considered to be an attractive material for supercapacitor applications. Contrary to ruthenium oxide, however, vanadium oxide (VOx) has limited conductivity ($\sigma = 1x10^{-4}/\Omega.m$ for VOx and $\sigma = 2.8x10^6 \Omega^{-1}.m^{-1}$ for RuO)[42], and thus conductive additives are required for applications in devices[49]. Several approaches allowed the preparation of a porous and uniform structure in VO_x[50]. These include electrodeposition[49], ALCVD[50], CVD[50, 51], APCVD[52, 53], and aerogel synthesis[41, 54]. The electrodeposition of vanadium oxide

onto CNT substrates yielded capacitances as high as 300 $F \cdot g^{-1}$ (Fig. 2.6). Although vanadium oxide has been the subject of significant research for supercapacitor applications, other forms of vanadium have been investigated: for example, devices with electrodes made from low-temperature synthesized vanadium nitrides yielded high values of capacitance: 1340 $F \cdot g^{-1}$ at a scan rate of 2 $mV \cdot s^{-1}$ or 554 $F \cdot g^{-1}$ at a scan rate of 100 $mV \cdot s^{-1}$[42]. These are values that compare very well to the previous results found with ruthenium oxide-based supercapacitors.

Vanadium oxide is also an attractive material for pseudocapacitive electrodes because it comes in a wide variety of oxidation states, which gives rise to its high theoretical capacitance. Changing the oxidation state by giving up electrons (during oxidation) or ions (e.g. protons) (during reduction) allows for the charge accumulation at the electrode surface needed for high capacitance to be achieved. The range of available vanadium oxides include: V_2O_5, a series of oxidation states of the form V_nO_{2n-1} (where $9>n>1$)[55], V_2O_3, VO_2, numerous intermediate phases of different compositions between $VO_{1.67}$ and $VO_{2[56]}$, and VO. In an ideal case, one would need to identify under what conditions (if any) we could cycle through all these oxidation states at the same temperature.

2.2.2.1 Crystal Structure of Vanadium Oxides:

The various VO_x have different crystal structures and morphologies. V_2O_3, for example, has a rhombohedral (hexagonal) corundum structure, R3c. This structure is composed of an approximately hexagonal close packed (h.c.p.) array of oxide ions (O^{2-}) in which trivalent cations (V^{3+}) occupy two thirds of the octahedral sites. Two stacking sequences are typically seen: the "ABCABC" stacking sequence and the "ACBACB"

stacking sequence (see Fig. 2.7). The lattice parameters a and c are 0.4954nm and 1.40083nm, respectively (c/a = 2.83)[9].

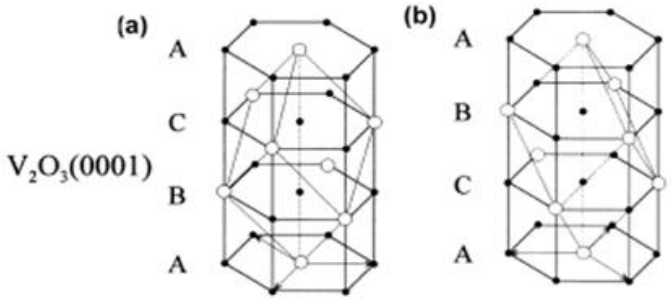

Figure 2.7. Crystal structure of V_2O_3 with different stacking sequences. Taken from[9]

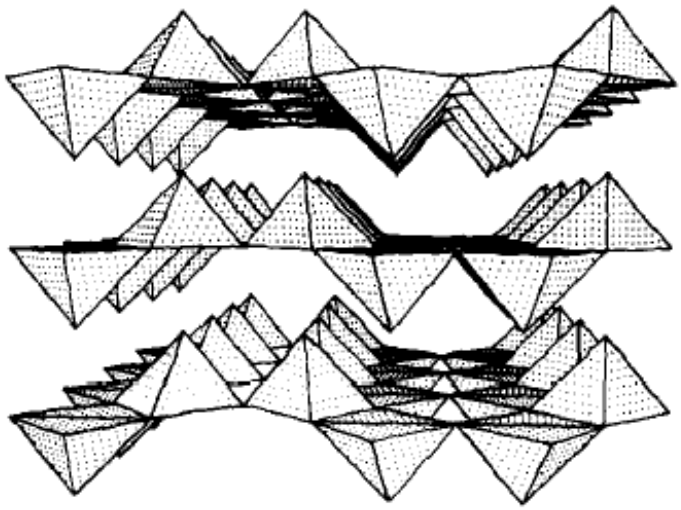

Figure 2.8. Crystal structure of V_2O_5. Taken from [10].

VO_2 also possesses a distorted h.c.p. array of oxide ions. V_2O_5, on the other hand, has an orthorhombic crystal structure, with the lattice parameters a, b, c, being 1151.2pm, 356.4pm, and 436.8nm, respectively (Fig. 2.8). It belongs to the Pmmn space group and has distorted trigonal bipyramidal (V) geometry[57]. Galy *et. al*, describe it as "a layered structure, built up from VO_5 square pyramids sharing edges and corners, with V_20_5 sheets held together via weak vanadium oxygen interaction, V-O = 2.791 Angstroms.

The differences between these geometries may lead to a large energy barrier for cycling between all of the oxidations states of vanadium in the same device. Going from V_2O_3 toVO_2 would be simple because they have similar structures, but going from V_2O_3 to V_2O_5 involves a distortion and expansion of the crystal structure. While this expansion facilitates ion transport (the large open structure of V_2O_5 may lead to an enhanced ionic transport), the energy barrier may impede the reaction, and the added stresses may mechanically degrade the electrode, leading to poor device performance.

2.2.2.2 Diffusion vs. Charge Transfer Responsible for Device Kinetics in VOx Electrodes:

It is necessary to identify whether the charging process is limited by charge transfer or mass transport (diffusion) for the range of the selected VO_x electrodes, as the limiting step will determine the overall kinetics of the electrochemical reaction. The charging process in EDLCs is governed by mass transport. The charging process in pseudocapacitors, on the other hand, can be governed either by charge transfer (the kinetics of the electron transfer reactions) or by mass transport (e.g. diffusion of electrolyte ions through the electrode and back to the current collector). Once the kinetics for charge transfer have been understood, it will be easier to determine a corresponding electrolyte and thus suitable operating parameters (voltage and temperature range, rate of charge/discharge, etc…) for our supercapacitor device. Understanding these kinetics can be achieved by performing experiments with EDLC-only electrodes having identical porosity and comparing the electrochemical results to those of the pseudocapacitive samples.

2.3 Synthesis of Transition Metal Oxides for Pseudocapacitor Applications

Transition metal oxides can be deposited onto different substrates via such processes as electrodeposition, chemical vapor deposition (CVD), atomic layer deposition (ALD), and sol-gel or aerogel synthesis. While there is yet to be any research on ALD deposition of vanadium oxide for supercapacitor applications, this approach should work better than the already-proven CVD methods, as ALD will allow for monolayer-thick control of the desired deposition thickness by using the same basic principles as the CVD methods.

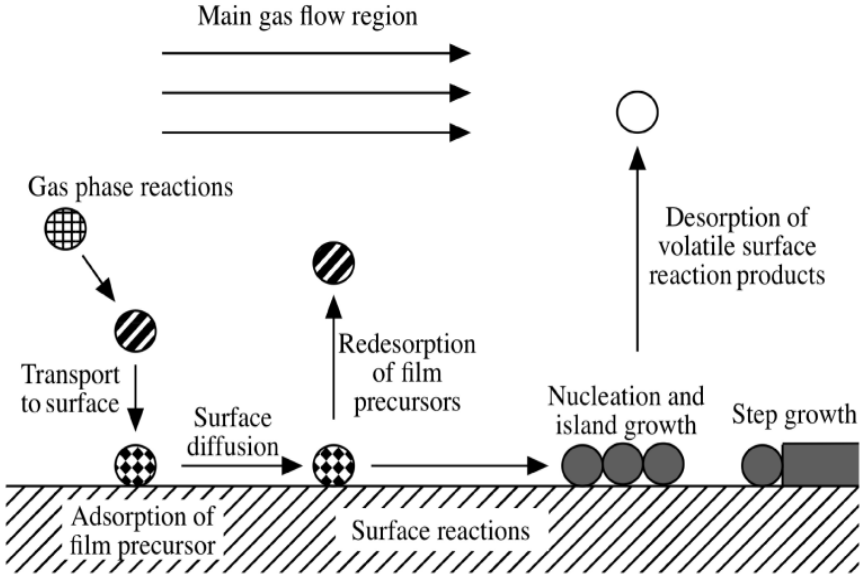

Figure 2.9. Schematic depicting CVD process. Taken from .[1]

I have deposited uniform films of vanadium on various substrates via Atomic Layer Deposition (ALD). During the ALD process, a precursor is introduced into a heated chamber that decomposes and deposits the desired material onto a substrate. The chamber is flushed with inert gases to remove by-products of this reaction. The main difference between the CVD and ALD mechanisms is the way in which the chemical reaction leading to deposition is allowed to proceed in the chamber. In CVD, carrier gases

transport the precursor and other source vapors continuously, allowing the reaction responsible for deposition to proceed continuously for as long as is necessary to deposit the desired thickness (Fig. 2.9). In ALD, the precursor and other sources vapors are pulsed into the chamber one at a time, separated by purging or evacuation periods. Each pulse step commonly deposits a sub-monomolecular layer of the precursor onto the substrate, while the purge or evacuation step limits the reaction to the surface by removing the excess reaction gases (those not adsorbed onto the surface) (Fig. 2.10). As such, ALD allows precise and uniform deposition of coatings on porous substrate surfaces, provided enough time is allocated for the diffusion of the precursor gases into (and out of) the porous structure of the substrate during both the pulse and purge periods. The key advantage of ALD is excellent conformality and uniformity of the coatings achievable[58].

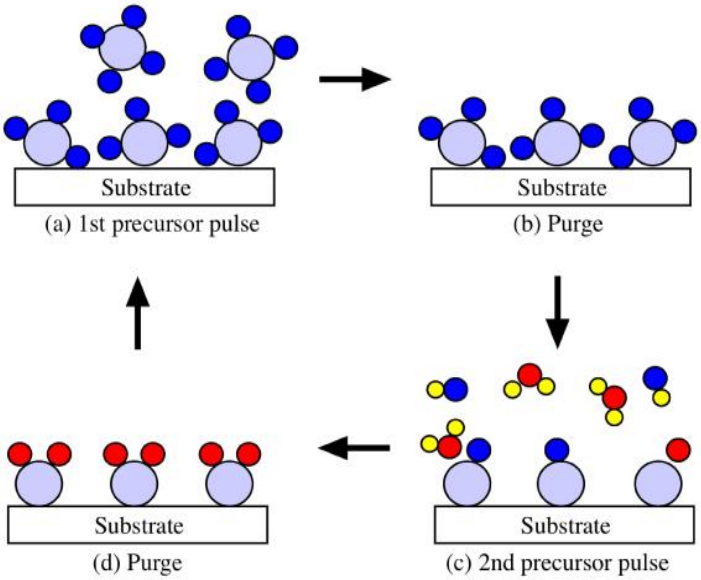

Figure 2.10. Schematic depicting ALD process. Taken from http://cnx.org/content/m25737/latest/

An example of the chemical reaction to deposit vanadium oxide (e.g., V_2O_5) for this project is given below:

$$2VO(OC_3H_7)_3 + 3H_2O \rightarrow V_2O_5 + 6HOC_3H_7$$

The precursor used is Triisopropoxyvanadium(V) oxide- $C_9H_{21}O_4V$ or $VO(OC_3H_7)_3$. The carrier gas used should be an inert gas (such as Ar or He). The other source vapor is H_2O.

An atmospheric pressure CVD method for depositing uniform films of V_2O_5 was developed by Parkin *et.al[52]*. Two precursors were investigated: $VOCl_3$ and VCl_4. The carrier gas used was Ni and the other source vapor was H_2O. The chemical reactions responsible for this deposition are:

$$2VOCl_3+3H_2O \rightarrow V_2O_5+6HCl$$

$$2VCl_4+5H_2O \rightarrow V_2O_5+8HCl+H_2$$

Due to different molecular structures (the main difference is the presence of a VO bond in $VOCl_3$ and its absence in VCl_4), the precursors require different decomposition conditions: the $VOCl_3$precursor needs to be heated to 90°C and the VCl_4 precursor needs to be heated to 100°C. Both of these routes yielded uniform, pure films of V_2O_5 at a rate of ~300nm min^{-1} at 500 °C.

2.3.1 Kinetics of Deposition Reactions:

Numerous factors affect deposition rate for the CVD and ALD processes. As stated earlier, there are four major steps that determine a successful deposition. First is transport of an appropriate source (precursor) to the substrate. Because the substrates used in this experiment are porous (and nanoporous), even though diffusion of the precursor to the substrate can be achieved easily, diffusion into the material so that deposition can occur on the surface of the inner pores as well as on the outer surface of the material might be

slow. To overcome slow diffusion, care must be taken to ensure that the deposition process is controlled by the surface reaction kinetics and not by the diffusion kinetics (in other words, that surface reaction is sufficiently slow that sufficient time is allowed for the diffusion to proceed) in order to produce as pure and uniform a coating as possible.

The deposition of the film onto the substrate occurs in two steps: adsorption of gas onto the substrate followed by a chemical reaction on the substrate resulting in deposition. The temperature of the reaction chamber is important: it must be elevated enough to provide enough energy to allow for the reaction to proceed, but it should be low enough to allow for the reaction to proceed at a speed which allows for uniform deposition. The time it takes to form a single complete monolayer of gas onto a surface in a CVD reaction when there are no diffusion limitations (i.e. on any flat surface) is[59]: $t_m = 4[nv_{rms}d^2]^{-1}$, where n is the number of molecules per unit volume, d is the diameter of the molecule, and v_{rms} is the average velocity of the molecules: $v_{rms} = [3kT/m]^{1/2}$, where k is the Boltzmann constant, T is the temperature, and m is the mass of the molecule. At high temperatures the substrate coverage n becomes lower since it follows the following trend: $n = R\tau_a = [R/v_o]\exp[\Delta G_{des}/kT_s]$, where τ_a is the mean residence time of atoms onto the surface of the substrate, ΔG_{des} is the change in energy associated with desorption, T_s is the substrate temperature, and v_o is related to the desorption rate v_d according to the following relation: $v_d = v_o\exp[-\Delta G_{des}/kT_s]$

The overall nucleation rate during CVD is a function of these two competing reactions (impingement vs. desorption) and is found to be: $N = [2\pi]^{1/2}r^*a_o\sin\theta\ PN_A/(MRT)^{1/2}n_s\exp[(E_{des}-E_s-\Delta G^*)/kT]$. This expression can be separated into three sections: the critical area for nucleation, the atom impingement rate onto the nucleus, and

the equilibrium concentration of nuclei. By determining the nucleation rate of the CVD/ALD depositions, it becomes easier to set one of the many parameters affecting deposition success: the length of time of the deposition.

Another important step in a CVD or ALD reaction is mass transport of the "waste" byproducts away from the substrate. It is important to identify the appropriate reactions and determine which is the slowest as it will be the rate-determining step. This can be achieved by doing control experiments and comparing them to additional experiments (such as changing the distance from the gas inlet to the substrate or from the substrate to the gas outlet, changing the porosity of the substrate to affect the gas diffusion rate inside the sample, or changing the temperature and pressure) where factors that can affect the length of each step are altered. Control of different parameters will aid in obtaining a successful deposition. For example, it is important to keep the pressure of the reaction chamber sufficiently low to increase the mean free path of the precursor molecules prior to decomposition and material deposition to allow for uniform growths. For example, it is important to keep the pressure of the reaction chamber as low as possible as this will lead to more uniform growths. Other parameters that affect mass transport include: reactant concentration, diffusivity, boundary layer thickness, pressure, gas velocities, temperature distribution, reactor geometry, and gas properties such as viscosity[59]. All of these parameters must be evaluated and optimized to yield the best quality thin film of metal oxide for supercapacitor applications: one that is pure, uniform, and open (porous).

2.3.2 Obtaining Pure and Uniform Distribution During Deposition

Optimal device performance can be expected if the deposited metal oxide film is both pure and uniform throughout. In the ideal case, the nanoporous substrate will see a thin coating of metal oxide in all of its pores. However, there are many considerations to take into account before one can obtain a pure and uniform coating. Thin film growth on epitaxial substrates can be divided into three different regimes: Volmer-Weber (WB), Frank-van der Merwe (FM), and Stranski-Krastanov (SK) growth (see Fig. 2.11). The difference between the three regimes lies in the way nucleation and growth occur on the substrate. In WB growth, three-dimensional adatom clusters/islands are formed because adatom/adatom interactions are stronger than adatom/surface interactions. During FM growth, the adatoms preferably attach themselves to the substrate surface, resulting in atomically smooth, uniform layers. FM growth is also known as "layer-by-layer" growth, and results in a very smooth epitaxial film because each monolayer of atoms is deposited before a new one is begun. The SK growth regime is located between FM and WB: both two dimensional atomically smooth layers and three-dimensional islands are formed.

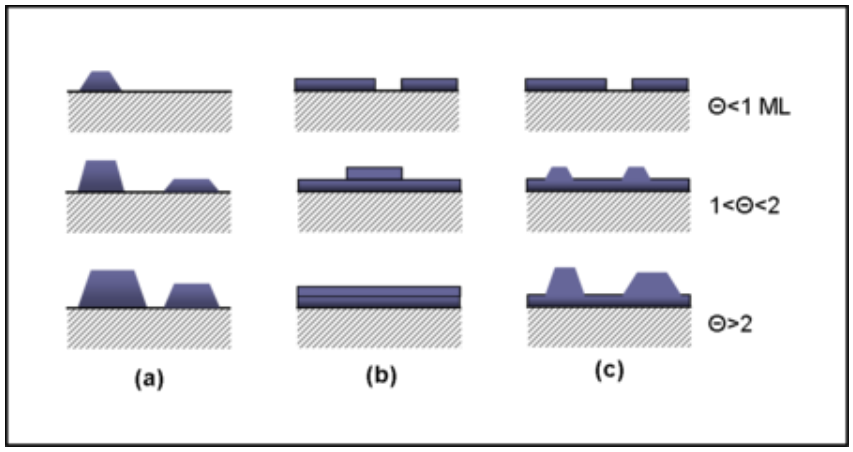

Figure 2.11. Illustration of Different growth regimes: (a) Volmer-Weber growth (b) Frank-van der Merwe Growth (c) Stranski-Krastanov Growth. The Φ is indicative of how many layers have been grown.

Determining which growth regime you are in depends entirely on the chemical potential of the system. Markov proposed a model[60] for the layer chemical potential per atom:

$\mu(n) = \mu_\infty + [\varphi_a - \varphi'_a(n) + \varepsilon_d(n) + \varepsilon_c(n)]$, where μ_∞ is the bulk chemical potential of the adsorbate material, φ_a is the desorption energy of an adsorbate atom from a wetting layer of the same material, $\varphi'_a(n)$ is the desorption energy of an adsorbate atom from the substrate, $\varepsilon_d(n)$ is the per atom misfit dislocation energy, and $\varepsilon_c(n)$ is the per atom homogeneous strain energy. These values are dependent on the thickness of the growing film as well as the lattice misfit between the substrate and the growing film. The growth regimes can thus be expressed as inequalities in terms of the potential. If $d\mu/dn<0$, we are in VW growth mode. If $d\mu/dn>0$, we are in FM growth mode. During SK growth, both regimes are present so both inequalities apply: during the initial steps of the growth the behavior follows FM behavior as strain energy is accumulated in the deposited layers and the chemical potential differential is positive; at a critical thickness the chemical potential differential becomes negative, and it becomes energetically favorable to nucleate islands by a VW type mechanism.

J. Maier identified the effects of different variables on the chemical potential of the system[61]. For example, the introduction of point defects into the electrode has differing thermodynamic effects. The high cost in locally free energy associated with the creation of each point defect is offset by the gain in configurational entropy that is a result of the numerous possible arrangements of these point defects[61]. The defect concentration will affect the chemical potential of the system; if these defects are dilute and randomly

distributed, a Boltzmann distribution is used to describe the chemical potential: $\mu = \mu^{\circ}+RTlnc$

At higher concentrations, defects have to worry more about other defects in their vicinity and thus a decreasing number of available sites (or quantum states) and the Boltzmann distribution is not enough to model the chemical potential. Different considerations force the chemical potential to adopt the following form:

$$\mu_j = \mu_j^{\circ} + z_jF\Phi + \mu_j^{\circ ex} + RTln\ c_j + \mu_j^{c,ex}$$ [61]

The $\mu_j^{c,ex}$ term is representative of the effect of interfacial energy on chemical potential (especially if the structure abruptly changes at an interface). Similarly, the $z_jF\Phi$ term is there to account for electrical effects on the chemical potential. Finally, the $\mu_j^{\circ ex}$ term is representative of the effect of the mean curvature (1/r) of the grains (grains with higher curvatures will have enhanced internal pressure which leads to an increase in the chemical potential by (at least) 2(y/r)v, where v is the partial volume) on the chemical potential. Note that for thin films 1/r approaches 0.

Interfacial spacing affects chemical potential significantly. For example, interfacial structural changes can penetrate numerous atomic layers due to elastic effects, and even (if small enough), the entire substrate. In that case, the chemical potential will vary depending on position in the substrate and will be different from the bulk single-crystal value.

The chemical potential represents the increase in free energy if the concentration of the species is slightly increased. As such, the contributions listed above which affect the chemical potential will lead to what Maier describes as “true size effects”. The change in chemical potential can lead to phase changes, the formation of heterolayers, and

penetrating accumulation zones. These considerations allow researchers to identify what kind of material is needed for a device that should allow for rapid ionic movement in nanochannels or pores. The researchers should select a material in which the considerations mentioned above (grain curvature and size, interfacial spacing, defect concentration) are kept at a value that minimizes the chemical potential. A small value for μ_j indicates there will be very little increase in free energy during the reaction. Large increases in free energy will make the reaction unfavorable, and it is necessary to minimize this as much as possible. The chemical potential is also critical in achieving uniform deposition and it should be optimized to achieve the most uniform and smooth growth.

Coating uniformity can also be improved using some simple methods described by K.L. Choy. These methods include translating/rotating the substrate during deposition, improving precursor mixing by stirring the reactants and/or reversing the gas flow direction periodically, and tilting the substrate to enhance the projection of downstream substrates into the boundary layer, and/or create a temperature gradient across the substrate[62].

2.3.3. Post-deposition Annealing Treatment

The as-deposited oxide films grown by ALD and CVD techniques are often amorphous and further treatment is needed to obtain a crystalline form. For example, crystalline vanadium oxide films can be obtained by annealing the amorphous films in air at 500°C for 2 hours[63]. One undesirable effect to consider when annealing amorphous vanadium oxide film covered substrates is that thermal stresses arising from different thermal expansion coefficients in the substrate and film can lead to high stress in the

electrode[40], which can mechanically degrade it and thus worsen supercapacitor performance. Moreover, the carbon substrates that will be used in these experiments can be burnt off at these elevated temperatures in air. As such, it is important to monitor and control the post-deposition annealing process accordingly (e.g. by using inert atmosphere instead of air).

In order to investigate the effect of the initial oxidation state and microstructure on the electrochemical performance of metal oxides in anodes and cathodes of pseudocapacitors (if asymmetric design is employed) or in both electrodes (in the case of symmetrical design), we need to identify conditions required for the growth of the controlled phases. The regions of thermodynamic stability of various vanadium oxides can be identified through the use of Ellingham diagrams that plot changes in Gibbs free energy versus temperature for various reactions, such as those describing the formation of oxides. These diagrams are commonly used to estimate which reactions are favorable in different conditions (temperature, pressure, atmosphere), with the aid of thermodynamic variables, such as entropy (which can be determined from the change in free energy and the temperature $d\Delta G/dT = - \Delta S$). Generally, reactions that lead to an increase in entropy of the entire system and surroundings should have a higher probability of occurring. Also, because the signs of the free energy and the entropy are opposites, spontaneous reactions (where the change in free energy is negative) will have a positive value for ΔS, and a positive slope on the Ellingham diagram.

Another useful aspect of Ellingham diagrams is that these diagrams can be altered to account for different ambient atmospheres. For example, if the desired material can only be deposited onto the substrate in an O_2-containing atmosphere (such as is the case for

the deposition of VO), then in the Ellingham diagram the axe representing changes in free energy can be replaced with one representing $-RTlnPO_2$ ($\Delta G° = -RTlnPO_2$ in the presence of O_2) , or appropriate versions of this equation for different combinations of gases (such as H_2/H_2O ($\Delta G° = -RTlnPH_2$) and CO/CO_2($\Delta G° = -RTlnPCO_2$)) to identify these temperature stability regions in different atmospheres.

The Ellingham diagrams for the VO system has been constructed by Mizuta et. al[9]. and Hanglund, Jr. et. al[55] (see Fig. 2.12) over different temperature ranges. Different regions of stability for the numerous vanadium oxides in different atmospheres have also been identified by J.S. Anderson and A.S. Khan[56]. Once an appropriate vanadium oxide is selected for the study, the use of these diagrams will help us in choosing the most appropriate growth conditions for it. For example, the Ellingham Diagram shows that V_2O_5 is stable at 300°C in air. As such, we can identify the range of starting conditions needed to deposit the V_2O_5 film on the carbon substrates.

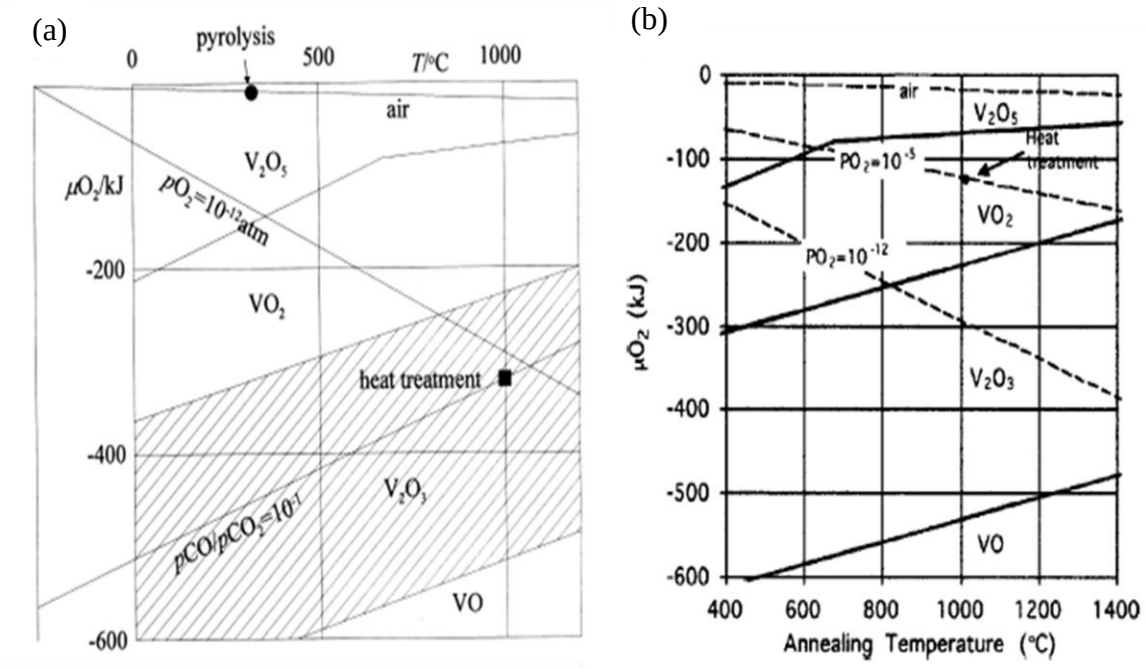

Figure 2.12: (a) Ellingham diagram for the V-O system developed by Mizuta et.al extending from 0-1000°C. [9] (b) diagram for the V-O system developed by Hanglund, Jr. et.al extending from 400-1400°C[55] . Notice the vertical axis is in terms of chemical potential of O_2 (the values that are read-off apply in an O_2-containing atmosphere) .

The Ellingham diagrams can also be used to identify useful post-deposition treatments. For example, annealing the as-deposited VO in the range of 300-500°C in air should lead to the formation of V_2O_5. In order to produce V_2O_3, one would have to anneal somewhere between 500 and 1000°C. This same logic can be applied with Ellingham Diagrams for many different metal oxides. As such, analysis of these diagrams can help identify which metal oxides will be easiest to grow into the desired form and can help save researchers a lot of time and effort.

Note that the quality of the interface between VO and the C may affect the charge transfer process. One potential complication for the proposed project is the strain between the carbon substrate and deposited film (e.g., as a result of different coefficients of thermal expansion), which may affect the efficiency of the composite architecture or

affect the cycle life for the supercapacitors. For example, V_2O_3 films that were deposited on α-Al_2O_3 were observed to shrink 1.8% along the a-axis while the substrate contracted only about 0.81% in the a-direction at 1000°C[9]. This aspect should be investigated for the materials used in the temperature range they will be exposed to and its effect minimized as much as possible.

2.4 Impact Of Electrolyte On Supercapacitor Performance

An appropriate electrolyte is essential for correct device performance. In many cases, the electrolyte can be the limiting factor for use in certain applications, as they are usually sensitive to such external factors as temperature and operating voltage. Electrolytes used in supercapacitor applications fall into three categories: aqueous electrolytes (acids, solution of salts[39], alkalis, etc..), organic electrolytes, and ionic liquid electrolytes[25, 64-66]. Aqueous electrolytes offer high ionic conductivity and a high dielectric constant at a low cost, but will decompose at low operating voltages (~1.23V) and thus limit high voltage supercapacitor applications[29]. Organic electrolytes can operate up to higher voltages (~2.5V), allowing for a higher maximum energy density for the device[49]. In case of EDLCs, organic electrolytes often do not induce irreversible changes within the electrode and the EDLC devices made with them tend to have longer lifetimes. Ionic liquids are low temperature molten salts (liquids composed solely of ions). They are environmentally friendly and can be used in temperature ranges necessary for hybrid car application (~60°C)[64, 67]. However, these liquids are highly viscous (>50cP). The high viscosity decreases mobility of the ionic species[65, 68] according to Walden's Rule, resulting in low conductivities (<5mS cm^{-1})[66]. The ionic salts have to be placed in different solvents for different applications : for example, protic (the solvent has a

hydrogen atom bound to an oxygen or a nitrogen i.e. a molecular solvent which contains dissociable H^+) ionic liquids are more suitable in fuel cells, while aprotic (lacking an acidic hydrogen) ionic liquids are those most suitable for supercapacitor/battery application and zwitterionic (a dipolar chemical compound that has a net neutral charge) liquids are most suited for ionic-liquid based membranes (Fig.2.13).

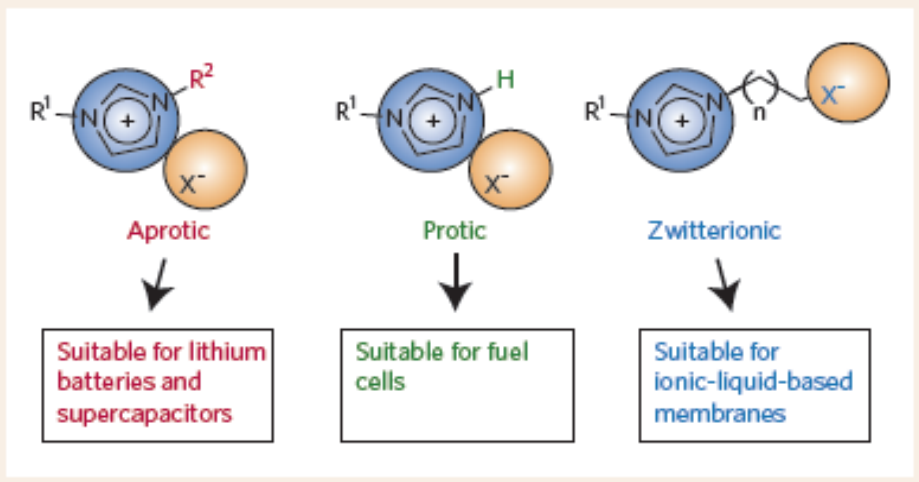

Figure 2.13. Schematic showing different ionic liquid types and their uses. Taken from[5]

Selection of an appropriate electrolyte has been demonstrated to affect energy and power density, device lifetime, and overall characteristics of the supercapacitor devices. While it is widely accepted that choice of salt and solvent will have a considerable effect, there is still little understanding as to why use of certain solvents will lead to better electrochemical performance than others in the same carbon/salt systems. For example, Taberna *et. al.[12]*compare the performance of supercapacitors in polycarbonate (PC) and acetonitrile (AN) solvents, observing faster response of the EDLC devices with AN solvent and attributing this effect to the lower viscosity of the AN solvent. The carbon/solvent interfacial energy, the solvation energy and size of the solvation shells were not considered to impact the electrolyte performance. Moreover, the possible impact

of carbon/solvent interfacial energy on ion adsorption in pores of different size was not discussed. This effect has been described by numerous other groups. For example, faster response and higher power of (microporous carbide-derived carbon – based) EDLCs was also seen [69-72] with AN solvent than with PC solvent and slightly higher capacitance in AN in the temperature range from -30 to +60º C when measured using all the common electrochemical techniques (galvanostatic charge-discharge, cyclic voltammetry and electrochemical impedance spectroscopy). Once again, little discussion was provided to explain this higher capacitance in AN than in PC (in spite of the AN's lower dielectric constant: 36.6 for AN vs. 66 for PC), except for the lower ionic resistance of the electrolyte and "*weak specific adsorption of anions in AN solvent*". Similarly, the influence of carbon/solvent interfacial energy on ion adsorption in pores of different size was not discussed. This same effect was described but remains unexplained by other research groups studying the performance of both mesoporous carbon- and microporous carbon- based EDLCs in AN and PC-based electrolytes[73]. Interestingly, R. Kotz et al. (and occasionally P. Simon et al.) observed the opposite trend: slightly higher capacitance in PC in the temperature range of 10-60°C (but again, no explanation or insights were provided)[16]. The fact that using AN versus PC solvent in porous carbons results in either higher or lower capacitance indicates that factors other than viscosity, ion solvation shells' sizes or dielectric constant (typically used to explain these differences) are responsible for this behavior. Such a factor could be the carbon walls/electrolyte interactions which govern the adsorption capacitance of ions in micro- pores.

Another major factor often cited as influencing the performance of EDLCs is electrolyte wettability. Multiple authors[67, 74] noticed that if the electrolyte solvent

exhibits poor wetting on porous carbons, the carbon specific capacitance will decrease considerably. In case of aqueous electrolytes, these authors noticed that when these carbons are oxidized (either by heat treatments in air or in CO_2 or by wet chemistry) the carbon surface becomes both more hydrophilic (thus increasing the wettability with aqueous solutions) and also exhibit higher specific capacitance. However, many unknowns still exist in regards to this claim. First, after oxidation the carbon surface not only becomes more hydrophilic, but also becomes covered by various functional groups. These functional groups may (i) exhibit pseudo-capacitance (and thus will greatly increase the measured specific capacitance of carbon) and (ii) additionally may interact with the solvation shells of the ions, decreasing the average carbon surface-ion separation distance, and thereby increasing specific capacitance[14, 75]. Second, the application of the electric field to electrolyte is known to greatly increase the wetting by electrolyte (performance of EDLCs is tested after several charge-discharge cycles, which shall induce wetting).

Enhancement of electrolyte wetting in porous carbons can also be accomplished via the addition of surfactants [76-79]. However, it is important to note that due to their relatively large dimensions (~0.5-2nm), surfactants cannot aid in increasing wetting in the smallest pores, and thus their overall contribution to the maximization of capacitance is minimal, and can in fact be detrimental if they obstruct the opening of the smallest pores. However, their use in the larger mesopores can improve ion transport and thus rate capability and power density in supercapacitor electrodes[79]. Once again however, special attention must be paid to maintaining the concentration of the surfactants below

the critical micellar concentration, at which point the large micelle structures will obstruct the pores and negatively affect the supercapacitor device properties[79].

In order to elucidate these mysteries, a powerful characterization technique such as small angle neutron scattering (SANS) can allow us to probe the sites of ion electro-adsorption and to study how the material parameters (electrolyte / microporous material of the specific chemistry and microstructure) affect the ion adsorption in pores of different sizes.

2.4.2 Ion Electroadsorption

Ion electroadsorption has many similarities to gas adsorption. As such, adsorption isotherms similar to those used in the analysis of gas adsorption can be used to describe the adsorption of ions under the application of an electric field. In this case, the applied voltage determines the concentration of ions found along the surface of the material, as well as their surface coverage inside of the pores, and the effect of temperature is minimal [80-82]. The concentration of ions on the electrode surface depends on numerous factors, and will be distributed such that the balance between the changes in enthalpy and entropy results in the minimum possible total Gibbs free energy of the system[83]. This effect has been reported in EDLCs and in some pseudocapacitive materials[84, 85]. In other pseudocapacitive materials, the presence of pseudocapacitance will result in a sharp volatge peak at specific values[85]. This difference is due to the range of enthalpies of the ion adsorption sites on the electrode surface and their distribution. For a broad range of enthalpies corresponding to the ion adsorption sites, the first case will be applicable; otherwise the second case will be applicable.

Another important factor affecting ion electroadsorption in supercapacitor electrodes is (as described previously) electrolyte accessibility to the inner pores of the electrodes. Recent research has demonstrated tha the traditional model (based on the Helmholtz electric double layer model) which predicted this accessibility on how tightly ions and their solvation shells could fit into the inner pore volume was wrong[4, 86]. As stated previously, in many cases the concentration of ion electroadsorption sites will vary linearly with the applied voltage. Th e Helmholtz electric double-layer (EDL) model is used to describe how this ion surface coverage translates to capacitance, and is based on the geometric fit of solvated ions (that is, ions and their solvation shells) inside of the electrode's nanoporous system. According to this model, maximizing the number of pores and their size (thereby maximizing the number of ions that can fit along the surface of the electrode to create the EDL) will maximize the capacitance of the device. In this case, it is clear that the internal specific surface area (SSA) should correlate linearly with capacitance. However, this was proven wrong in a systematic analysis and comparison of different porous carbons with different porous architectures [4]. In this study, increasing SSA with a simultaneous increase in the average pore size was shown not to increase the specific capacitance either. In this case, SSA was calculated using BET and DFT analysis of N_2 sorption experiments. While gas soprtion has long been used to determine internal specific surface area of porous materials, there exist many differences between the size of gas ions and that of electrolytic ions used for energy storage applications. Subsequent studies compared the inner pore volume accessible to ions in organic and aqueous electrolytes to those accessible by N_2 gas, to determine the validity of using gas sorption experiments to determine the inner pore volume of supercapacitor electrodes[87]. Many

of the commonly used ion/solvent combinations were investigated, and the size of these ions were compared to that of the commonly used N2 gas molecule (their relative size is: Li^+(propylene carbonate solvent) > TEA^+(propylene carbonate solvent) > BF_4^- > Cl^- (aqueous) ≈ Na^+(aqueous) ≈N2 (gaseous). Since this study, much attention has been made to designing supercapacitor electrodes with inner pore volumes that can accommodate these ion/solvent combinations. Later reports focused on the distortion of the ion solvation shell and on the resulting smaller separation charge distance between the ion center and the electrode surface, which can account for an increase in capacitance in the smallest pores[3, 88-90], and which will depend both on the ion and on the solvent's nature and size. However, it is important not to minimize the pore size beyond a critical limit, as this may restrict ion access and limit the rate of ion transport inside of the electrodes. It seems that the electrode architectures most optimal for rapid charging and discharging do not include bottle neck or strongly curves pores and mostly possess stright (in some cases aligned) pores above some critical size [91].

These studies allowed for the development of newer models of electrosoprtion which focused on the formation of an ion monolayer which was 'squeezed' into tight pore walls, representating the squeezed ions as an ion wire inside a cylindrical pore[92]. This distortion of the solvation shell is dependent on many characteristics, including solvation size, solvation energy, and pore wall-solvent interactions. The solvent will also affect key properites of the electrolyte, such as wettability[74, 93-95], viscosity, and pH [96-98], which may impact both the rate and capacitance of energy storage devices. Other important solvent parameters such as dielectric constant and ionic conductivity have also been experimntally determined to affect the capacitance of energy storage devices. Thus,

the choice of solvent is of critical importance in maximizing the energy storing capability of a particular device, and a method to elucidate how ions flow in different solvents under applied potentials is becoming of critical importance to the energy storage community.

Traditionally (and still to this day, due to lack of a better experimental technique), supercapacitor electrodes were evaluated using gas sorption experiments and analysis of these measurements by different models, such as BET (a simple model that does not accurately represent gas sorpion in microporous solids[99]), DFT (which is based on simplified pore shapes such as infinitely long slit shaped and cylindrical pores[100]), and BJH. These measurements ignore many factors of importance which can contribute to the capacitance of the device, such as pore shape, microstructure of the electrodes, and concentration of functional groups and defects.

Moreover, these measurements depend entirely on the acessibility of the inner pores by gas molecules, which (as discussed in another section of this dissertation), can be entirely different from accessibility by electrolytic ions. These considerations were confirmed by the studies of Centenno et.al. of porous carbons in various aqueous and organic electrolytes[101-104]. Additional experiments making use of materials with well defined pores [105] or with different types of pore volumes[106] are better suited to resolving some of the still unknown questions about ion adsorption in supercapacitor electrodes, such as the impact of electrolyte solvent-carbon pore wall interactions. For example, a recent study by Kajdos et.al. investigated the effect of pore alignement on the kinetics of charge and discharge in supercapacitor electrodes[106]. Electrochemical characterization of electrodes with different levels of pore alignment showed that ion

transport and frequency response could be improved by up to three orders of magnitude by creating clear channels for ion transport devoid of obstacles to ion diffusion.

Another important factor affecting electrolyte solvent-carbon interactions and thus ion electroadsorption is the pH of the electrolyte. Many studies have investigated this factor in aqueous electrolytes, and concluded that the pH will impact pseudocapacitance, self-discharge, and the electrolyte stability window[107-109]. For example, in a recent study by Demarconnay et.al., neutral electrolytes were better than acidic electrolytes in improving low potential stability, and were better than basic electrolytes at improving high potential stability in symmetric carbon/carbon supercapacitors[108].

2.5 Impact of Conductive Carbon Substrates on the Performance of Metal Oxide-Based Composite Supercapacitor Electrodes

The use of highly conductive pure carbon-based EDLC electrodes as a base substrate for depositing transition metal oxides may combine the charging mechanisms of both EDLCs and pseudocapacitors into one more efficient device. High conductivity, well developed porosity, often low cost and high surface area make porous carbons the most logical choice for a suitable electrode material for EDLCs. These highly porous structures allow for effective penetration of the electrode by the electrolyte ions because of their large surface area, and this has been shown to increase specific capacitance[110]. Other important characteristics of porous carbon include good corrosion resistance and high temperature stability. Pore size, pore alignment, surface area, microstructure, surface chemistry and electrical conductivity of carbon were all found to play a key role in the device performance.

The morphology of the carbon substrate (surface chemistry, defects, pore shape and size, etc.) affects both the metal oxide deposition conditions as well as the electrochemical performance of the composite in supercapacitors. For example, an analysis of pore size can indicate how easily the electrolyte can access the electrode for ion exchange during the electrochemical experiments. Similarly, the diffusion and the VO CVD growth regime will be affected by both the carbon surface chemistry and pore size distribution. Finally, the morphology of the VO films themselves (dense vs. porous of different pore size) is expected to strongly affect the electrolyte diffusion into the metal oxide matrix during electrochemical reactions.

Diffusivity during the CVD and ALD processes is a function of position (jump frequency will depend on local atomic arrangements and defects). This is because more open structures with higher jump frequencies possess a lower energy barrier to overcome than other microstructures. As such, using substrates/electrodes with many of these features should allow for easier deposition of the desired metal oxide.

2.5.1 Impact of Specific Surface Area of the Electrode on Electrochemical Performance of Supercapacitor Electrodes

The capacitance of an EDLC is dependent on the specific surface area of the carbon material (SSA) and on the area-normalized double layer capacitance (DLC) of the electrode (specific capacitance C_s = SSA*DLC). As such, one would expect a linear relationship between surface area and specific capacitance. This was proven untrue[111], and to relate the area to the capacitance it is important to differentiate between the surface areas of the electrode material accessible to fully solvated ions, accessible to de-solvated ions and not accessible to any. In some studies, the surface area accessible to fully

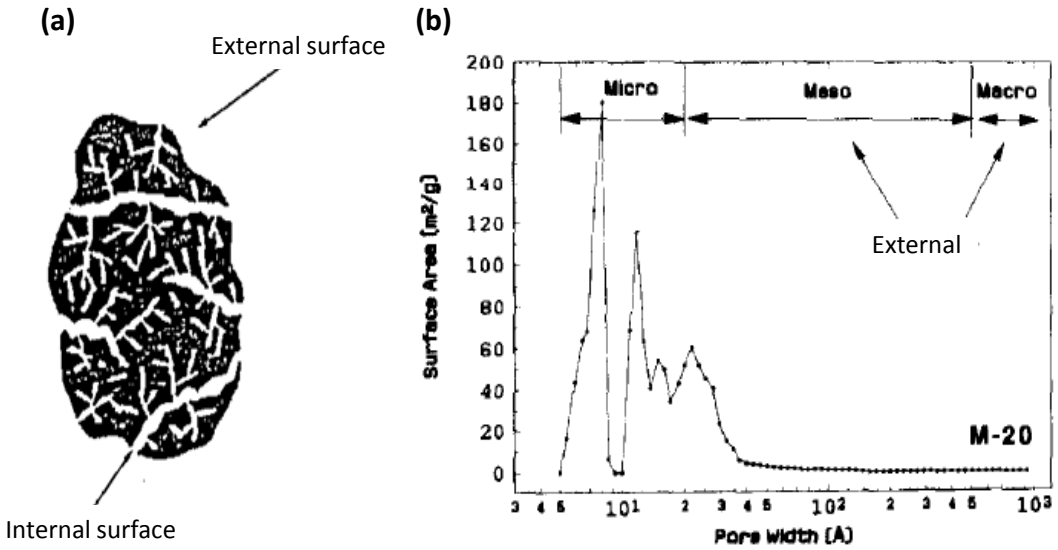

Figure 2.14. (a)Schematic illustrating external and internal surface area of a porous carbon.(b) Pore size distribution of activated carbon classified as external and internal surface areas. Taken from[4].

solvated ions is approximated as the so-called *external* surface area, which includes the area of all the outer surfaces of secondary particles, and of all cracks that have a larger width than depth (Fig. 2.14)[111]. The internal surface area is often approximated as the surface area accessible to at least partially desolvated ions. It is comprised of all pores and cracks that are deeper than they are wide[27]. The external surface area is much more accessible than the internal surface area to the electrolyte. As such, it is this surface area which is linearly proportional to specific capacitance. The internal surface area may have either higher area-normalized capacitance (when ions access it but their solvated shells are distorted) or lower area normalized capacitance (when electrolyte does not access some of the smallest pores), as discussed in more details below.

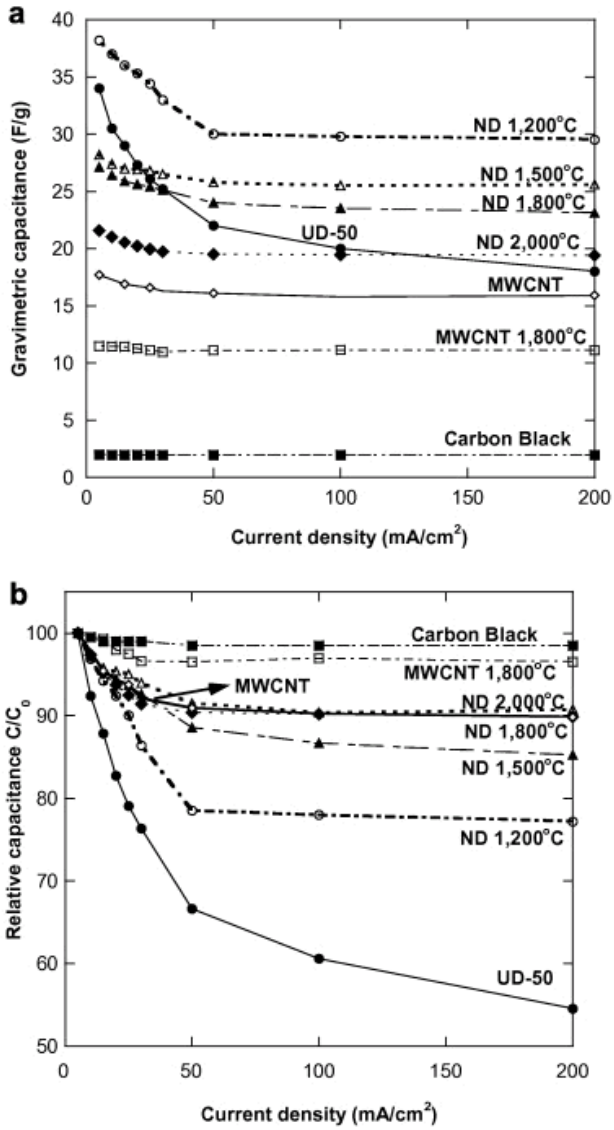

Figure 2.15. Capacitance variation with current density: gravimetric capacitance (a) and relative capacitance C/C_0 (b), where C_0represents the capacitance measured at 5 mAcm^{-2}.

Taken from [14].

Additional studies demonstrated that surface area was not the only important factor impacting the gravimetric and relative capacitance of supercapacitors. In Portet et.al.'s 2007 experiments, nanodiamond-based samples were annealed at different temperatures. The annealing steps did not affect the porosity of the nanodiamond samples, but rather

introduced defects or edge planes in the carbon lattice that enhanced interaction between the carbon surface and the ions in electrolyte. The effect of introducing these defects was to increase capacitance and to decrease capacitance retention at higher current densities. Thus it was shown that the electrode microstructure had a significant effect on device performance (Fig. 2.15)[14].

2.5.2 Pore Size Effect

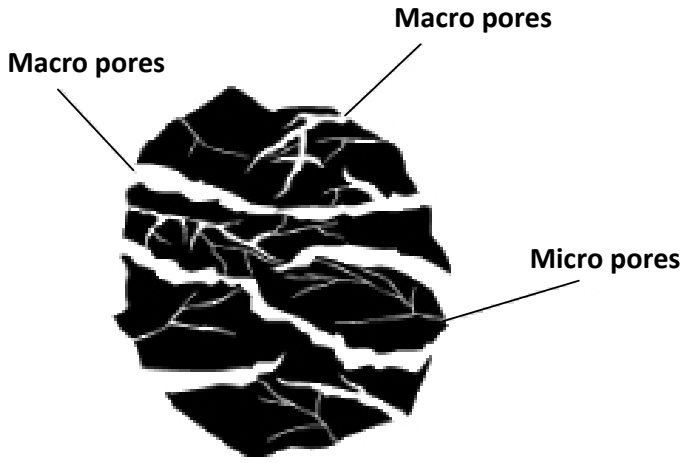

Figure 2.16. Schematic illustrating types of pores. Taken from [http://sujatacarbons.com/gifs/activated-carbon3.jpg]

Pores in materials are classified according to their size: micropores are smaller than 2 nm, macropores are larger than 50nm, and mesopores are located between the two (Fig. 2.16). Porous materials that have micropores are usually preferred for supercapacitor electrodes for numerous reasons. They possess a high surface area to volume ratio, and exhibit greater adsorbent-adsorbate affinity due to an overlay of adsorption forces from opposing surfaces. Pores that are too small or too big will lead either to ion impediment or a waste of useful area. Experimentally it was found that pores with diameters in the of 0.6-1.2 nm range commonly lead to the combination of high capacitance and good frequency response (see Fig. 2.17)[21]. To find the most appropriate pore size, it is

important to compare it to the size of the ion and its solvation shell. If the pore size is equal or larger than twice the solvated ion size, layers of ions can reside on both sides of the pore walls that define the pore and provide high capacitance. If the pore size is smaller than single diameter of a solvated ion, one may expect the ions not to fit inside the pore and the resulting capacitance to be negligibly small. To demonstrate this, Chmiola et.al. used porous carbons made from carbides with very good control over the pore size and uniformity. It was hypothesized that as the size of the pores became smaller than that of the ion and its solvation shell, the capacitance would become negligible. The results they observed were surprising, there was a large increase in capacitance in these smallest pores. This increase was attributed to a distortion of the solvation shell which allows the center of the ion to be closer to the electrode surface than in the other cases, leading to a large increase in normalized capacitance[86] (Fig. 2.17).

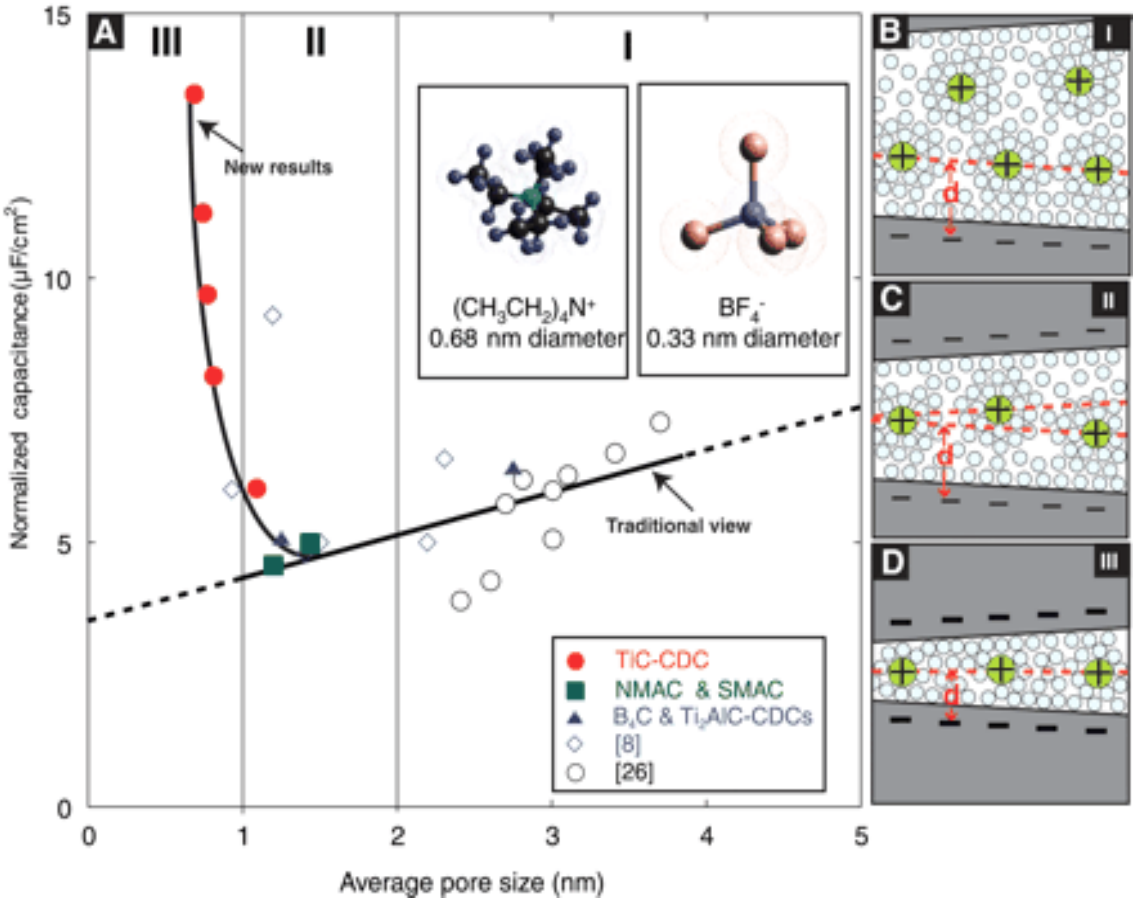

Figure 2.17. Diagram illustrating effects of pore size on normalized capacitance. Taken from[3]

This distortion of the solvation shell was recently experimentally proven through NMR spectroscopic studies of porous carbons in organic electrolytes. Researchers used the NMR technique to demonstrate that in carbon molecules with sufficiently large pores (> 1nm), electrolyte molecules tend reside closer to pore walls than solvent molecules (seen through a chemical shift in the NMR peak of the ion molecules – see Fig. 2.18). Removal of the solvent through vacuum evacuation resulted in a removal of the solvent molecules (seen by the absence of the solvent peak in the NMR spectrum after the vacuum evacuation step – see Fig. 2.18) which brought the electrolyte molecules even closer to the pore walls. The researchers showed that if adsorbed in pores smaller than

1nm, the electrolyte molecules did not exhibit an intact solvent shell, suggesting that in small pores the solvation shell did not exist [19].

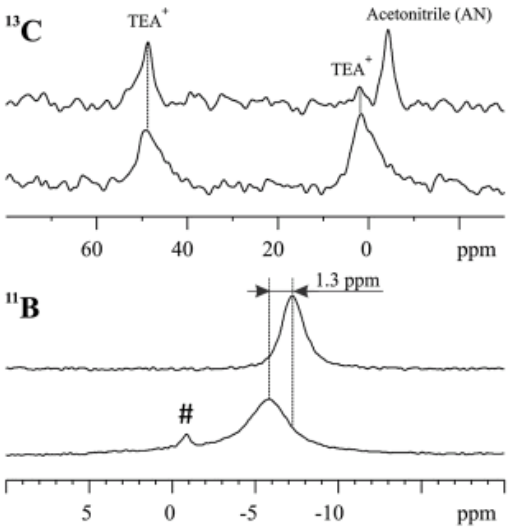

Figure 2.18. Chemical shift of NMR peak before (top) and after (bottom) evacuation of electrolyte by vacuum. Taken from[19].

Discoveries such as these outline the fact that little is known about ion adsorption for energy storage applications. These results indicate that a limiting pore size for the electrode material should be based on the size of ion used in the electrolyte. However, there is a clear absence of knowledge regarding carbon/solvent interface energy, the effects of solvation energy, and the effect of the size of the solvation shell. While it has been accepted in the research community that different solvents and ions(electrolytes) will lead to different device characteristics (energy and power density, specific capacitance, etc…), new *in-situ* studies capable of revealing the ion adsorption sites are required to gain better fundamental understanding of the origin of this phenomenon.

Pore size distribution is also an important factor for the charge-discharge frequency of supercapacitors. If the pore sizes in the electrode are fairly equal and uniform, the resulting device will exhibit impedance that approaches the ideal capacitive behavior at

low frequencies (this will resemble a vertical line on the impedance spectrum). Penetration of the ac signal is different for pores of the same size at the same frequency[110]. Electrolyte accessibility will become easier for larger pores and more difficult for smaller ones. As such, a pore size distribution in the material will not lead to effective charging and discharging of the entire electrode at any one frequency. This trend also holds when looking at varying frequencies. Low frequencies allow sufficient time for the ions to completely penetrate the depth of the pores. At higher frequencies, there is not enough time to do so, which leads to incomplete penetration of the pores by the electrolyte. Because of this, materials with large open structures (three-dimensional porous structures) such as the metal oxides mentioned above, facilitate ion transport and reversibility and are thus ideal candidates for supercapacitor electrode[63].

A new heuristic theoretical model that takes into account pore curvature and size has been developed by Meunier *et. al.* This model can be used regardless of what type of carbon materials and electrolyte are used and allows researchers to correlate supercapacitor properties with pore size, specific surface area, Debye length, electrolyte concentration, dielectric constant, and solute ion size[92].

It is possible to construct a carbon electrode with desired pore sizes by using inorganic templates such as zeolyte[112, 113], porous alumina, or silica[51, 114]. After finding a template with the desired microstructure and pore size distribution, carbon is deposited onto the template. The template is then etched away with a powerful etchant (such as HF), leaving the carbon with the desired pore architecture. Zeolyte-templated carbons have been shown to exhibit excellent capacitance characteristics[112, 113].

2.5.3 Microstructure Effects on Electrochemical Performance of Supercapacitor Electrodes

An ideal electrode possesses a microstructure tailored for maximum electrolyte accessibility and highest ion adsorption density. As mentioned previously, pore size distribution will affect this: larger pores will allow for fastest access of electrolyte to it, and smaller pores may lead to a large increase in specific capacitance due to the solvation shell distortion effect. Surface area normalized by the volume of the electrode increases for smaller pores (more pores per volume), and specific capacitance is related to surface area. As such, in many cases it is advantageous to increase the surface area of small pores. This means that there is a trade-off between surface area and pore size and a correct balance must be determined to make most efficient use of the architecture. Larger pores will allow for high power discharge applications (they can be accessed quicker by more ions than smaller ones) but a large surface area per unit volume may allow for more energy to be stored. The tradeoff thus becomes one of specific energy versus specific power, and the microstructure must be tailored to meet desired specific needs[68].

2.5.4 Impact of Electrical Conductivity

Electrical conductivity of powder electrodes depends on the powder size (smaller size leads to higher resistance) and compaction (greater compaction pressure decreases resistivity) as well as the bulk material conductivity[115]. In ordered carbon materials, such as graphite (graphene) and carbon nanotubes, the conductivity changes according to crystallographic orientation[67]. In EDLCs, slow ion transport, and not electrical resistance of electrodes, limits the rate of charging or discharging of a device.

2.5.5 Types of Carbon Materials used in Supercapacitor Electrodes

Several types of carbon materials have been used in supercapacitors: exfoliated graphite / graphene, activated carbon, carbon-derived carbon (CDC), templated carbons, carbon nanoparticles (carbon onions, carbon aerogels) and carbon nanotubes (CNT).

Graphite is composed of numerous hexagonal graphene layers stacked on top of each other. When considering graphite it is important to distinguish between different crystallographic orientations as these affect conductivity and reactivity. The crystal structure has two orientations: an edge (along the height of the crystal structure) and basal (perpendicular to the graphene layers) orientation. Edge sites are more reactive than basal sites and as such they are often associated with unpaired electrons. Because of this, the edge sites exhibit conductive behavior while basal sites exhibit semiconductor properties. This results in a larger double layer capacitance along the edge orientation than on the basal layers. Resistivity measurements have confirmed this: resistivity was measured experimentally to be 10^{-5} Ω.cm along the a-direction (edge direction) and 10^{-2} Ω.cm along the c-direction (basal layer)[68].

Activated carbon is carbon that has been chemically or thermally activated. Activation is a process employed to increase surface area and pore volume in carbon substrates, which leads to high specific capacitance. Activation also leads to lowered resistivity since the intrinsic resistivity increases with increasing surface area. The specific capacitance of the activated carbon materials is also dependent on crystallographic orientation (edge is preferable over basal orientation).

CDC is formed by high temperature chlorination of carbides. It possesses good mechanical properties, which translates to a longer lifetime for the supercapacitor[68]. It

has 50-80% pore volume, and it is possible to get atomic-level porosity control by exploiting the host carbide lattice as a template. However, appropriate carbide precursor with the desired crystal structure must be selected. Host carbides include α-SiC (rhombohedral structure), TiC (cubic structure), Mo_2C (hexagonal structure), B_4C (rhombohedral structure), and Al_4C_3 (rhombohedral structure)[72]. The selection of a precursor carbide was found to affect numerous properties, including series capacitance, series resistance, time constant, diffusion resistance, and charge-transfer resistance. Supercapacitors with electrodes made from CDCs using ZrC and TiC as precursor host carbides were found to have maximum specific capacitance values of 190 and 150 $F \cdot g^{-1}$, respectively[31].

CNTs combine small size with large conductivity and can be regarded as the smallest possible electrodes with diameters in the sub-nanometer range[116]. They possess good mechanical, electrical, thermal, and electrochemical properties. The nanotubes are extremely conductive because all bonds are sp^2 hybridized orbitals, and they are spread out as conjugated double bonds (alternating single and double bonds), which allows for rapid movement of delocalized electrons and thus high conductivity. Pre-treatment of CNTs has been found to affect electron-transfer rates. One such treatment is acid purification of the CNTs. This is done by boiling the CNTS in acid (usually a mixture of nitric and sulfuric acids)[117]. During this step, the reactive and highly strained CNT caps are removed, leaving open-ended tubes which facilitate ion transport during supercapacitor operation. The acid also cleans the side of the CNTs of dangling groups and bonds, leaving a clean surface which will not impede ion transport later. Finally, the acid shortens the tubes, which facilitates dispersion and can, when coupled with filtering,

lead to the formation of a binder-free electrode. CNTs have been used in electrodes for supercapacitor applications through the use of many different techniques: they have been directly grown on graphite electrodes[118], electrodeposited onto current-collectors[49], painted onto Cu current collectors with the use of Ag paint[119], made into a paste electrode[120], or used in combination with a binder to form the electrode.

Carbon nanoparticles[14, 121-123] can be used in conjunction with a binder such as PTFE (polytetrafluoroethylene) or PVDF (polyvinylidene fluoride) to create high surface area electrodes. This binder is usually not conductive, and as such it must be used sparingly to avoid formation of an electrically insulating layer between the carbon particles. Excessive amounts of binder have been shown to increase electrode resistance and contribute to an overall increase in capacitor ESR through greater particle contact resistance[124].

2.5.6 Impact of Functional Groups

Because of processing conditions, functional groups are often introduced on the surface of the carbon electrodes. These functional groups affect access of electrolyte to the porous carbon electrode, conductivity, surface area, stability, and wettability[68]. Dangling groups and surface functionalities impede ion transport at high current densities[67], as they may restrict ion movement towards the internal volume of particles. Some functional groups can increase conductivity (such as hydrocarbyls) while others can contribute to pseudocapacitance (nitrogen or oxygen containing functional groups can undergo redox reactions and this gives rise to pseudocapacitance)[68].

However, many of the functional groups that give rise to pseudocapacitance only do so in certain potential windows that must be identified. Functional groups are sometimes

introduced on the surface to make it hydrophilic or hydrophobic, depending on the desired application. Surface oxides can also be introduced on the electrode surface. Acidic surface oxides can be added by exposing the carbon substrate to O_2 at 200°C-700°C[68]. Unfortunately, acidic groups were found to decrease the stability of devices and greatly increase the rates of self-discharge[125]. The basic and neutral surface oxides (which are commonly introduced at room temperature) are much more stable and do not commonly lead to rapid self-discharge[67].

The functional groups present on the electrode (both carbon and VO_x) surface are known to affect access of the electrolyte to the surface, electrical conductivity of the compacted electrode powder, the specific surface area, and the wettability of electrodes by the selected electrolyte and the resulting overall ionic resistance (particularly at high current densities)[115]. It is thus important to identify their presence (via the use of surface characterization techniques such x-ray photoelectron spectroscopy) and investigate their effect on the electrochemical performance of the produced electrodes in different electrolytes. Both the wet and dry chemistry routes could be used to remove and selectively place the desired functional groups on the electrode internal surface.

Due to the wide ranging nature of the effects of functional group and the general surface chemistry of the electrode materials on the supercapacitor device operation, it is necessary to analyze the surface chemistry of these electrodes in order to try and tailor it to suit these supercapacitor applications. Numerous techniques, such as Energy dispersive X-ray Spectroscopy (EDS), Auger Electron Spectroscopy (AES), Rutherford backscattering (RBS), X-Ray Photoelectron Spectroscopy (XPS), and Secondary ion mass spectrometry (SIMS), can be used for surface chemistry analyses.

2.4 Effects of Assembly Methods, Temperature and Voltage on Supercapacitor Device Performance

Experimental methods and laboratory procedures can significantly alter results obtained, and as such it is important to evaluate different supercapacitor electrodes along the same guidelines. Stoller and Ruoff outline some of the key parameters which must be followed during supercapacitor testing in one of their most recent papers[126]. To ensure reproducibility, electrode thickness should be measured as it will affect the equivalent series resistance of the device (Stoller *et.al.* recommend that the thickness of the electrodes remains between 10 and 100 μm). The generation of Nyquist plots from the impedance data is especially useful in determining the equivalent series resistance (ESR) of the device. The ESR of a device is inversely based on cell size and depends on many factors, including electrode spacing, electrolyte, and package type, among others. (Fig. 2.19). Moreover, this value should agree very well with the ESR value which can be calculated from the voltage drop at the beginning of the discharge curve [ESR = (IRdrop)/(total change in current applied)] of the constant current charge-discharge plots. As such, by checking the values obtained from the impedance data with that obtained from the constant-current data (or vice-versa), one can check the reliability of the experiments and the values calculated from the data.

R. Kotz *et. al.* investigated the temperature and voltage-dependent behavior of commercial supercapacitors[16]. Elevated temperatures will degrade the supercapacitor electrodes and thus affect their lifetime, and it is important to provide information which allows estimating the lifetime for conditions that deviate from the recommended specifications, especially temperature and nominal voltage. Supercapacitors typically

only operate in the (-70 to +70°C) range because of constraints imposed by the electrolyte (the type of electrolyte used will also fix the operating voltage range)[105]. In a recent study, zeolite templated carbons were used as electrodes in supercapacitors retaining up to 86% of their energy density at ultra-low temperatures, opening up new possible applications in high altitude aerial vehicles, polar regions, and extreme altitudes[105].

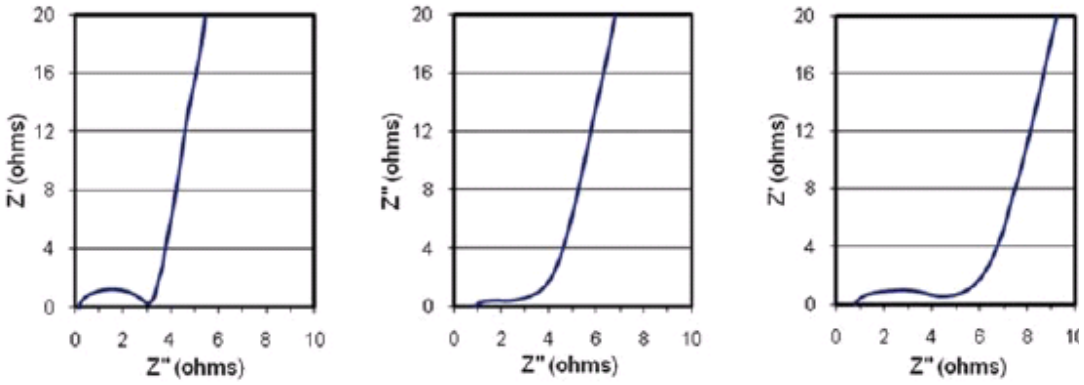

Figure 2.19. Nyquist plot of supercapacitor cell with (left) packaged cell (middle) two electrode test cell with Celguard separator, and (right) two electrode cell with separator from package. Taken from[13]

Kotz et. al. determined that a decrease in temperature lead to an increase in the equivalent series resistance of the device at high frequencies (i.e. the Nyquist plot shifts to the right at lower temperatures - see Fig. 2.20). The high-frequency resistance, on the other hand is mainly dominated by the distributed part (45° region) of the Nyquist plot. The lifetime of a supercapacitor can also be determined by using accelerated life tests which take into account the effects of elevated temperatures and potentials. The authors tested the lifetime of their supercapacitor electrode against that of a commercially available one and discovered that aging of the capacitor is accelerated by a factor of 1.5-2 for an increase in maximum cell voltage by 0.1V while an increase in temperature of 10°C will result in an accelerated aging factor between 1.7 and 2.5[16].

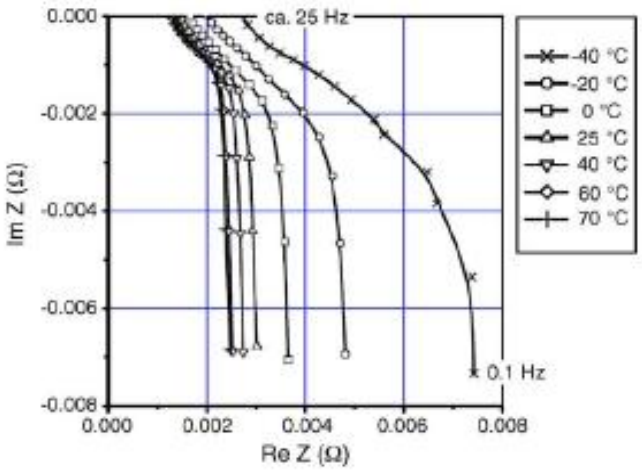

Figure 2.20 Temperature dependence of Nyquist plot for commercial supercapacitor. Taken from [16].

CHAPTER 3

MATERIAL CHARACTERIZATION TECHNIQUES

3.1 Introduction

A list of the major characterization techniques used through these studies is supplied, along with a brief description, in the sections below. A good understanding of these techniques, including their advantages and limitations, is necessary to evaluate the work which was performed over the course of this dissertation.

3.2 Scanning Electron Microscopy (SEM)

Scanning Electron Microscopy (SEM) is an imaging technique used to observe the topography and surface of samples. Here, an electron beam (of order 0.2keV-40keV) is generated from an electron gun (usually thermionically) and focused onto the sample. The electrons in the beam interact with a sample, and lose energy by repeated random scattering and absorption. High energy electrons are reflected due to elastic scattering, while secondary electrons are generated from inelastic scattering in the sample. Detectors are placed around the sample and measure the energy exchange between the incoming electron beam and the reflected electrons. By rastering the beam onto the surface of the sample, the topography can be imaged.

While SEM is a very useful and versatile characterization technique, it does have its limitations. Imaging via SEM requires use of a vacuum atmosphere due to the necessity of generating an electron beam. The presence of a vacuum is needed to generate the electron beam, as the presence of particles within the SEM chamber could interact with the beam. As such, samples need to be dry and secured in the chamber. Secondly, the

elevated energy of the beam can also destroy fragile samples, and this must be taken into consideration when preparing samples.

3.3 X-Ray Diffraction (XRD)

X-ray diffraction (XRD) is a characterization technique which uses X-rays to identify crystalline phases in a sample. In this technique, X-rays are generated and directed at a sample. These x-rays will diffract off of the electrons that are in the atoms that compose the sample and will hit a detector. The angle and relative intensity of these diffracted beams allows researchers to determine the crystal structure of the sample. This can be achieved because XRD reveals the average spacing between layers or rows of atoms. It also allows for the determination of the orientation of a single crystal or grain. Finally, it can also be used to measure the stress of small crystalline regions within the sample. Because it does not require a special atmosphere, XRD can be used on a wide variety of samples, the only limitation being materials that are X-ray sensitive.

3.4 Small Angle Neutron Scattering (SANS)

Small Angle Neutron Scattering (SANS) is a technique used to characterize the structure of samples. Radiation is elastically scattered by a sample and the resulting scattering pattern is analyzed to provide information about the size, shape, and orientation of some component of the sample. Here, neutrons generated either from a nuclear reactor or from a spallation neutron source (using a particle accelerator or synchrotron to generate high energy proton beams which, given enough energy, will blast away nuclei from a target) are shot at a target sample, and information about this sample's structure is determined from the resulting scattered pattern. Because of this, SANS is an expensive technique which cannot be used in a typical laboratory. However, use of neutrons has two

advantages over more traditional characterization techniques such as small angle X-ray scattering (SAXS). First, because neutrons have similar wavelengths to X-rays (neutron radiation is typically in the 0.01-3nm range) with lower energy (energy of 0.15nm wavelength neutron is ~36.4meV whereas energy of 0.15nm X-ray photon is ~8.2KeV), they can be used in fragile samples in which molecular degradation should be avoided, such as biological samples, colloids and polymer samples. Secondly because neutrons scatter off nuclei, and not the electrons surrounding the atomic nuclei (such as X-rays, or photons – see Fig. 3.1), the neutron scattering cross section does not increase linearly with increasing atomic number Z, and even isotopes of the same element can have different neutron scattering cross sections (for example, Hydrogen and Deuterium will scatter differently during a SANS experiment due to their different scattering lengths – b_H = $-3.739*10^{-13}$cm and b_D = $6.671*10^{-13}$ cm)[127]. This is an important aspect of SANS which is used in numerous experiments: by combining hydrogenous and deuterated forms of a specific medium, one can isolate the SANS profile of adsorbed layers alone (this process is known as contrast matching). Moreover, because the interaction of neutrons with matter is weak, neutron radiation is very penetrating especially when compared with X-rays. This allows for characterization of much thicker samples. Finally, because neutrons possess small magnetic moments, there is also a possibility of scattering from interactions between the neutron and from the spin and orbital magnetic moments present in a sample containing atoms with unpaired electrons[128].

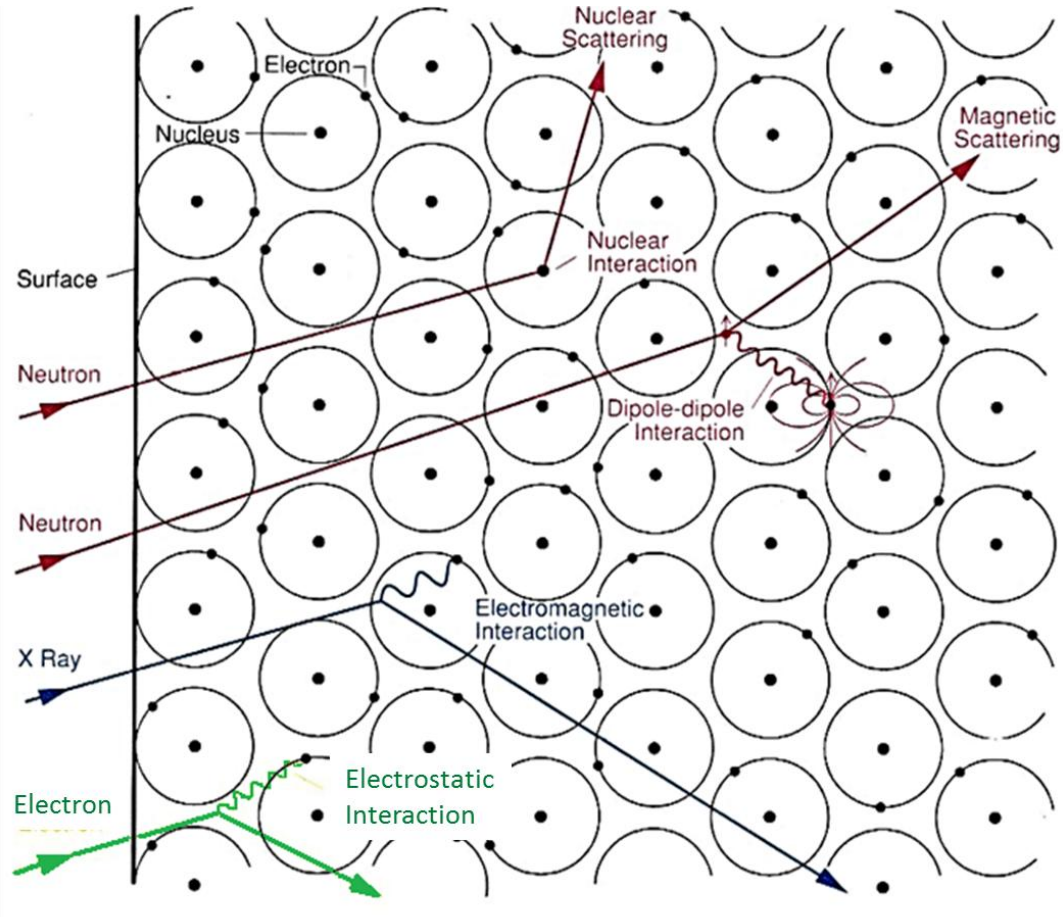

Figure 3.1. Illustration of neutron scattering compared to other scattering techniques (from SANS presentation by Samuel Ghebru).

The SANS technique can be used to reveal the size and shape of particles dispersed in a homogeneous medium by calculating the differential cross section. Because of these considerations, SANS has already been used to probe the structure of porous carbon aerogels[129], and is an ideal candidate for characterization of porous carbon electrodes such as those used for supercapacitor applications. Moreover, hydrogen's nucleus (a single proton) has a mass which is very similar to that of a neutron. Because of this, elastic collisions between neutrons and hydrogen nuclei result in the most efficient energy transfer between neutrons and atoms, and this means that materials with a high hydrogen content efficiently absorb neutrons travelling through them[130]. Thus,

hydrogen is easily detectable by neutron scattering, and the fact that most of the electrolytes used in supercapacitor devices contain hydrogen either in the ion or in the solvent means that small angle neutron scattering is an ideal technique to identify the presence of these ions during supercapacitor operation.

3.5 Raman Spectroscopy

Raman spectroscopy is a vibrational spectroscopic technique used to study the chemical composition of gaseous, liquid, or solid samples. Monochromatic light (usually a laser in the visible, near-ultraviolet, or near infrared range) is targeted at a sample. A small percentage of photons from this light source interact with molecular vibrations, phonons, and other complex elements within the sample. Due to inelastic scattering from these complex elements, a small number of the emitted photons will have their frequency either shifted up or down. The majority of emitted photons, however, will not interact with these elements, and will thus remain at the same frequency (known as Rayleigh or elastic scattering). The Raman spectra which are generated are thus dependent on chemical bonds and on the symmetry of the molecules being analyzed. As such, Raman spectroscopy can be used to quickly identify a sample by comparing collected spectra with a large database of stored chemical bonds and molecular structures.

There are numerous advantages to Raman spectroscopy. It is a rapid characterization technique which requires little to no preparation and can be performed in ambient atmosphere. Because water is a weak scatterer, it is compatible with wet samples and can be used for organic and aqueous samples.

3.6 X-Ray Photoelectron Spectroscopy (XPS)

XPS allows for the determination of numerous factors, including elemental composition, empirical formula, and electronic state of the elements that make up a material. XPS can identify these elements in the surface layers of the material (top 1-10nm of the material surface), and thus can help identify functional groups, contaminants (impurities), and the level of uniformity of elemental composition across the surface of the electrode. XPS can also be used to create a depth profile of the sample by looking at the uniformity of elemental composition as a function of ion beam etching.

XPS spectra plot binding energy vs. number of electrons counted. Because only electrons from the top 1-10 nm of the electrode will be detected (deeper electrons will end up recaptured or trapped in various excited states throughout the material), the surface chemistry of the sample can be analyzed. Also, because XPS uses X-rays and not an electron beam (like other techniques such as AES or EDS), the XPS analysis does less damage to the sample surface than other surface analysis techniques. Modern sources use monochromatic x-ray sources that harm the electrode surface even less. This is of vital importance in supercapacitor research where a device must be constructed after the surface chemistry has been analyzed.

XPS has numerous advantages over other surface analysis techniques. For example, XPS can identify all of the elements in the periodic table from Li to U. While the detection limits are similar to those of EDS, AES, and RBS (~0.1-1 at%) and much larger than that of SIMS ($\sim 10^{-6}$ at%), only XPS (and to a lesser extent AES) has the ability to inform the researcher on the nature of the chemical bonding and valence states of the elements in the sample. XPS provides more detailed information on chemical bonding

than AES because the line widths are considerably narrower than those associated with Auger transitions. For these reasons, XPS is also known as ESCA (Electron Spectroscopy for Chemical Analysis). However, AES allows for the highest lateral special resolution over which analysis can be performed (~500 A vs. ~0.1mm for XPS).[59]

While XPS is a suitable technique for surface analysis of electrode surfaces, there are some drawbacks which must be kept in mind when considering its use. Quantitative chemical analysis with AES and XPS is problematical with error bounds of a few percent[59]. Also, as stated earlier, XPS does not have the best detection limit (SIMS does), and its lateral resolution is one of the largest (only RBS is larger). Another problem is that because XPS is very sensitive to the ambient atmosphere, an inert atmosphere sample-preparation box is usually required to prepare the samples and load them into the XPS instrument. This makes sample preparation much more complicated and time consuming. Another major problem comes with the identification of XPS peaks as specific bonds. In order to do this, the experimental spectra are usually compared with a large database of stored identified spectra. XPS looks at the chemical shift (there is a change in electrostatic potential on an atom when valence electrons are added or subtracted) of an element to identify its chemical bonds. The accuracy of this method is dependent on our ability to model different factors such as the local partial charges and molecular geometry. This ability, and thus the accuracy of the XPS instruments decreases with heavier elements. As such, comparative chemical shift data from different research laboratories usually does not agree to better than 0.3-0.5 eV[131]. XPS measurements are also prone to another source of inaccurate measurements: XPS samples are usually insulated during irradiation. This leads to an accumulation of negative charge on the

sample surface, which also leads to an increase in measured binding energies. To deal with this, the spectrum must be compared to a reference photoelectron line such as the C_{1s} line and calibrated. Another problem arises from analysis of the XPS spectrum itself. The peaks which are indicative of binding energies and thus responsible for elemental and chemical identification are usually difficult to define, and this becomes more difficult when other factors such as multiplet interaction or Plasmon interactions, which reduce peak symmetry, come into play.

The high sensitivity of XPS coupled with its non-destructive nature makes it an ideal candidate for the study of delicate surfaces like those of supercapacitor electrodes.

3.7 Electrochemical Characterization

Electrochemical testing (cyclic voltammetry, impedance spectroscopy, charge-discharge experiments) is necessary to understand the underlying mechanisms responsible for charge generation and transport. Depending on the type of experiment, numerous equations can be applied in order to study the electrochemical data and gather information about the device being tested. It is thus of crucial importance to understand the thermodynamics governing these reactions. The standard free energy change arising from conversion of reactants to products is:

$\Delta G° = -nFE°$ (or, more generally, $\Delta G = -nFE$), where n is the number of electrons transferred during the reaction, F is Faraday's constant (96485.339 C mol^{-1}), and E° is the cell potential. The laws of chemical equilibrium yield the following relation:

$\Delta G = \Delta G° + RT \ln Q$, where R is the gas constant (8.314J $mol^{-1}*K^{-1}$) and Q is the reaction quotient ($Q = \Pi\{activity_{products}\}/\Pi\{activity_{reactants}\}$ = [products]/[reactants]). Substituting $\Delta G°$ and ΔG for the previous expressions we get:

$-nFE = -nFE° + RT \ln Q$, which can be re-arranged to yield the Nernst Equation:

$$E_{cell} = E° - RT/nF \ln Q$$

Thus, cell potential is only dependent on temperature, the activities and concentrations of the products and reactants, and the number of electrons transferred during the reaction. It is important to note that the Nernst Equation only applies to solutions with very dilute concentrations of ions. For more concentrated solutions, the reaction quotient Q must be expressed in terms of activity instead of concentration ($a = \gamma C$, where a is the activity, γ is the activity coefficient, and C is the ion concentration). In order to determine the activity coefficients, electrode potentials measure activity directly in solutions of known concentration. It is important to note that at equilibrium, $\Delta G = 0$ and the equilibrium constant K is used.

The formation of new defects (dislocations, vacancies, grain boundaries, etc…) within the solid particles or formation of functional groups on the surface of the solid during the electrochemical testing may drastically alter device performance. These defects can either aid or impede ion movement during device operation. For example, vacancies facilitate ion diffusion through the bulk of the electrode particle (it is especially effective if the ion diffusion within the solid occurs via a vacancy-hopping mechanism), which in turn improve supercapacitor operation if this step is the rate-limiting step of the reaction. Grain boundaries and dislocations within the solid metal oxide particles can act as source for vacancies, and as such their presence can be beneficial. On the other hand, the formation of dislocations can lead to mechanical fracture of the particles and reduce device lifetime. Particular care must be given to selecting materials that will not impede ion transport rates.

3.7.1 Cyclic Voltammetry

Cyclic voltammetry (CV) is an electrochemical technique in which positive and negative potential sweeps are applied to a sample electrode while the current response is monitored. Thanks to this technique, the capacitance of the sample electrode can be determined from the scan rate and current. This is because capacitance is defined as the change in charge over a specific change in potential. Simplifying this equation to obtain the specific capacitance of individual electrodes can be accomplished via the following equation, where, C is capacitance of the supercapacitor device, $C_{specific}$ is the capacitance of a specific electrode, Q is charge of the electrode, V is the potential, dV/dt is the scan rate, i is the current, and m_1 and m_2 are the masses of both electrodes.

$$C = dQ/dV = (dQ/dt)(dt/dV) = i/(dV/dt) = C_{tot}/2$$

$$\Rightarrow \quad C_{specific} = 2i/(dV/dt)*(1/m_1+1/m_2)$$

Moreover, this technique allows for facile analysis of redox reactions. For example, redox reactions can be identified by the presence of peaks in the I vs. E *voltammogram* at relevant potentials. The reversibility of these redox peaks (which will influence cycle life of supercapacitor) can be determined by symmetry of voltammogram.

3.7.2 Chronopotentiommetry

Another electrochemical technique useful for analyzing supercapacitors is chronopotentiommetry (or charge-discharge experiments). Here, the supercapacitor device is subjected to alternating constant positive (charging) and negative current (discharging) steps while the voltage response is monitored. This technique allows for estimation of capacitance from the slope of discharge curve (similarly to the way it is calculated in cyclic voltammetry, gravimetric capacitance is calculated as C =

2i/m*[dV/dt], where *i* is the current, and *dV/dt* is the slope of the discharge curve in potential vs. time plot). Additionally, the voltage drop which can be identified at the beginning of the discharge curve allows one to calculate the resistance of the device (ESR = {IRdrop}/{total change in current applied }). This technique is also the most accurate electrochemical measurement tool as this is the way commercial supercapacitors are used (charged/discharge) in commercial applications, and as such is used extensively for monitoring life cycles of devices.

3.7.3 Electrochemical Impedance Spectroscopy

To evaluate the performance of a supercapacitor, electrochemical testing must be done on a sample of interest (devices usually consist of two electrodes separated by a separator and immersed in conductive electrolyte). Electrochemical impedance spectroscopy (EIS) can be used to determine capacitance of the sample device, to evaluate the frequency-stability range of the device and to evaluate different components of the device setup (such as resistances of the electrolyte, electrode, capacitance of the double layer, and effects due to such processes as adsorption and diffusion which are of critical importance for the supercapacitor system) by fitting the data to an equivalent circuit. Because of this, EIS is used today in much of the supercapacitor research to evaluate devices for real-life applications and to gain a fundamental understanding of the capacitive nature of the supercapacitor.

EIS is a very useful technique which measures an alternating current generated in response to an applied voltage addressed at an electrode interface. This technique can be used to help determine many critical components of the supercapacitor device: the internal resistance, the capacitance change with the frequency, and the DC potential

dependence of charge transfer resistance and pseudocapacitance. In addition, EIS may allow one to distinguish between the surface vs. bulk ion adsorption. EIS also allows for resolution of the individual components of the total resistance, including the electrode resistance, the electrolyte resistance in the porous structure of the electrode and the total resistance at frequencies where full access to the storage charge is available by fitting the impedance data obtained during experimentation to an equivalent circuit. EIS data can serve as a basis for comparing similar supercapacitors.

3.7.3.1 Supercapacitor Models and Use of EIS for Evaluation of Supercapacitor Performance

Many models have been devised through the years to understand the double-layer mechanism and its application in porous electrodes. One of the earliest models was introduced by de Levie in 1963[8]: the electrode surface is assumed to consist essentially of "circular cylinders of uniform diameter and of semi-infinite length" (the pores) which will be filled by the electrolyte solution and have a uniformly distributed resistance and capacitance per unit length (Fig 3.2). This model ignores the effect of faradaic reactions

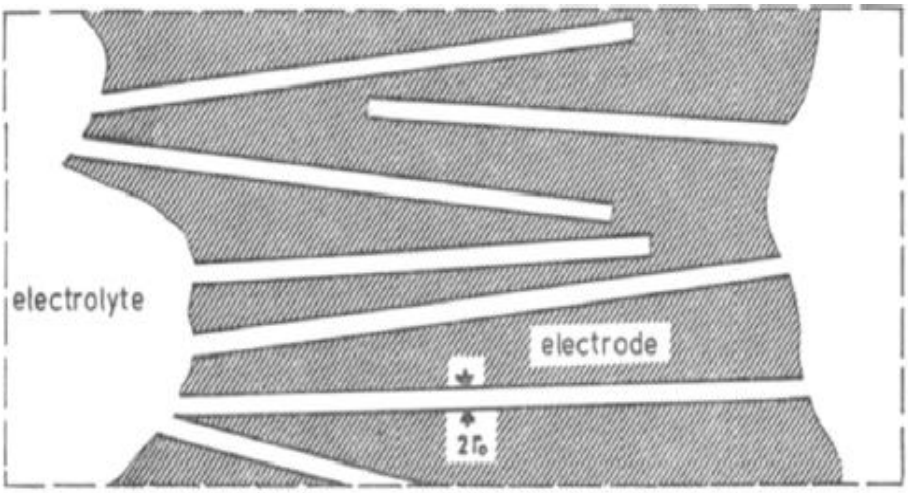

Fig. 3.2 De Levie's model of a porous electrode[6].

such as the ones responsible for pseudocapacitance and thus can only be used to model EDLC supercapacitor electrodes. It also ignores the electrode material resistance for simplicity. By looking at an infinitesimally small section of the pore (Fig. 3.3), one can determine the capacitance and resistance of the device as a function of penetration depth. With greater penetration by the electrolyte (determined mostly by frequency) comes both increased capacitance and resistance. This is commonly known as the transmission line model.

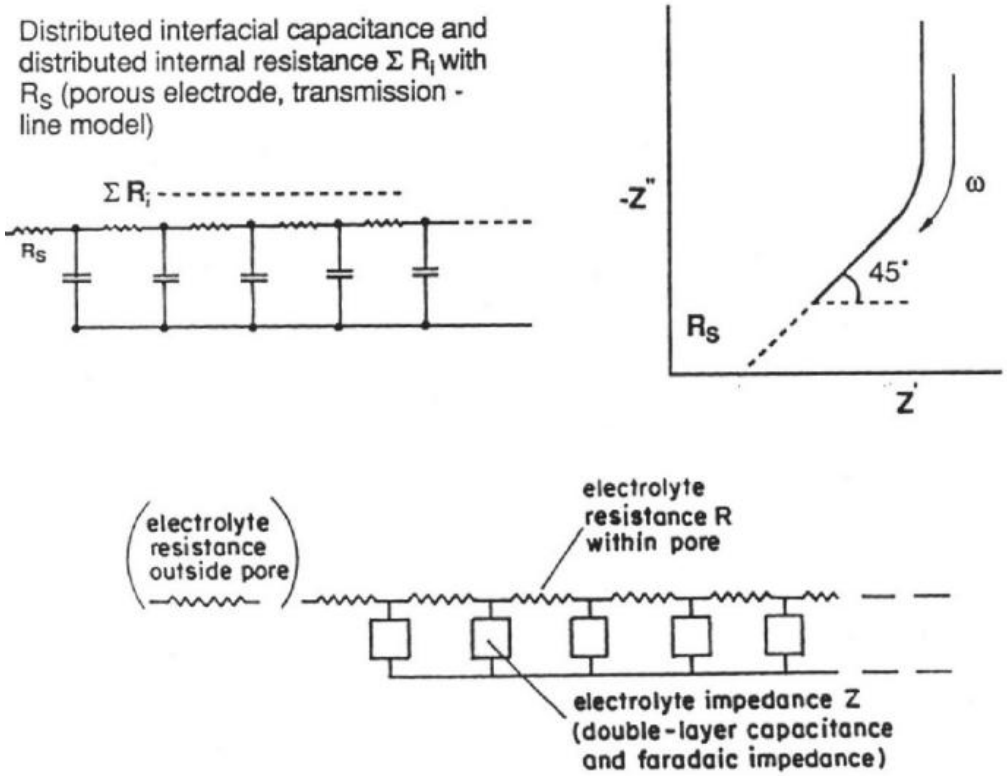

Fig.3.3 Equivalent circuit for infinitesimally small section of the pore according to Transmission Line Model. Taken from[8].

De Levie also calculated the characteristic time constant for this system as a function of the penetration depth into the pore (z),

$$\tau = \frac{1}{4} z^2 RC$$

The author determined that the phase angle between the potential imposed on a pore at its orifice (z=0) and the charging current is 45°, which is analogous to the "Warburg" diffusion impedance of a flat electrode. This model is good at simplifying the double-layer mechanism, but many of the assumptions upon which it is based are rarely true. For example, the pores in electrodes usually do not possess uniform diameters, and it is rare for them to be cylindrically shaped. However, the fundamental results de Levie explains with this model hold: penetration depth of the pore by the electrolyte solution will increase with time. As such, after short times (at very high frequencies), one will only measure the capacitance effects of the external surface area of the electrode (the electrolyte cannot access the pores). In contrast, at low frequencies, the influence of the pores becomes more important, especially since this inner surface area is usually much larger than the external area.

De Levie also investigated the radial diffusion within a small cross-section of a pore to determine the effect of frequency on capacitance and to look at the effects of pseudocapacitance by introducing electro-active species in the solution. He begins with Fick's second law in cylindrical coordinates, and claims that the simple equations (and thus his model) for plane diffusion can only be used if $Dt/r_0^2<10^{-3}$, where D is the diffusion coefficient, t is the time, and r_0 is radius of the pore[8]. The frequency dependence of diffusion is also important for supercapacitors: at very high frequencies the diffusion layer becomes so thin that it behaves as a plane-parallel film on the electrode surface (no matter the shape). On the other hand, at lower frequencies accessibility to the pores is facilitated and concentration of electro-active species in solution is less than for planar diffusion. The presence of the electro-active species

changes the equivalent circuit and adds a leakage and a leakage-part of the capacitance to the previously described transmission line model.

Because the surface area of the electrode accessible by the electrolyte determines the capacitance of the supercapacitor device, determining this value can be very helpful in evaluating a supercapacitor electrode. Armstrong *et. al[15]* suggested a way to calculate this accessible surface area solely by using this impedance data, and the method used may arguably be more accurate (at least in the evaluation of EDLC with very uniform pores) than the more generally used B.E.T. gas adsorption technique. The authors begin by looking at the impedance Z_0 of a single pore and the length of the pore which is penetrated by a signal of specific frequency (ω):

$$Z_0 = E_0/I_0=(Z_1R)^{1/2}\text{cotan}(\rho l_0)$$

Where Z_0 is the impedance of the pore, Z_1 is the capacitive impedance per unit pore, σ is the conductivity of the material, and ρ is the reciprocal penetration depth ($\rho=(R/Z_1)^{1/2}$). The total admittance of the electrode can be found by summing the admittance of all these pores (since they are all in parallel), such that:

$$\sum_{n=1}^{N0}\frac{1}{Z_0}\Rightarrow jwC_{dl}A$$

As such, by determining the double-layer capacitance of the measured electrode via cyclic voltammetry or charge-discharge experiments, and by confirming these results through the use of the impedance data, one can calculate the total surface area accessed by the electrolyte for double-layer capacitance. The authors also recognized different key variables which will alter the values for surface area obtained with this method. These

variables include the volume of sample that is immersed in the electrolyte (see Fig. 3.4), varying pore sizes, and frequency dependence of the impedance data. Complete penetration of the pores by the electrolyte requires very low frequencies. At higher frequencies, the specific area which is calculated with this method decreases since the signal is restricted to progressively larger pores.

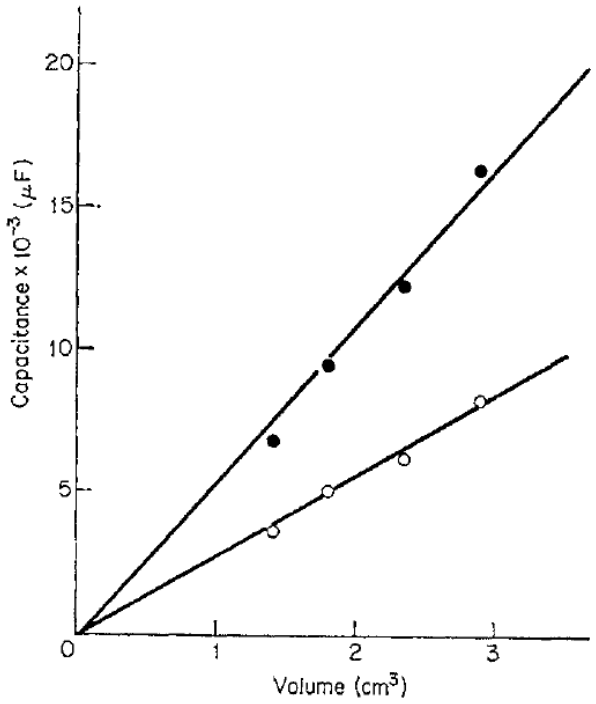

Fig 3.4. Correlation between calculated capacitance and volume of sample immersed in electrolyte. Taken from[15].

P.L. Taberna *et. al.* used EIS data to analyze carbon-carbon supercapacitors (the most common type of EDLC electrode)[12]. In order to validate their experiment, the authors also measured their electrodes via constant-current charge-discharge measurements and compared the results obtained with each other. To analyze the EIS data, the authors propose two equivalent circuits. The first is one of the simplest ways of

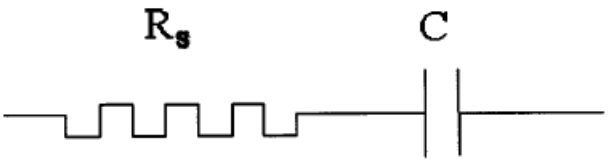

Fig. 3.5 Simple equivalent circuit used to model supercapacitor. Taken from[12].

describing supercapacitor frequency behavior and consists of a resistor and capacitor in series (see Fig. 3.5). From this model the impedance is calculated as:

$$Z = R_s + \frac{1}{jC\omega} = \frac{1 + jR_sC\omega}{jC\omega}$$

From this relation it is easy to see that as $\omega \rightarrow 0$, the admittance $Y \rightarrow jC\omega$. Another (slightly more complex) model describes the resistance and capacitance as frequency dependent. This model is more complex but also more correct: frequency will determine both the resistance and capacitance of the device as it will determine electrolyte access to the electrode (this frequency-dependence increases for systems with larger numbers of pores). In this case the impedance becomes:

$$Z = R(\omega) + \left[\frac{1}{jC(\omega)\omega}\right] = \frac{1}{jK\omega}$$

where K is the complex supercapacitance of the device (K=C'-jC"). Rearrangement of this relation yields equations for the individual real and imaginary parts of the capacitance:

$$C' = \left[\frac{C(\omega)}{1 + R^2(\omega)C^2(\omega)\omega^2}\right]$$

$$C'' = \left[\frac{C^2(\omega)R(\omega)\omega}{1 + R^2(\omega)C^2(\omega)\omega^2}\right]$$

Thus by converting the impedance data to the real and imaginary capacitance, one can determine the frequency-dependent behavior of the capacitance of the device, the

capacitive loss received during the charge/discharge steps, and (from the characteristic time constant determined by finding the peak of the C" vs frequency plot) the rate at which the supercapacitor is able to deliver its stored energy(see Fig. 3.6).

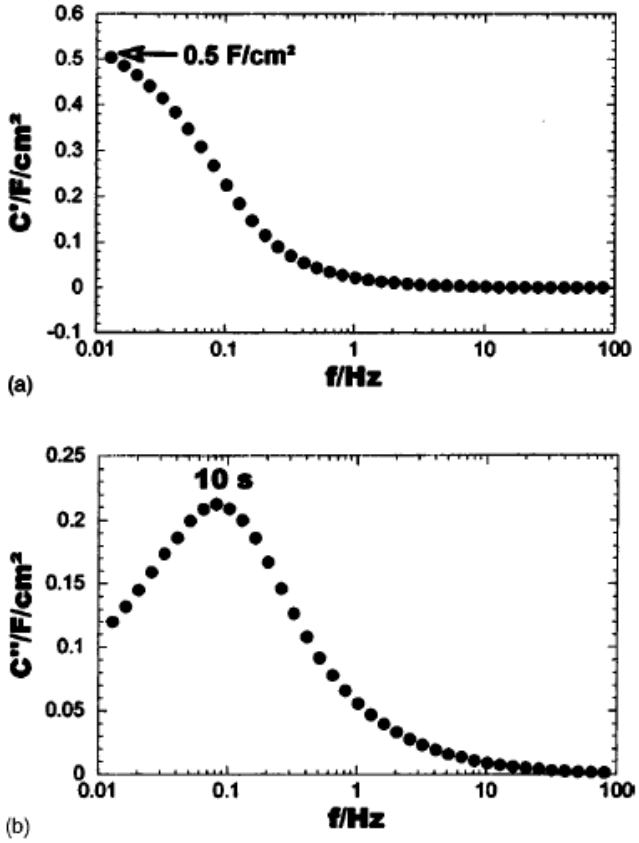

Fig. 3.6. (a)Real and (b) Imaginary Capacitance vs. frequency for typical carbon-carbon supercapacitor. Taken from[12].

In addition to this data, the Nyquist plot (Imaginary Z vs. Real Z – see Fig. 3.7) of a supercapacitor device can be broken down into three separate parts to yield information about the device. At the highest frequencies, the supercapacitor will behave like a resistor, and the equivalent series resistance of the device can be determined by finding the intercept of the Nyquist plot with the real Z axis. At the lowest frequencies it will behave like a capacitor, with the imaginary part of the impedance sharply increasing and the plot will tend to a vertical line characteristic of capacitors. In the middle frequency

range, the influence of electrode porosity and thickness on the ion migration rate from the electrolyte can be observed. Here the plot will behave according to the transmission line model described above, and will be quite linear in this frequency range.

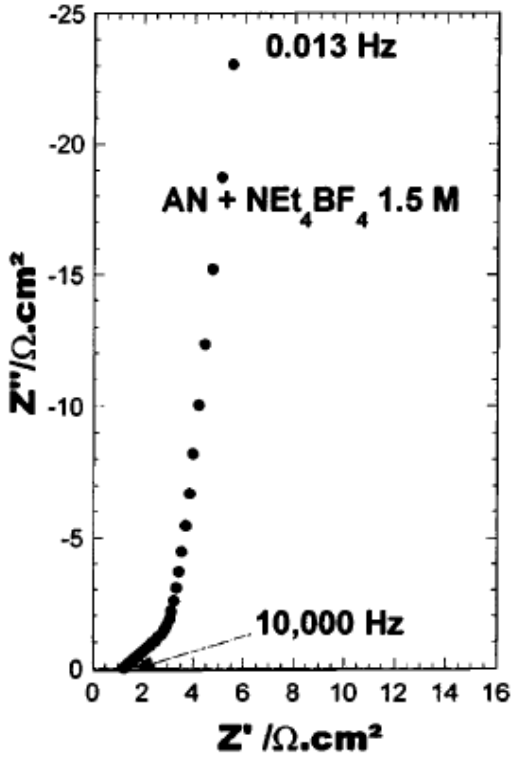

Fig. 3.7 Typical Nyquist plot for carbon supercapacitor. Taken from. [12].

3.7.3.2 EIS for Analysis of Complex Systems

In his textbook on electrochemical supercapacitors, B. E. Conway associates certain specific capacitances, resistances, and impedances with specific interfacial effects present in the supercapacitor devices[2]. All supercapacitors will possess some double-layer capacitance C_{dl}, a solution resistance R_s in series with the electrode interfacial impedance, a faradaic impedance associated with any potentially-dependent Faradaic charge-transfer resistance, a Faradaic resistance R_f (corresponding to the process of charging a pseudocapacitance through an electron transfer reaction) which tends to increase with a

greater kinetic reversibility of the reaction, and finally (when applicable) a pseudocapacitance C_p(this pseudocapacitance is a function of the potentially-dependent coverage θ of the electrodeposited species and of the amount of charge which can be accommodated on the electrode, i.e. $C_p=qd\theta/dV$)). If one wants to be more rigorous and approximate real world electrochemical systems, other elements that can be present include ohmic solution resistances, ohmic inter particle contact resistances, and (at high potentials of charge) a faradaic leakage resistance due to overcharge or due to Faradaic redox reactions caused by impurities[2]. These kinetic leakage processes that are faradaic in origin include faradaic charge transfer processes arising from interfacial redox reactions of impurities or surface functionalities at carbon surfaces, and electron charge-transfer reactions involved with the charge/discharge of pseudocapacitors. Another important value to consider is the time constant of the equivalent circuit. This time constant is of both fundamental and practical importance in determining and understanding the rate at which electrical response of a capacitor device can take place, and will thus also determine its power capabilities on discharge or recharge, and thus its applications for practical utilizations.

Conway then proceeds to list final equivalent circuit elements which can appear for supercapacitor systems[2]. For example, one can obtain another faradaic or chemical potential-dependent R_f' arising in parallel with the equivalent circuit if the potential is beyond the under potential deposition (this enables intermediates that give rise to C_p to become desorbed or combined to form an overall product of the reaction). One can also get the rise of an additional series capacitance C_2 to represent, say, some blocking oxide

film. All of the elements discussed above are included in the equivalent circuits and associated Nyquist plots in Fig. 3.8.

EIS has been used to evaluate the electric and dielectric properties of materials in aqueous systems for a long time. The research and development of high power, high energy supercapacitors requires such a technique in order to evaluate the performance of the device. EIS can resolve and determine specific values of individual components of the device being measured (e.g. electrode and electrolyte resistance, double-layer and faradaic capacitance, etc…) by fitting the data to an appropriate equivalent circuit. Moreover, the EIS data allows researchers to determine the frequency dependence of many of the supercapacitor's properties, including capacitance and resistance. The research and development of supercapacitors will continue for a long time because of their numerous desirable properties, and its success and rapid commercialization will depend on the use and development of the EIS technique.

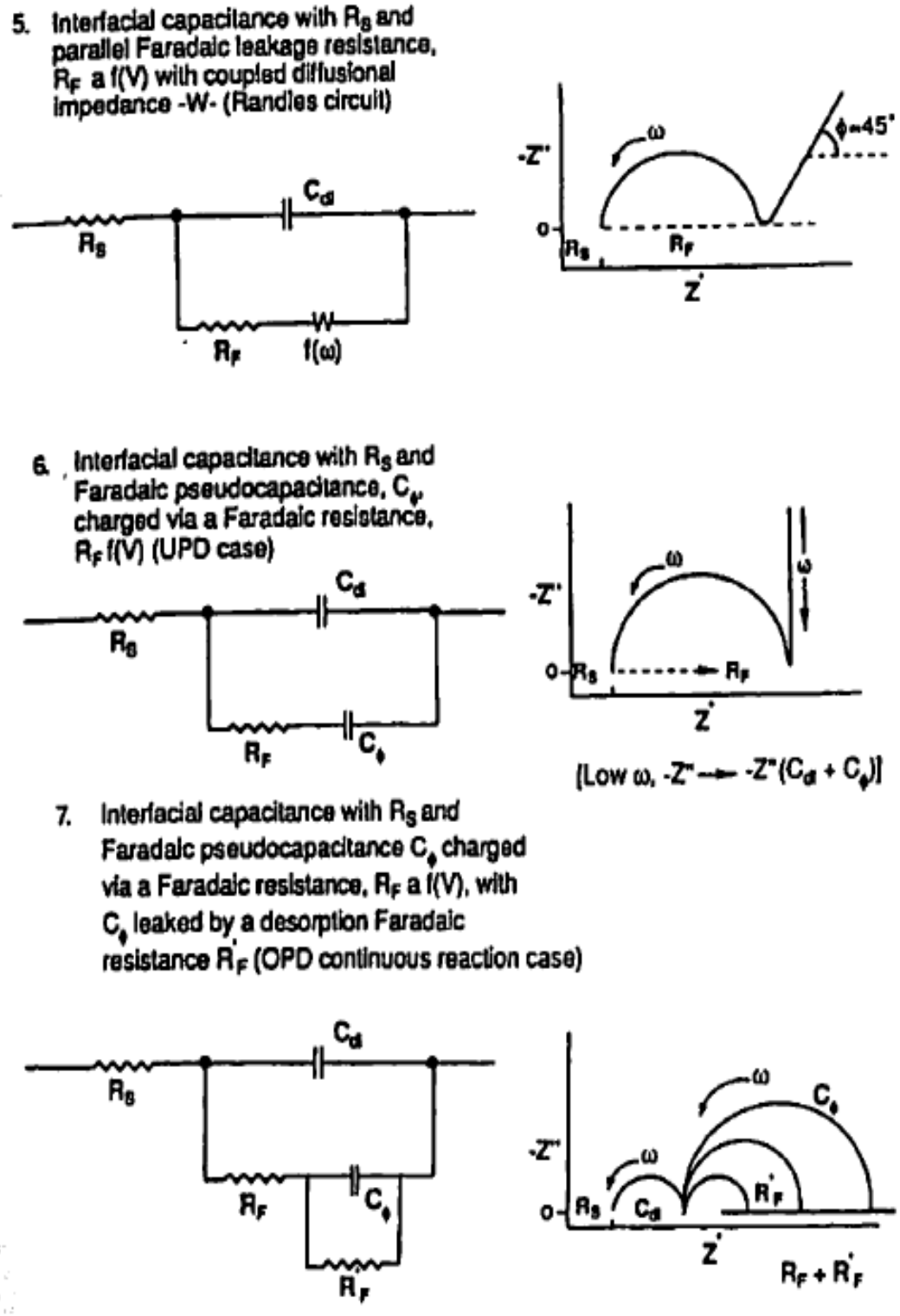

Fig. 3.8 Equivalent circuits and respective Nyquist plots of possible supercapacitor devices. Taken from[2].

CHAPTER 4

CURRENT STATE-OF-THE-ART AND PRIMARY OBJECTIVES OF THIS STUDY

4.1 Current State-of-the-Art in Quantitative and Qualitative Analysis of Ion Electro Adsorption in Supercapacitor Electrodes

EDLCs have been investigated extensively by the scientific community, and many factors are thoroughly analyzed in scientific studies that demonstrate their effect on device performance. These factors include electrode microstructure and porosity, the type of electrolyte used (its conductivity, its dielectric constant, its viscosity), and the electrolyte-electrode interactions (which has been investigated minimally) and which depends on such factors as the effect of the carbon/solvent interfacial energy, the effect of solvation energy, the effect of ion size, and the penetration of ions in the sub-nm pores (which was shown to have a very large effect on capacitance[3]).

In the literature, the following assumptions are usually made regarding the effect of solvent on supercapacitor device performance: (1) a solvent with higher dielectric constant shall result in higher capacitance, (2) lower viscosity of the solvent permits better ion movement through the porous networks of the electrodes, leading to a higher capacitance and access to all pores at faster rates, and (3) higher ionic and molar conductivity of the solvent leads to smaller resistance on ions during device operation, also resulting in higher capacitance and in a faster access to pores of all sizes. However, a thorough literature review yields the following information in regards to these assumptions: (1) use of solvents with higher dielectric constants can lead to lower

capacitance values (see table 1 below), (2) viscosity is a macroscopic effect, which cannot be used to account for performance in the smallest sub-nm pores, and (3) use of solvents with better electrolyte conductivity can lead to lower capacitance values (see table 4.1 below). For example, Fig**.** 4.1 and 4.2 demonstrate the effect of solvent on the performance of carbon based electrodes (altering the shape of the cyclic voltammogram and thus the capacitance of the device, and affecting the frequency and rate capability of the device[7]), specifically by looking at the influence of the following commonly-used solvents: acetonitrile, r-butyrolactone, propylene carbonate, and dimethyl ketone.

Table 4.1. Effect of solvent properties on capacitance. Values obtained from[69, 132].

Solvent	Viscosity (Pa s^{-1})	Dielectric constant	Bulk Electrolyte Resistivity (Ωcm)	Capacitance CV @ 10 $mV \cdot s^{-1}$ (F)	Capacitance CD @ 0.5 A (F)	Capacitance EIS @ 10mHz (F)
Acetonitrile	0.369	36.64	19.6	25.6	22.7	25.6
Γ-butyrolactone	1.72	39.0	57.1	26.0	22.8	26.0
Propylene Carbonate	2.513	66.14	76.9	22.8	21.6	22.8
Dimethyl ketone	0.306	21.01		20.4	19.5	23.9

A thorough study of these additional factors is required to fully understand the mechanisms responsible for energy storage in these devices, and such studies will require a new experimental methodology to investigate the influence of each of these individual factors on ion adsorption in pores of different sizes.

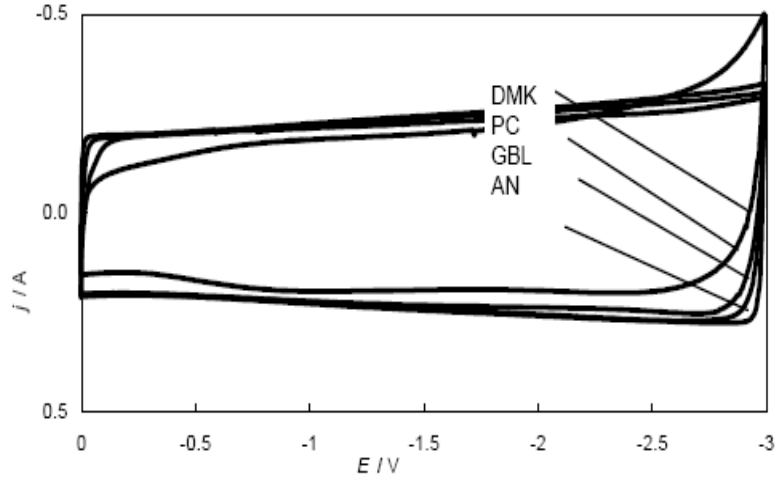

Fig. 4.1 Effect of solvent on cyclic voltammogram . Taken from[7].

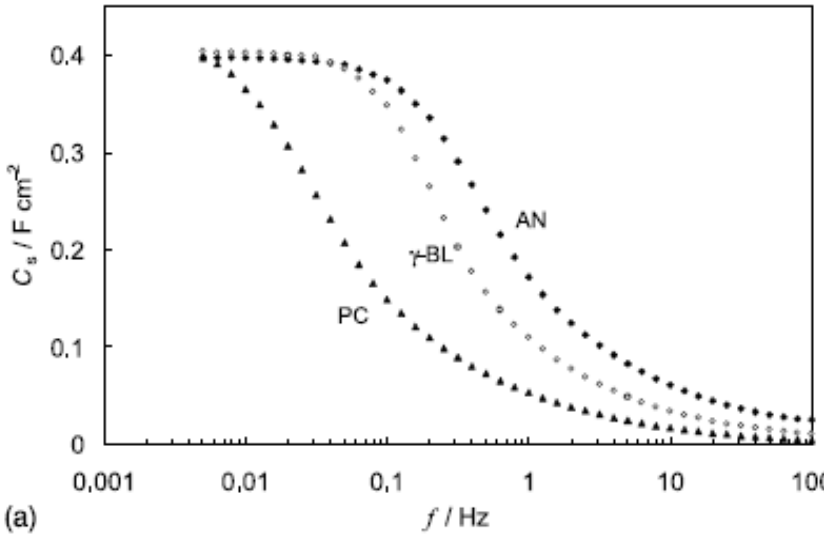

Fig. 4.2 Effect of solvent on frequency stability of supercapacitor device. Taken from[7].

4.2 Current State-of-the-Art in Pseudocapacitive/Carbon Nanocomposite Supercapacitor Electrodes

The major research which has been accomplished in the field of pseudocapacitive/carbon nanocomposite supercapacitor electrodes has been focused on the choice of pseudocapacitive material (focusing on polymers, metal-oxides, or the introduction of functional groups, all of which possess large capacitance due to the presence of many redox states) and on the choice of conductive EDLC-type substrate (usually carbon based) upon which the pseudocapacitive material is deposited. For example, the original pseudocapacitor, based on ruthenium, achieved high capacitance and conductivity while maintaining a long cycle life[133], but due to the expensive nature of the material, its use was prohibited in most applications. Other transition metal oxides, such as vanadium oxide[17] and manganese oxide[18] have been studied due to their high capacitance and inexpensive nature. However, the low conductivity of these materials is a large barrier which researchers have attempted to overcome by coupling these materials with high conductivity carbon materials. In general, these nanocomposites are created through the use of chemical vapor deposition, electrodeposition, or through a mixing of the carbon and metal-oxide powders which is turned into a slurry and coated onto different current collectors. The uniformity of the produced composites is generally poor, which likely limited their performance characteristics. Improving uniformity and tuning the size of metal oxide can be achieved effectively through the use of ALD, which has thus become an integral part of this PhD study.

I specifically chose to investigate vanadium oxide as a starting point of this research for several reasons. First, ALD of vanadium oxide has already been developed for use in

the development of chemical sensors. As such, I already had a starting point for the choice of precursors and deposition parameters which needed to be refined for the supercapacitor applications. Secondly, vanadium oxide possesses many redox states which are electrochemically active at different potentials. This makes vanadium oxide a suitable supercapacitor material as it possess many different electrochemical ranges in which it can be used, and can thus permit study in different electrolytes which operate in different voltage ranges. Additionally, vanadium oxide is a widely abundant inexpensive material that makes it a more readily available material for commercial applications. More specifically, the vanadium oxide which is most widely used for supercapacitor applications is V_2O_5 and it is this form of vanadium oxide which is the most important form from an industrial perspective, as it is the principal precursor to many alloys of vanadium and is a widely used industrial catalyst. Thus, many of the properties of vanadium oxide are known, making systematic studies of the effect of coating thickness and of the impact of the present VOx phases present easier to accomplish.

4.3 Technical Objectives

Throughout the course of this PhD study, two major research thrusts have been investigated with the aim of contributing to the development of supercapacitor technology. The overall objective has been to generate new knowledge and improve the fundamental understanding on how the microstructure, physical and chemical properties of the electrodes affect their electrochemical performance in different electrolytes. In order to accomplish this, the investigation was accomplished in two parts. First, fundamental absorption studies of ions in electrolyte during supercapacitor operation were performed. Secondly, carbon-metal oxide nanocomposite electrodes were designed

in order to create supercapacitor electrodes with large specific energy and specific power densities.

Specific objectives for each research thrust are summarized below:

1. ***Fundamental Electro-Adsorption Studies using in-situ Small Angle Neutron Scattering(SANS)***
    - Objective 1.1: develop the methodology to perform *in-operando* SANS measurements on EDLC electrodes for gaining quantitative insights on the ion adsorption and desorption in the pores of various sizes
    - Objective 1.2: reveal the changes in the ion concentration within the carbon pores as a function of the applied potential, carbon pore size, electrolyte properties and electrolyte solvent/carbon interaction.

In order to achieve these objectives, EDLCs have been investigated and constructed, and the electrode samples were characterized using SANS at rest and during supercapacitor operation (charging/discharging of individual electrodes) in order to distinguish between the surface vs. bulk ion adsorption in different environments (electrolyte type, polarization of specific electrodes, etc…). A more detailed description of the tasks is given below.

SANS Studies: An experimental setup for the characterization of electrodes using small angle neutron scattering was designed and constructed in order to allow for *in-situ* studies of supercapacitor devices during operation (charging/discharging) and at rest in specific electrolytes. Electrolytes were compared to their deuterated form to use contrast matching to determine location of ions at different stages of the charge-discharge cycle.

The SANS experiments were performed at Oak Ridge National Laboratory (TN, USA) using the beam line at the High Flux Isotope Reactor.

EDLC Electrochemical Performance: Carbon-based EDLC electrodes were designed and assembled. Surface area of the porous nanostructures is of critical importance for EDLC-based supercapacitor power characteristics (since total surface area of the sample is responsible for capacitance for EDLC type supercapacitors), so BET analysis was used to determine this value for the constructed electrodes and to aid in tailoring the desired architecture.

Material Characterization: All materials investigated during this project were characterized effectively in order to take into account all factors responsible for absorption. This characterization includes Scanning Electron Microscopy (SEM) and Electron Dispersive Spectroscopy (EDS) and was used to identify the morphology of the carbon and of the deposited oxides. X-Ray Diffraction (XRD), X-ray photoelectron spectroscopy (XPS), Raman spectroscopy, and Transmission Electron Microscopy (TEM) experiments were also used to identify and tailor the carbon and oxide microstructures and to complement the SANS data for analysis.

Cell Assembly: Electrochemical supercapacitor cells were constructed for research applications in the testing frame described above. Low cost aqueous electrolytes (such as H_2SO_4) were investigated, along with organic electrolytes in order to generate a good understanding of supercapacitor operation in its many operating environments. Factors, such as separation distance between the electrodes, electrode thickness, electrolyte concentration, and ambient temperature may affect the data and were thus monitored.

2. Design, fabrication, and characterization of metal oxide-carbon nanocomposite electrodes

- Objective 2.1: Identify process parameters to achieve uniform deposition of ultra-thin coatings (5-100 nm) of vanadium oxide on carbon nanotube substrates.
- Objective 2.2: Reveal how the size, morphology and microstructure of the metal oxides affect their electrochemical performance (specific capacitance, frequency response, capacity retention at different current densities, temperature range of operation, degradation mechanisms and overall long-term stability) in different electrolytes

In order to achieve these objectives: (a) porous carbon matrix electrodes with different pore size, microstructure and surface chemistry were first produced; (b) an ALD system for deposition of metal oxide was designed and assembled, and (c) the growth parameters for uniform and pure coating of metal oxides onto nanoporous carbon substrate were optimized; (d) the synthesized materials were characterized; (e) supercapacitor cells were assembled, and (f) electrochemical characterization was performed to analyze the possible changes in microstructure after long-term cycling. A more detailed description of the tasks is given below.

Carbon Synthesis:. In order to construct the carbon matrix electrode, CNT substrates were produced onto which the desired transition metal oxide (vanadium oxide) was deposited. Surface area of the porous nanostructures will also be of critical importance for supercapacitor power characteristics, so BET analysis was used to determine this value for the constructed electrodes and to aid in tailoring the desired

architecture. For the CNT electrodes, a binder-free CNT paper was developed, as it eliminates the added resistance brought on by binders.

Metal Oxide Deposition: Deposition of the desired metal oxide was accomplished via ALD. To the best of my knowledge, deposition of metal oxides via ALD for supercapacitor applications had never been attempted prior to my experiments. For this deposition mechanism, optimal growth parameters (including deposition time, pressure, temperature, and gas flow rates) were determined in order to control the thickness and morphology of the deposited transition metal oxides. Post-annealing experiments were done in order to obtain the most appropriate oxide microstructure.

Material Characterization: SEM and EDS were used to identify the morphology of the carbon and of the deposited oxides. XRD, Raman spectroscopy, and TEM experiments were used to identify and tailor the carbon and oxide microstructures.

Cell Assembly: Two types of electrochemical supercapacitor cells were constructed for research applications: beaker cells and coin cells. Coin cells are smaller and air tight and were used for testing in organic electrolytes. They require using less material overall and lead to high reproducibility. Beaker cells are simpler to make and disassemble. They were used for low cost aqueous electrolytes (such as H_2SO_4) and were composed of two electrodes submerged in a beaker filled with an electrolyte solution. Factors, such as separation distance between the electrodes, electrode thickness, electrolyte concentration, and ambient temperature may affect the data and thus were monitored. The advantage of beaker electrodes is that they are simpler to make and allow for an immediate check of the electrode's condition after electrochemical measurements.

Electrochemical Characterization: Once an appropriate electrode had been constructed, several electrolytes were investigated. Surface chemistry, redox chemistry, viscosity, permissible voltage and temperature ranges vary from one electrolyte to another and selection of the electrolyte will reflect this. Electrochemical measurements such as CV and C-D permitted study of the redox reactions governing the supercapacitor behavior as well as study of the supercapacitors' power characteristics, performance, and lifetime. EIS was used to determine internal resistance, estimate the capacitance change with the frequency, study the DC potential dependence of charge transfer resistance and pseudocapacitance, and distinguish between the surface vs. bulk ion adsorption. EIS also allowed for resolution of the individual components of the total resistance, including the electrode resistance, the electrolyte resistance in the porous structure of the electrode and the total resistance at frequencies where full access to the storage charge is available.

Chapter 5

FUNDAMENTAL ELECTRO-ADSORPTION STUDIES USING SMALL ANGLE NEUTRON SCATTERING (SANS)

5.1 Overview

Transport and adsorption of electrolyte ions in porous carbons under applied potential control the performance of double layer capacitors for rapidly emerging high power energy storage applications[134, 135], capacitive deionization devices for water purification and desalination[136] [137], rotational motors for artificial muscles, microfluidic devices and nanorobotics[138].

The importance of the solvent for ion transport has been primordial in numerous fields that make use of nanoporous materials with high internal volumes and surface areas. The internal architecture of these materials determines the concentration of ions in the pores, as well as how rapidly these ions can penetrate and extract themselves from pores of different sizes. The transport mechanism responsible for changing this concentration of ions and its optimization is essential in maximizing the capacitance of these devices, and in maintaining these high values of capacitance at the more rapid rates that are needed in today's powerful and varied electronic devices and systems. For these reasons, the design of electrodes used in many wide ranging industries have been influenced by the transport of ions in the electrode's nanoporous channels. Many of the factors that affect the transport and speed of ions in these nanoporous channels, such as wettability and viscosity, and other factors that influence capacitance of electrochemical capacitive devices, such as dielectric constant and specific conductivity, are directly influenced by the type of solvent in which ions flow. Although these factors have been

acknowledged as having some effect on the performance of electrochemical capacitors, their specific importance has not been determined. Moreover, the importance of other factors such as solvation energy and solvent-pore wall interactions have been overlooked due to the complexity of designing physical experiments that can quantify this importance.

Electrochemical analysis techniques combined with structural and chemical characterization of porous carbons offer limited prognostic abilities. The inter-related effects of the size of pores, the properties of ions and electrolyte solvent molecules and the resulting ion-solvent, ion-pore and pore-solvent interactions on electro-adsorption are poorly understood. Several studies revealed significant impact of structural defects in carbons on their electrosorption properties[14] and the enhanced ion adsorption in sub nanometer pores[3, 87, 88] in selected materials systems. The observed phenomena, however, were not always confirmed in other carbons or electrolytes, and the universality of such observations remains a topic of debates in the scientific community. The challenge comes from the difficulty of independently tuning various material properties needed for systematic experimental studies and from the very high complexity of realistic materials systems for *ab-initio* simulations. For example, prior studies observed a noticeable impact of organic electrolyte solvents on the carbon capacitance [73, 139, 140]. The majority of such studies focused on acetonitrile (AN) and propylene carbonate (PC) used in commercial electrochemical capacitors. While AN offers higher ionic conductivity and is more polar, it exhibits nearly 45 % lower dielectric constant than PC. Interestingly, in different porous carbons the AN-based electrolytes inconsistently showed either higher[7, 73] or lower capacitance [140] than PC-based ones with an

identical salt. To gain better insights into adsorption phenomena, computer simulations were performed in model systems[89, 134, 141-145], with a stronger emphasis on ionic liquid (IL) electrolytes[134, 142-144], which don't contain solvent molecules and thus simplify the calculations. A recent study emphasized the importance of taking into consideration a more realistic structure of porous carbons[146]. While the obtained modeling results are insightful, development and adoption of complementary experimental techniques is critically needed to directly identify both the ion transport[147] and adsorption sites in a broad range of microporous solids as a function of the applied potential, verifying the molecular mechanisms previously proposed and providing guidance to future modeling efforts. In spite of the significant efforts, rather limited fundamental understanding of the solvent effects has been demonstrated so far. The proposed small angle neutron scattering (SANS) experiments will demystify the impact of the solvent on the ion adsorption in pores of different sizes.

Recent studies have demonstrated that small angle neutron scattering (SANS) can provide unique, pore-size specific information on the adsorption of confined fluids and may be used to evaluate the density of the adsorbed molecules in nanometer and sub-nanometer pores [148]. In this thesis a unique method that utilizes the unique capability of *in-situ* SANS to directly visualize changes in the electrolyte ion concentration in pores of different size as a function of the potential applied to any nanoporous material is described and explored. SANS patterns are analyzed based on three-phase model developed and applied recently for quantifying the adsorption of supercritical fluids and gases in carbon nanopores[149]. In contrast to prior studies[3, 87, 88], the distribution of ion density within the pores of different sizes can be measured within the same material.

Since materials with different pore size distributions inevitably exhibit different microstructures and different concentrations of defects and surface functional groups, the proposed method offers a unique and very important ability to study the effects of the pore size and surface chemistry independently.

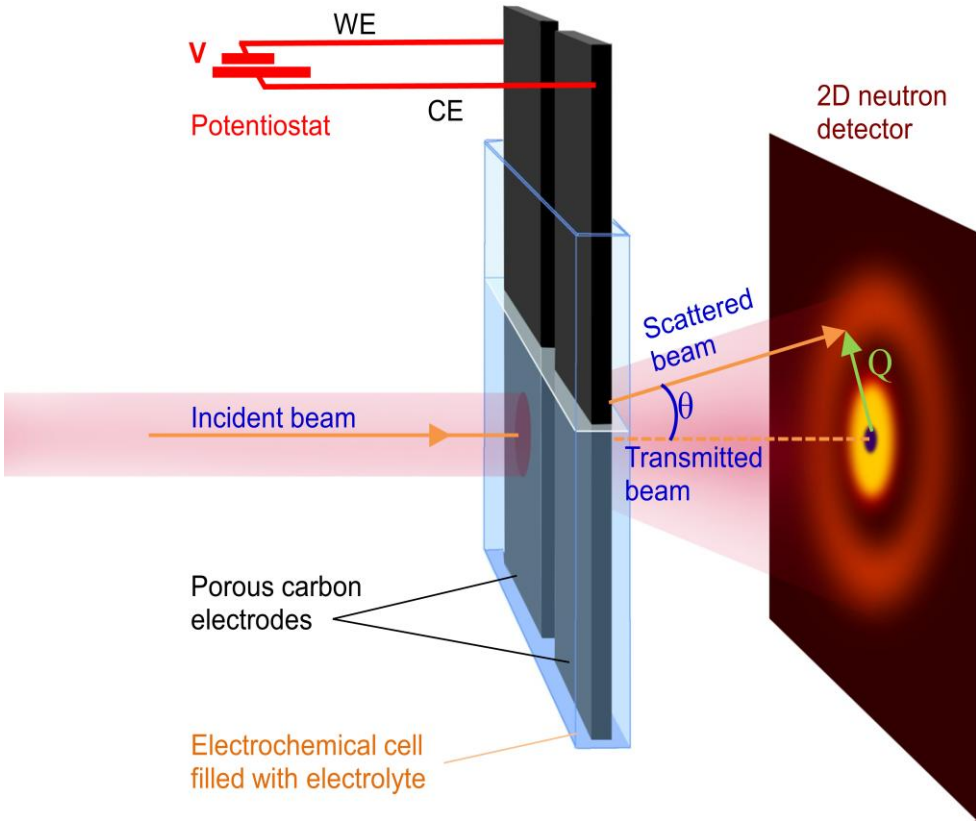

Figure. 5.1 Schematic of the experimental setup for *in-situ* studies of ion adsorption on the surface of microporous carbon electrodes.

The majority of electrolytes contain hydrogen atoms in either their solvent molecules or ions or both. By monitoring changes in the distribution of hydrogen in the nano-confined electrolyte upon the application of external potential to porous carbon electrodes one can elucidate where the ion adsorption takes place. A simplified schematic of the experimental setup is shown in Fig. 5.1. Microporous activated carbon fabric (ACF) was used as binder-free conductive electrodes for these studies (Fig. 5.2).

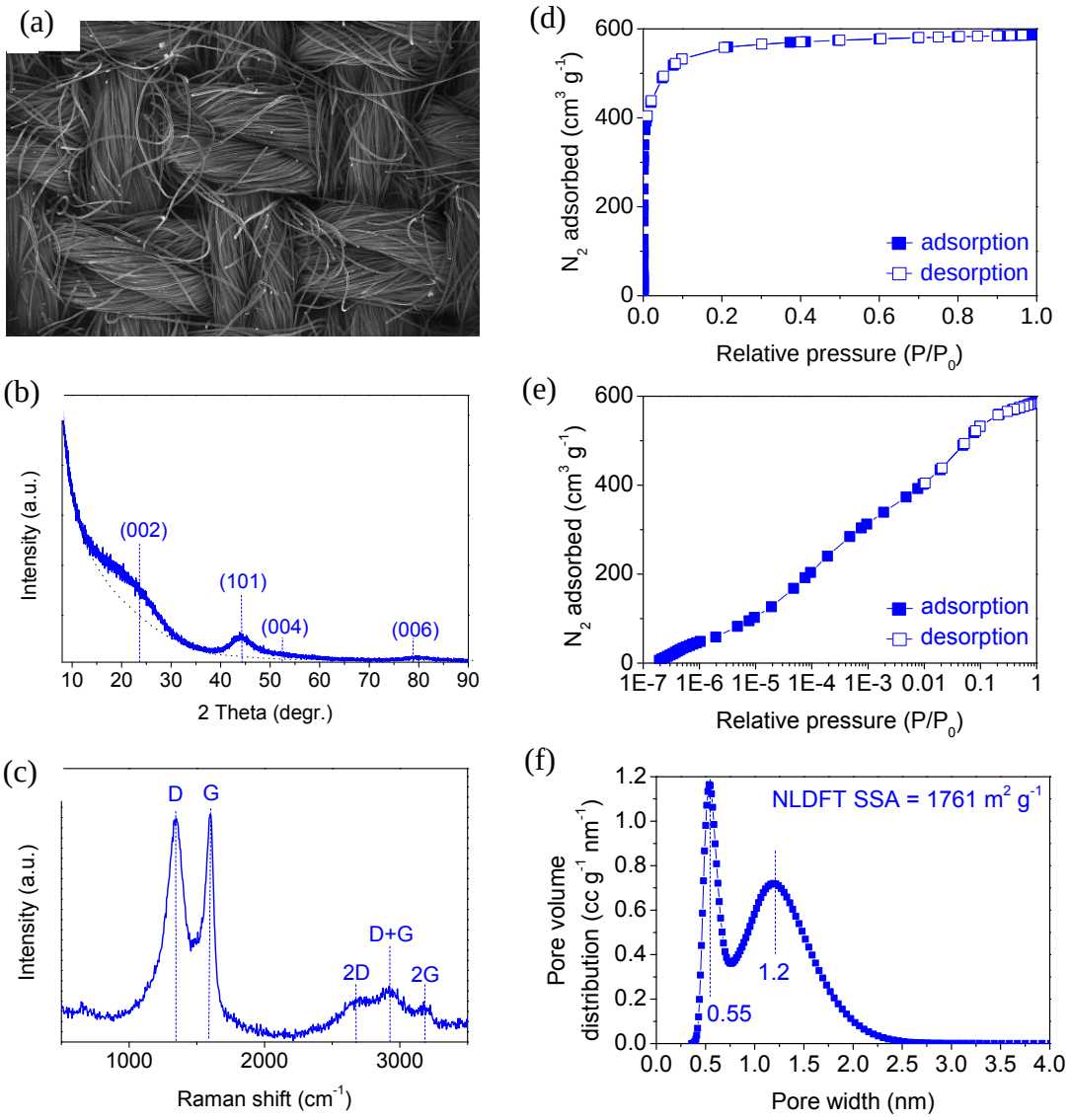

Figure. 5.2 Characterization of the activated carbon fabric structure: (a) SEM micrographs, (b) XRD pattern, (c) Raman spectrum, (d, e) N_2 sorption isotherms collected at 77K, (f) pore size distribution.

For these in-situ SANS experiments aqueous electrolytes based on H_2SO_4 solutions in H_2O and D_2O were initially used. This choice of electrolyte was motivated by a significant difference in the neutron scattering length density (SLD) of H_2O and C, and a small difference in the neutron SLD between D_2O and C. Additionally, both solvents exhibit similarly-sized solvation shells and have similar dielectric constants (78.5 for D_2O

vs. 78.4 for H_2O). Subsequent studies focused on organic electrolytes commonly used in supercapacitor testing in the scientific community, as well as on the effect of concentration on ion electroadsorption in these electrolytes.

5.2 Experimental Details

Commercially available ACF (ACC-507-20) were purchased from Kynol (USA) and used to analyze electro-sorption of ions in aqueous electrolytes. For electrochemical testing, the activated carbon fabric of ~ 300 µm in average thickness was cut into strips of approximately 1 cm. Four strips were used for WE and CE in *in-situ* experiments. These tests were performed in a symmetric two-electrode configuration using hermetically-sealed beaker-type cells (Fig. 5.1). For *ex-situ* electrochemical experiments the electrodes were assembled into a sandwich structure separated with 25µm thick GorTex separator (GorTex, USA). For the *ex-situ* we performed tests to measure response of the WE individually while insuring a minimal cross-contamination of organic solvents. Throughout the course of these experiments, aqueous and organic electrolytes were investigated. In the case of the aqueous electrolytes: H_2SO_4 (Sigma Aldrich, USA) which was diluted to 1M concentration in both DI H2O and D2O (Sigma Aldrich, USA). In the case of the organic electrolytes: 1M tetraethyl ammonium tetrafluoroborate (Sigma Aldrich, USA) which was diluted to 1M concentration in both deuterated acetonitrile (99.96%, Cambridge Isotope Laboratories, USA) and in deuterated dimethyl sulfoxide (99.9%, Cambridge Isotope Laboratories, USA) were investigated.

Electrochemical characterization of ACF was performed using electrochemical impedance spectroscopy (EIS), and cyclic voltammetry (CV). EIS measurements were performed on a Gamry Potentiostat from 1MHz to 0.1Hz at 10mV scanning amplitude..

Cyclic voltammetry was performed using the same Gamry Potentiostat with the potential being swept from -2.0V to 2.0V at scan rates of 1-1000 $mV \cdot s^{-1}$. The integrated-average gravimetric capacitance of each electrode was calculated from the CV data (in symmetric, two-electrode configuration) according to:

$$C_{electrode} = 2C_{cell} = \left(\frac{2}{(dU/dt) \cdot m} \right) \cdot \left\{ \int_{-0.6V}^{0.6V} I(U)dU - \int_{0.6V}^{-0.6V} I(U)dU \right\} \cdot \frac{1}{2} \cdot \frac{1}{1.2V},$$

where *dU/dt* is the scan rate, m is the mass of each electrode in a symmetric cell, and *I(U)* is the total current. For the three electrode measurements, the capacitance of the working electrode was calculated from the CV data (in a three-electrode configuration) according to:

$$C_{electrode} = \left(\frac{I(U)}{(dV/dt) \cdot m} \right)$$

where *dV/dt* is the instantaneous scan rate at the working electrode measured with the reference electrode, m is the mass of the working electrode, and *I(U)* is the total current.

Scanning electron microscopy (SEM) measurements were performed using a LEO 1550 microscope (Carl Zeiss, Germany). TEM experiments were performed using a Tecnai G^2 F30 (FEI, Netherlands) microscope operating with an accelerating voltage of 300kV. XPS experiments were performed on a Kratos Axis Ultra (Kratos Analytical, USA).

SANS experiments were conducted at ORNL General Purpose SANS instrument with a neutron wavelength of λ = 4.75 Å and a wavelength spread, $\Delta\lambda/\lambda$ of 0.13. Two sample-to-detector distances, 10 m and 0.3 m, were used to cover a Q range between Q_{min} of 0.008 $Å^{-1}$, and Q_{max} of 0.9 $Å^{-1}$, where $Q = 4\pi \cdot \sin(\theta)/\lambda$ is the scattering vector and 2θ is the scattering angle. The sample-to-detector distance was chosen to cover a broad range

of scattering vectors Q up to 0.9 $Å^{-1}$. Average acquisition time for each scattering curve was approximately 60 min. Scattering patterns were corrected for instrumental background, the transmission and detector efficiency. The raw 2D data were azimuthally averaged to produce the 1D profile, $I(Q)$ versus Q. The data were placed on an absolute scale (cm^{-1}) using pre-calibrated standards. The measurements were conducted at room temperature. SANS patterns were recorded from dry ACF electrodes, ACF with ultra-pure H_2O, D_2O, and H_2SO_4 solutions (0.5M and 1M) in H_2O and D_2O, ACF immersed on 1M TEATFB salt in d-DMSO electrolyte, and ACF immersed in different concentrations (0.5M, 1M, and 2M) of TEATFB salt in d-acetonitrile solvent, at different applied voltages to monitor the changes in the distribution of hydrogen ion concentrations as a function of pore sizes. For the experiments on comparative infiltration of ACF with ultra-pure H_2O and D_2O, the ACF samples were dried under vacuum at 60°C for 2 days prior to immersion of samples in these solvents for 24 hours. After pre-treatment, solvent-infiltrated ACF samples were sealed in the quartz sample holders with internal thickness 2 mm. The following equation was used for the deconvolution of the scattering intensity patterns into three terms:

$$I(Q) = \frac{A}{Q^n} + \frac{C}{1 + (|Q - Q_0|\xi)^m} + B$$

where the first term describes the scattering from the fiber surface (A is a constant and n is the fractal dimension), the second term describes the scattering from meso- and micropores (C is a constant, Q_0 is the position of the maximum, which is related to the characteristic spacing ξ between pores, and m is the Lorentzian exponent) and the constant B represents the incoherent background.

The normalized SANS intensities were obtained by dividing the scattering intensities measured at a certain potential (I(Q,V) by the scattering intensities measured at zero

(b) ial I(Q,V=0) as: (e)

$$I_{normalized}(Q,V) = I(Q,V) / I(Q,V = 0)$$

The relative changes in the normalized intensity as a function of scattering vector were obtained by subtracting the normalized scattering intensity measured at Q = 0.4 Å from the normalized intensity:

(c) $\Delta I_{normalized}(Q,V) = I(Q,V) / I($ (f) $= 0) - I_{normalized}(0.4\text{Å}^{-1}, V)$

This procedure was selected to show Q-domain (Q>0.4 $Å^{-1}$) corresponding to sub-nanometer pores in which the variation of the normalized intensity is most pronounced.

The statistical uncertainty of normalized intensity was calculated as follows:

$$\frac{\delta I_{normalized}(Q,V)}{I_{normalized}(Q,V)} = \sqrt{\left(\frac{\delta I(Q,V)}{I(Q,V)}\right)^2 + \left(\frac{\delta I(Q,V=0)}{I(Q,V=0)}\right)^2},$$

where $_{\delta I(Q,V)}$ is the measured uncertainty.

5.3 Study of Ion Electroadsorption in Aqueous Electrolytes

5.3.1 Electrochemical Measurements

Initial studies focused on comparing H_2SO_4 and D_2SO_4 in H_2O and D_2O solvents. Cyclic voltammetry (CV) studies performed in a symmetric two-electrode configuration in the voltage window between -0.6 and 0.6 V revealed nearly ideal capacitive behavior with a rectangular shape of the curves (Fig. 5.3a, b, Fig. 5.5 and 5.6). Analysis of CV

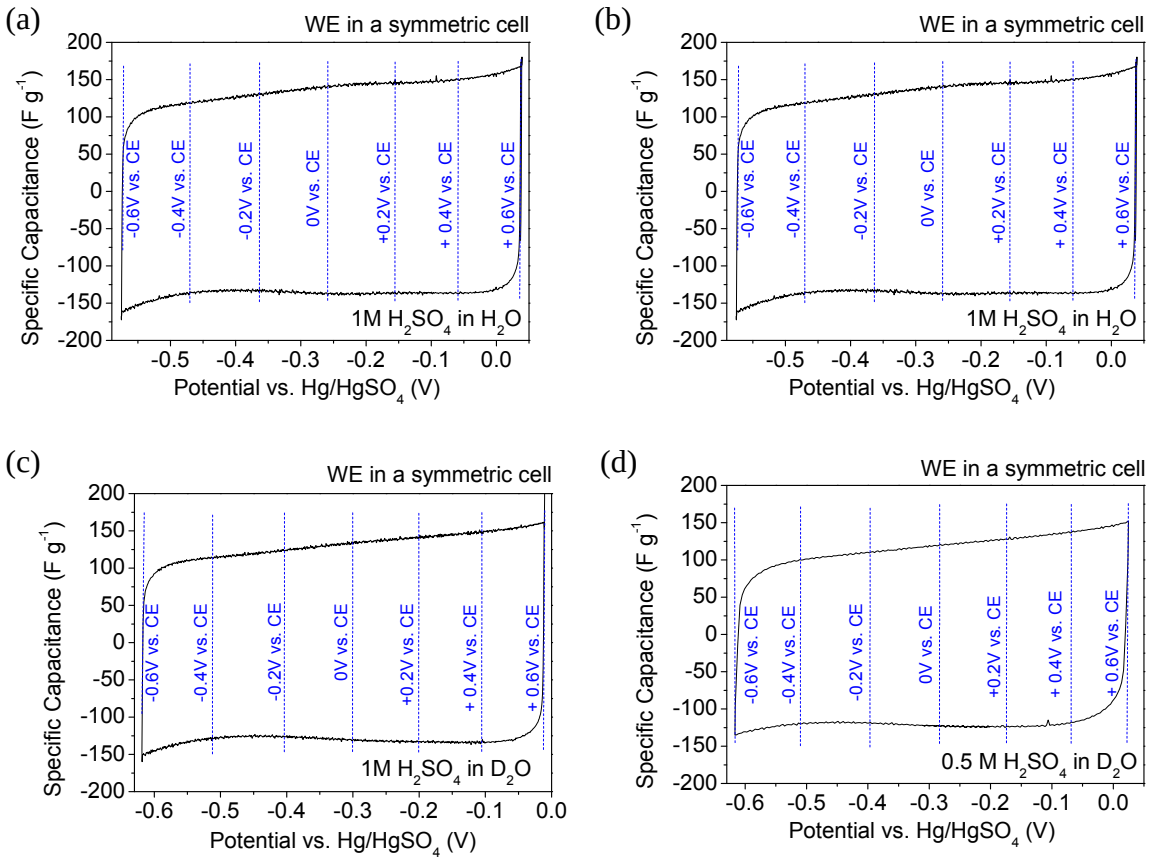

Figure. 5.3 Cyclic voltammetry of activated carbon fabric in symmetric cells with a reference electrode performed at the sweep rate of 5 mV s^{-1} in (a) 1M H_2SO_4 solution in H_2O, (b) 0.5 M H_2SO_4 solution in H_2O, (c) 1M H_2SO_4 solution in D_2O and (d) 0.5 M H_2SO_4 solution in D_2O.

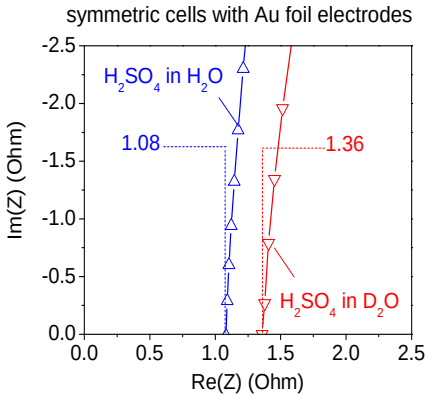

Figure. 5.4 Electrochemical imped ance spectroscopy performed on symmetric rectangular cells composed of 1 cm^2 Au foil electrodes immersed in 1M H_2SO_4 solution in H_2O and D_2O and separated by 3 mm.

curves showed noticeably higher ACF capacitance and better capacitance retention in a H_2O - based electrolyte (Fig. 5.5c and Fig. 5.5c). The experimentally determined higher ionic conductivity of the H_2O-based electrolyte (Fig. 5.4) may play a role in a better ACF capacitance retention (Fig. 5.5c). Higher strength of deuterium bonds over hydrogen bonds[150] results in a higher viscosity of D_2O than H_2O[151] and contributes to reduced overall mobility of electrolyte ions.

In the absence of Faraday processes and for a similar ion surface density the carbon capacitance per unit surface area shall increase with decreasing average distance between the pore walls and the center of charge of electrolyte ions near the surface. The size of the ion solvation shells in H_2O and D_2O is similar. At the same time, since D_2O is a weaker solvent, one may expect ions in the D_2O to approach the oppositely charged pore walls closer because of the lower solvation energy and smaller free energy barrier needed for the distortion of the solvation shell in this solvent. Because a small decrease in the carbon-ion charge separation leads to a large increase in the capacitance [141], one should expect ACF to exhibit higher capacitance in a D_2O - based electrolyte (in contrast to our observations, Fig. 5.6), if the average concentration of electro-adsorbed ions on the carbon surface were identical.

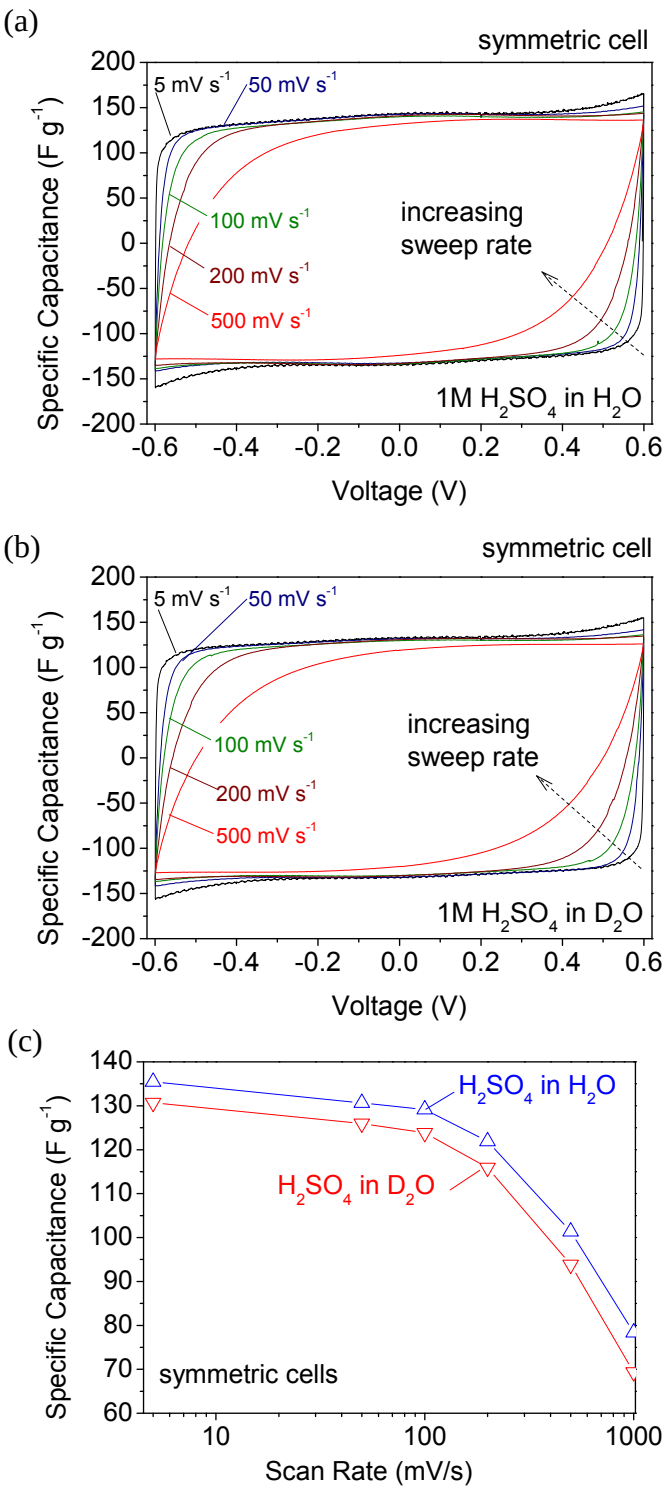

Figure. 5.5 Electrochemical characterization of the activated carbon fabric in symmetric cells: cyclic voltammetry performed at different sweep rates in 1M H_2SO_4 solution in (a) H_2O and (b) D_2O, (c) capacity retention as a function of sweep rate.

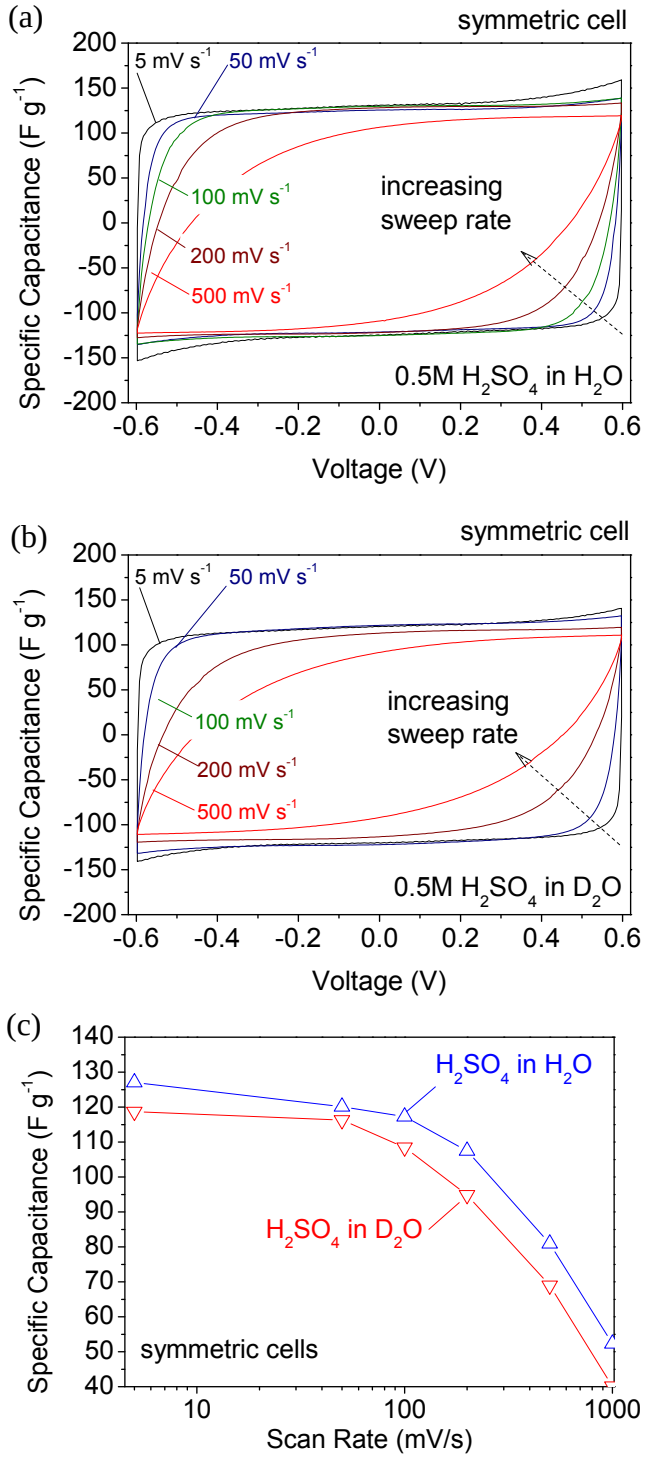

Figure. 5.6 Electrochemical characterization of ACF in symmetric cells: cyclic voltammetry performed at different sweep rates in 0.5 M H_2SO_4 solution in (a) H_2O and (b) D_2O, (c) capacity retention as a function of sweep rate.

5.3.2 Discussion of SANS Results

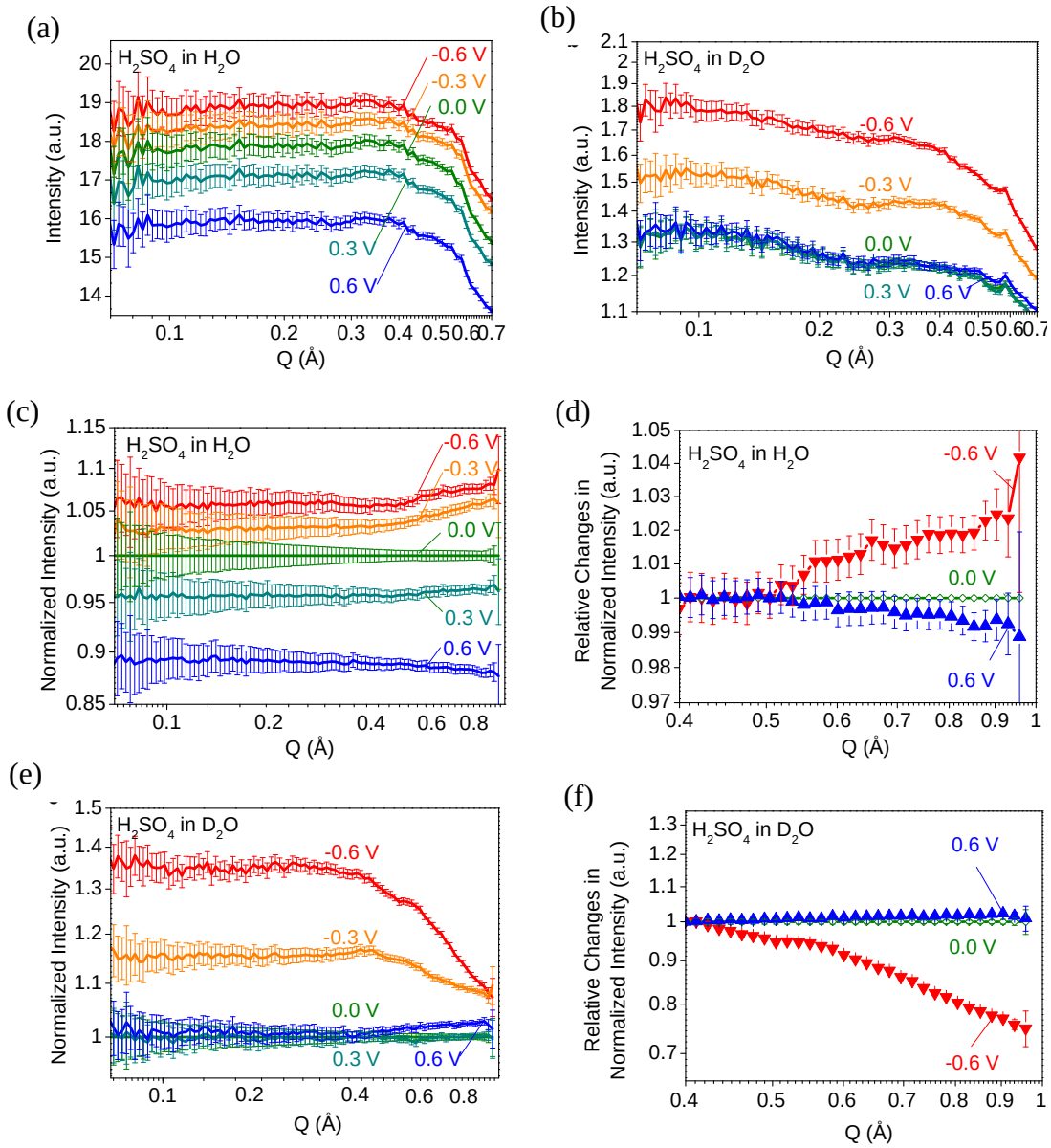

Figure. 5.7. In-situ neutron scattering experiments on ACF electrodes immersed into H_2O (a, c, d) and D_2O –based (b, e, f) electrolytes under an application of a potential between the WE and CE: (a, b) SANS patterns, (c, e) SANS profiles normalized by the 0V one, (d, f) relative changes in the intensity of the normalized SANS profiles.

The in-situ SANS studies shed light on the origin of the unexpected performance. Under the application of a negative potential to an ACF working electrode (WE) in a H_2SO_4 solution in H_2O, H-containing cations (such as H_3O^+, in the simplistic description)

replace anions (such as HSO_4^- and SO_4^{2-}) and H_2O molecules, thereby increasing the concentration of H in the vicinity of the ACF surface and thus increasing the intensity of the scattered neutron beam and shifting the intensity curve up to higher values (Fig. 5.7a). When a positive potential is applied to a working electrode, electrolyte anions replace both H-rich cations and H_2O molecules, thus decreasing the concentration of H in the vicinity of the ACF surface and decreasing the scattering intensity (Fig. 5.7a).

The application of a negative potential to an ACF working electrode in a H_2SO_4 solution in D_2O increases the intensity of the scattered neutron beam more than in the other case because of a dramatically weaker scattering of neutrons from deuterium in D_2O (Fig. 5.7b). Under the application of a positive potential to an ACF WE, the change in the H concentration becomes governed by the replacement of both cations (such as H^+, HD_2O^+) and D_2O solvent molecules by electrolyte anions (such as HSO_4^- and SO_4^{2-}, in a simplistic case). The replacements of D_2O by $SO_4^{(2-)}$ and of H^+ and HD_2O^+ by $HSO_4^{(-)}$ are expected to have little impact on the scattering intensities. Because the replacements of HD_2O^+ and H^+ by $SO_4^{(2-)}$ contributes to the decrease of H concentration in ACF pores, while the replacement of D_2O by HSO_4^-, in contrast, contributes to the increase in the H concentration, the change in the intensity of the scattered beam is determined by the balance of both processes. In our case, we see minimal changes in the scattering intensity when the potential of WE was increased from 0 to 0.6 V vs. a counter electrode (CE) (Fig. 5.7b).

To gain insights into the adsorption of ions within the pores of different sizes we normalized the SANS intensities to a zero voltage SANS profile (Fig. 5.7c, e). It is important to note that the variable Q is inversely proportional to pore size (large pores are

present at small values of Q and vice-versa). In the case of the H_2O solvent, under the application of -0.6V the scattering intensity increases by ~6 % (Fig. 7c), which represents the H enrichment of 6% within the relatively large pores. The smallest pores ($Q > 0.5$ $Å^{-1}$) of ACF exhibit even higher ion adsorption capacity, as manifested by higher H concentration in such pores at negative potentials and lower H concentration at positive potentials.

The effect of pore size on ion electroadsorption can be seen more clearly in Fig. 5.7d, where relative changes in the normalized scattering intensities are shown for both the negative and positive potentials applied to the ACF WE. Under the highest negative potential of -0.6V the H enrichment remains constant for pores corresponding to $Q < 0.5$ $Å^{-1}$ but increases in small pores corresponding to $Q > 0.5$ $Å^{-1}$. Under the highest positive potential of 0.6 V the H density decrease is enhanced in the smallest pores corresponding to the same Q (Fig. 5.7d). Such observations support the recent hypotheses of the enhanced ion adsorption in the smallest pores [3, 87, 88]. In contrast to these prior studies, where the impact of pore size was studied by analyzing completely different carbons exhibiting not only different pore size distributions but also different concentration of defects and functional groups, this investigation presents the first unambiguous observation of the different ion adsorption in the smallest sub-nm pores.

In case of a D_2O solvent (Fig. 5.7d, b, f), the negative polarization increases the neutron scattering intensity more dramatically because the scattering contrast between carbon and D_2O is much smaller than between carbon and H_2O. Under the application of -0.6V the concentration of H increases by ~35 % in large pores (Fig. 5.7e). However, in

sharp contrast to the H_2O solvent studies (Fig. 5.7c, d), cation adsorption is significantly reduced in smallest pores ($Q > 0.4$ Å^{-1}) in case of a D_2O solvent (Fig. 5.7e, f).

The apparently smaller surface area of ACF accessible to electrolyte ions explains the previously measured lower specific capacitance observed in a D_2O-based electrolyte (Fig. 5.5c). If the energy of solvent-pore wall interface could be neglected as traditionally assumed, the observed reduction of cations' adsorption upon changing the solvent (compare Fig. 5.7d and 5.7f) could not be explained, because ion solvation energy is, in fact, smaller in D_2O than in H_2O and thus a distortion of the solvation shells and permeation of partially desolvated ions into the smallest pores should be easier in D_2O. Therefore, it is more likely that D_2O-pore wall interactions obstruct ion access to a portion of the ACF surface. Such interactions should be greatly enhanced in the smallest pores, where interaction potentials of the solvent molecules with both sides of the pore walls overlap[152]. As a result, the relative concentration of ions becomes strongly reduced within sub-nanometer pores (Fig. 5.7f).

Two separate scenarios may lead to the reduced accessible surface area of the ACF in the D_2O-based electrolyte: either the attraction of D_2O to the pore surface is so strong in the smallest pores that the replacement of the surface-adsorbed D_2O molecules by cations becomes energetically unfavorable or, in contrast, the hydrophobic nature of the carbon surface combined with the higher carbon/D_2O – based electrolyte interfacial energy prevents the electrolyte access to the smallest pores. To identify which hypothesis is correct, the relative degree of the ACF pore filling by both solvents and the relative strength of the solvent-pore walls interactions was measured. SANS performed on dry ACF and on ACF infiltrated with H_2O and D_2O media provided valuable insights (Fig.

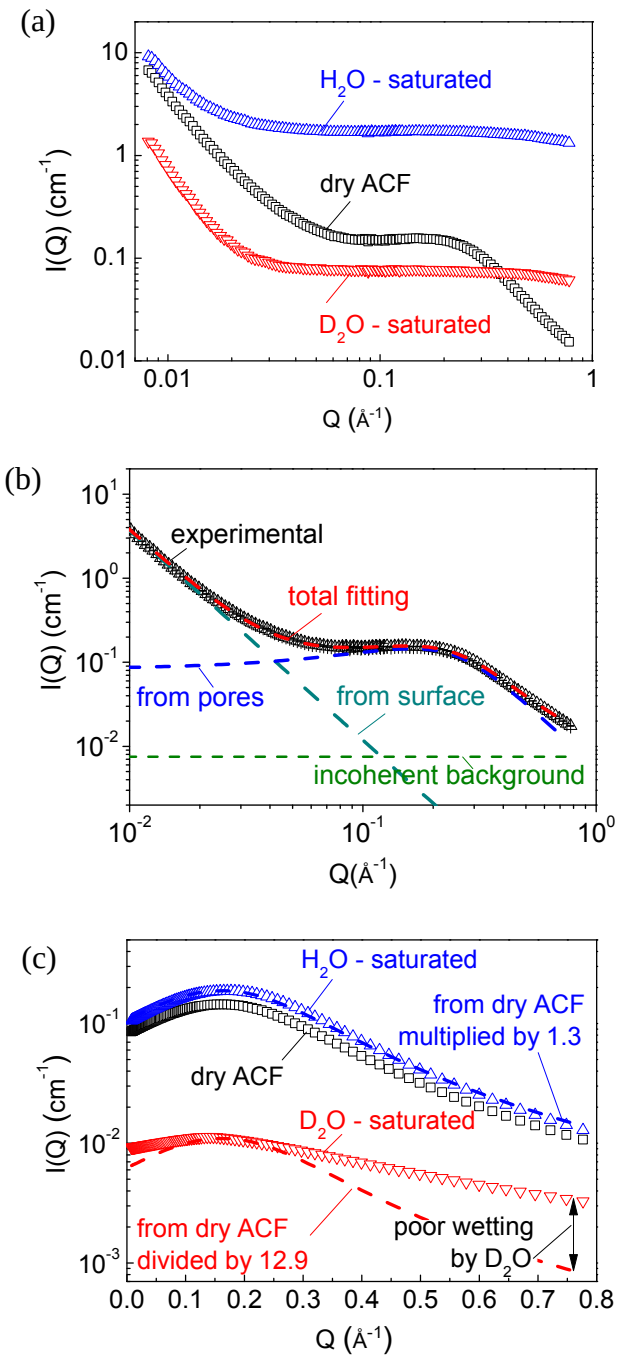

Figure. 5.8 Neutron scattering experiments on dry ACF electrodes as well as on ACF immersed into H_2O and D_2O: (a) SANS patterns; (b) deconvolution of total scattering from dry ACF into scattering from the incoherent background, fiber surface, and pores; (c) neutron scattering from meso- and micropores in the studied samples. In (C) dash lines represent scattering from dry ACF normalized to a maximum intensity of the neutron scattering curves of ACF immersed into two liquids: red dash line represents a normalization factor of 0.0775 and blue dash line represents a normalization factor of 1.3.

5.8). A negative SLD of H_2O ($-0.56 \cdot 10^{10}$ cm^{-2}) increases neutron contrast between carbon and H_2O saturated pores, leading to stronger scattering from H_2O saturated ACF (Fig. 5.7a). At the same time, a positive SLD of D_2O ($6.4 \cdot 10^{10}$ cm^{-2}) being close to that of carbon ($4 \cdot 10^{10}$ cm^{-2}) leads to a weaker scattering from D_2O saturated ACF (Fig. 5.8a). By deconvoluting the total scattering patterns (Fig. 5.8a) into the scattering from the fiber outer surfaces, scattering from pores and incoherent background (see Fig. 5.8b as an example) the degree of pore filling over a broad pore size range could be identified. The saturation of the ACF pores with H_2O leads to a parallel shift of the ACF scattering curve at all Q- values with a factor of ~1.3 (Fig. 5.8c), which is a ratio of the scattering intensities from H_2O-saturated and dry ACF at the value of the scattering vector corresponding to the maximum scattering intensity. This indicates that all the pores are evenly filled with H_2O. In contrast, saturation with D_2O leads to a Q-dependent decrease in the scattering intensity (Fig. 5.7c), indicating that a significant portion of the smallest pores ($Q > 0.3$ $Å^{-1}$) is not completely filled with D_2O. Vapor adsorption isotherms collected at 293K (Fig. 5.9) further confirm SANS results. H_2O adsorption was observed at slightly lower relative pressures, indicating stronger interactions with carbon pore walls. More impressively, nearly 250 cm^3 g^{-1} less D_2O was adsorbed on the ACF surface at a relative pressure of 0.8 (Fig. 5.9), indicating incomplete filling of pores by D_2O, as suggested by Fig. 5.7c.

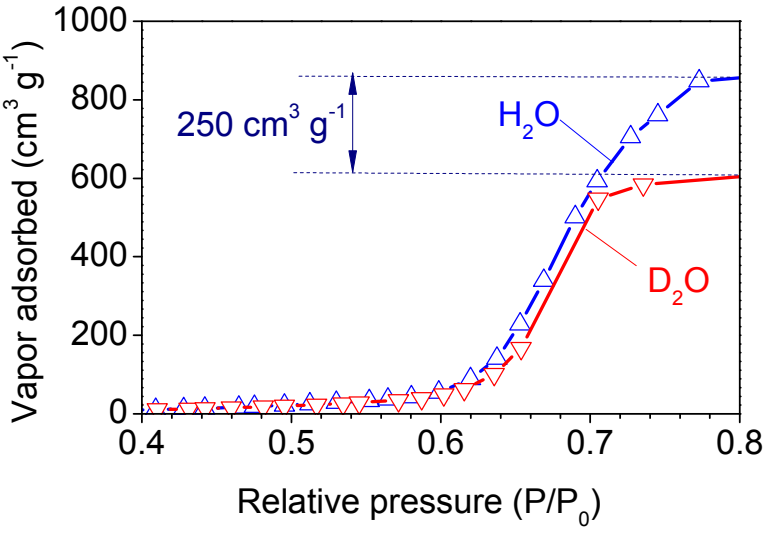

Figure. 5.9 Vapor adsorption isotherms collected on ACF electrodes in H_2O and D_2O

Since both SANS and sorption measurements indicate incomplete access of the D_2O to the small pores, it was concluded that the higher energy cost of maintaining a stronger deuterium bond network (compared to a hydrogen bond network) at the sub-nm proximity to the hydrophobic carbon surface is responsible for the formation of D_2O-based electrolyte depletion regions and for the dramatic difference between the electro-adsorption of D_2O- and H_2O- based electrolyte ions in the smallest carbon nanopores.

5.3.3 Conclusion

The idea that improved wetting properties may affect the specific capacitance of carbon is not a new one. Indeed prior studies observed higher surface area-normalized capacitance in porous carbons after surface oxidation, which improved electrolyte wetting[93]. These and similar studies, however, did not take into consideration that modification of carbon surface chemistry, increasing the concentration of defects and opening bottle-neck pores during oxidation which may similarly increase the capacitance.

Furthermore, no experimental studies have provided any insight on how the electrowetting phenomenon may counter-balance the insufficient carbon wetting by the solvent. As such, the impact of carbon wettability by the solvent on the specific capacitance has generated much controversy. In contrast, in these studies for the first time it was shown that the poor solvent wetting may indeed prevent electrolyte access to sub-nm pores even under the applied potential. More importantly, the capability of SANS to directly estimate the critical pore size, below which the inner surface area of carbons may not be accesible by electrolyte ions, was demonstrated.

Finally, it is important to note the unique capability of SANS to identify the degree of ion adsorption in pores of different sizes at an open circuit potential. This is an important question as the degree of pore filling affects the voltage dependence of the capacitance[153]. Several research groups suggested the opposite scenarios for ion filling small micropores. For example, Kiyohara et al. [154] suggest in their model that ions are expelled from small pores, when the porous electrode is not polarized. In contrast, Kondrat et al. assume the opposite based on the estimates of the role of image forces in the electrode that attract ions to electronically conductive pore walls[155]. By measuring lower neutron scattering intensity on ACF electrode immersed in pure solvents than in electrolytes based on such solvents (Fig. 5.10a and b) it was concluded that H-containing ions do enter the carbon pores under no applied potential in case of both H_2O and D_2O solvents. More importantly, this H enrichment is stronger inside the smallest pores in both of these solvents (Fig. 5.10c).

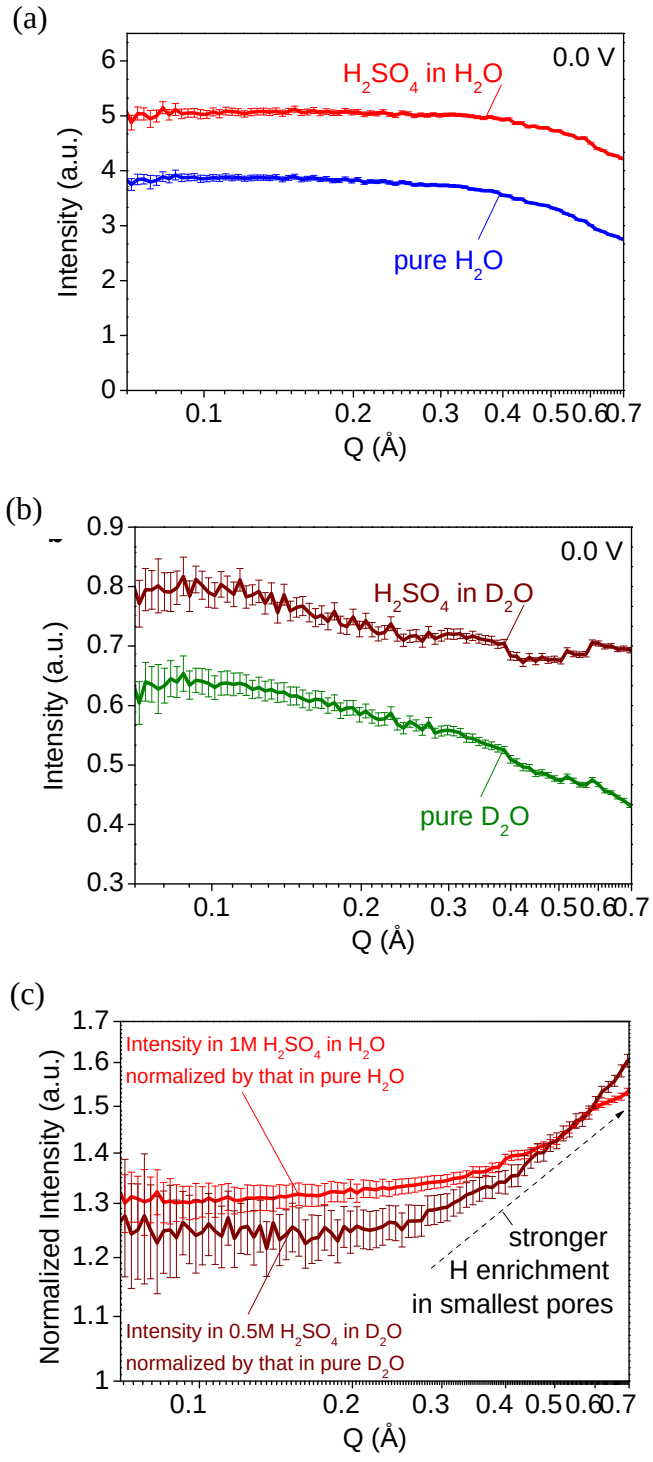

Figure. 5.10 Neutron scattering experiments on ACF electrodes immersed into various liquids under no applied potential (0V): (a) SANS patterns on ACF in pure H_2O and 1M H_2SO_4 electrolyte solution in H_2O, (b) SANS patterns on ACF in pure D_2O and 0.5 M H_2SO_4 electrolyte solution in D_2O, (c) SANS profiles on ACF immersed into electrolyte solutions and normalized by the SANS profiles on ACF immersed into pure solvent (either H_2O or D_2O).

5. 4 Study of Ion Electroadsorption in Organic Electrolytes

5.4.1 Motivation

Here the same approach to investigate the differences in ion adsorption in nanoporous carbon electrodes at the nanoscale was investigated in two different electrochemical systems commonly used in the design of high capacitance electrochemical capacitors: tetraethyl ammonium tetrafluoroborate (TEATFB) salt in acetonitrile and dimethyl sulfoxide (DMSO) solvents. TEATFB is typically used with different solvents to create electrolytes with appropriate electrical and electrochemical properties for use in high capacitance electrochemical capacitors. Because of the solvent's influence on the electrical conductivity, dielectric constant, wettability, and viscosity (among others), specific solvents are paired up with the TEATFB salt to create devices that fit specific requirements and standards. To improve the sensitivity of the small angle neutron scattering experiments to hydrogen, deuterated versions of the solvents were used. As such, in the systems studied the only source of hydrogen present in the electrochemical systems studied was in the cations (tetraethylammonium).

The differences between the two solvents being investigated also make this study very interesting in order to elucidate the effect of organic solvent on EDLC performance. For example, DMSO has a higher viscosity than acetonitrile (1.991 cP vs. 0.441 cP at room temperature). DMSO also has a higher dielectric constant than acetonitrile (47.7 vs. 38.8). Additionally, both solvents have similar scattering length densities (5.28×10^{10} cm^{-2} for DMSO vs. $4.92 \times 10^{10} cm^{-2}$ for acetonitrile), so that there is very little difference in the effect on scattering between both solvents (i.e. both solvents will contribute similarly to intensity profiles generated). As such, the only differences observed in the neutron

scattering experiments can be attributed solely to differences in ion electroadsorption in either solvent.

5.4.2 Characterization of ACF Electrodes

The electrodes used in this experiment are the same described in section 5.2, with characterization available in Fig. 5.2. In order to determine possible influence from other external factors, such as the presence of defects and functional groups, additional characterization was performed on the electrodes (TEM, SEM, XPS) and can be seen in Fig. 5.11. TEM was used to further analyze the microstructure of the electrodes. The electron microscopy measurements confirm that these electrodes are made up of long interwoven strands of carbon fibers roughly 10-15 μm in diameter (Fig. 5.11a). TEM confirms the presence of pores of various sizes, most of which are below 2nm in size (Fig. 5.11b). In the previous experiments N_2 sorption experiments were performed on the carbon fabric. The N_2 sorption isotherm had a type I shape, usually found in microporous materials with low volume of pores larger than 2nm. Moreover, these measurements verified the presence of sub-nm (<0.5nm) pores, and indicate that most of the internal pore volume is made up of pores of sizes 0.4-2nm. As such, these activated carbon fabric electrodes are excellent models for the adsorption of ions in microporous carbon materials. XPS was used to investigate the presence of functional groups on the surface of the electrodes, many of which can undergo faradaic redox reactions and thus influence capacitance of the electrodes. XPS measurements confirm the absence of such functional groups (Fig. 5.11c), and thus these studies will only look at the effect of ion electroadsorption in the specified organic electrolytes at different potential, without the effect of external factors.

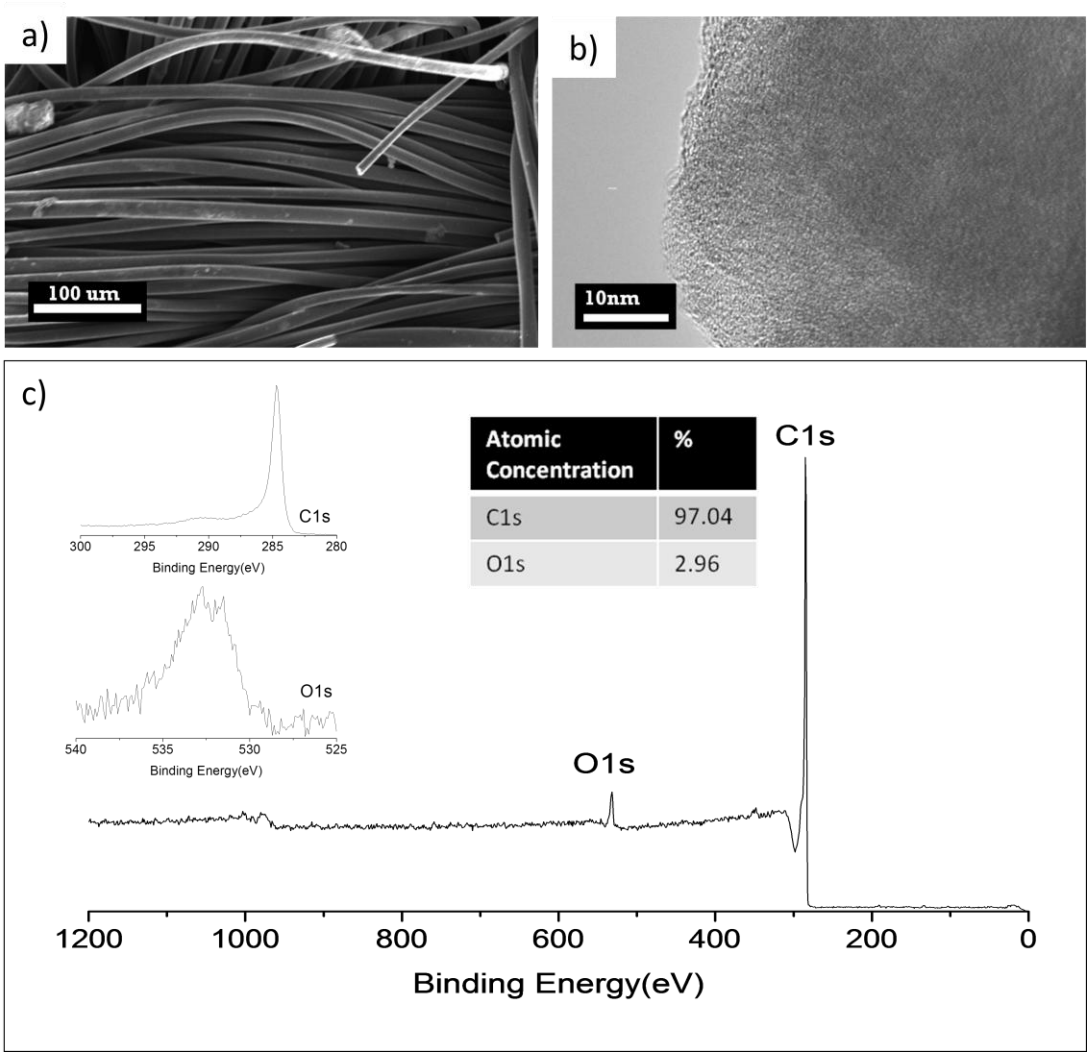

Figure. 5.11 Materials characterization of ACF electrodes: (a) SEM, (b) TEM, and(c) XPS results.

5.4.3 Discussion of SANS Results

The SANS experiments performed in d-acetonitrile and d-DMSO exhibit similar trends (Fig. 5.12). In both cases, the application of a negative potential results in an overall (across all pores and pore sizes) decrease in scattering intensity. Since the presence of hydrogen will increase the intensity much more than all other elements present in the electrolytes, it is the presence of adsorbed cations within the porous network of the ACF fibers which is responsible for the increase in intensity. As, the

negative potential is applied, the overall effect on the intensity profile is an increase in scattering intensity. This was expected, as the only hydrogen-containing molecule introduced into this system was the TEATFB cation (TEA^+), which is adsorbed into the pores under application of a negative potential, and expelled (replaced) with the non-hydrogen containing anion (BF_4^-) and solvent. These observations validate our methodology and corroborate trends observed in the previous studies.

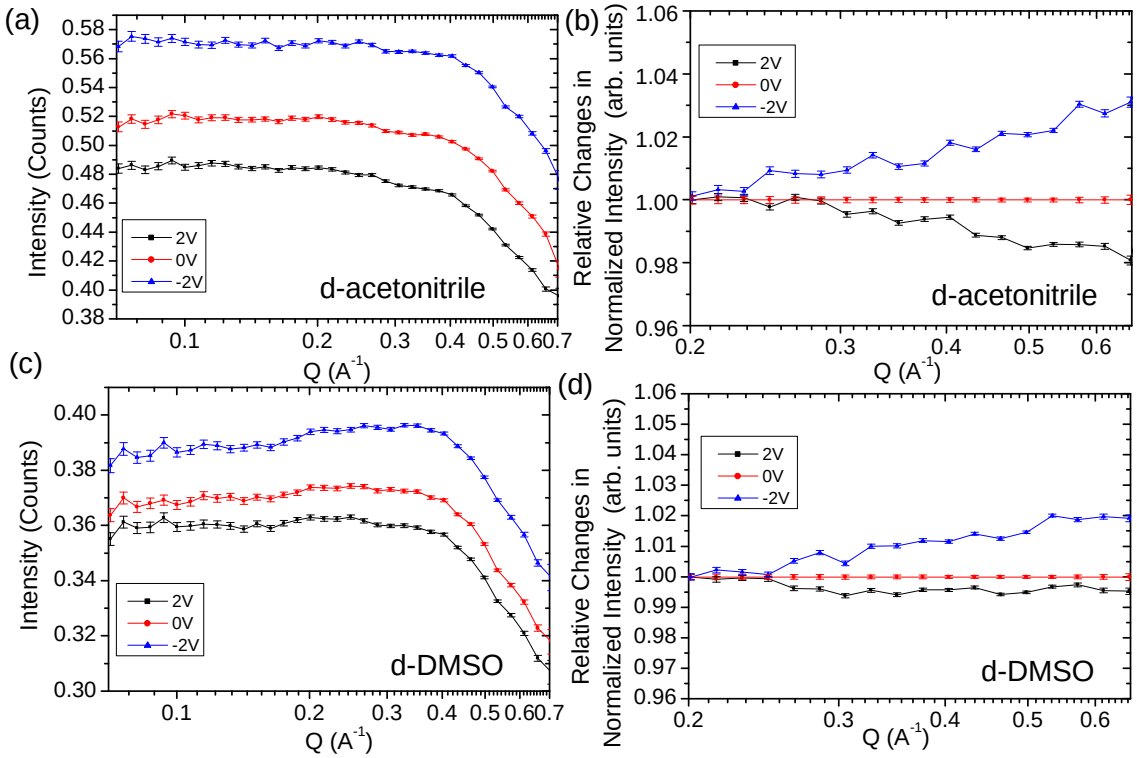

Figure. 5.12 In-situ neutron scattering experiments on ACF electrodes immersed into 1M TEATFB in d-acetonitrile (a, b) and d-DMSO (c, d,) electrolytes under an application of a potential between the WE and CE: (a, c) SANS patterns, (b, d) relative changes in the intensity of the normalized SANS profiles.

A more quantitative analytical examination of the data reveals other trends. For example, in the d-acetonitrile solvent, application of a negative potential results in a higher shift (~10-15% shift for all pore sizes) in intensity than the application of a positive potential (~5-8% shift for all pore sizes). This could indicate that more anions are adsorbed in the nanopores under no applied potential, although this difference in

relative change in intensity may also be attributed to the greater effect on intensity that the hydrogen-containing cations have along with the relatively larger size of the theses cations. This effect can also be seen in the case of the d-DMSO solvent (~5-7% shift for all pore sizes in the case of a negative potential versus ~2-3% shift for all pore sizes in the case of a positive potential). Since the only factor which has been changed between the two experiments is the choice of solvent, either the carbon-solvent interfacial energy or the difference in ion solubility (higher solubility in d-acetonitrile) might be responsible for this difference.

Focusing only on the smallest pores, it is apparent that this shift in intensity becomes more pronounced in the smallest pores in the case of both potential and negative applied potentials. Once again, both the shift in intensity and the range in shift in intensity become more pronounced in the smallest pores in the case of a negatively applied potential, and is most likely due to the presence of hydrogen in the cation. The difference in intensity profiles between the larger pore range and the smaller pore range could be due to either the solvation shell distortion in the smallest pores (if small pores were fully accessible to electrolyte at zero potential) or to the electro-wetting phenomenon (if the smallest pores were not fully wetted with electrolyte, as previously observed with a D_2O solvent, but the application of the potential could wet the smallest pores). In the last case, the significant impact of electrowetting in organic electrolyte (as opposed to D_2O, previously discussed) may be attributed to the less polar nature of the solvents than water and heavy water, and to the higher applied potentials used here (2V vs. 0.6V).

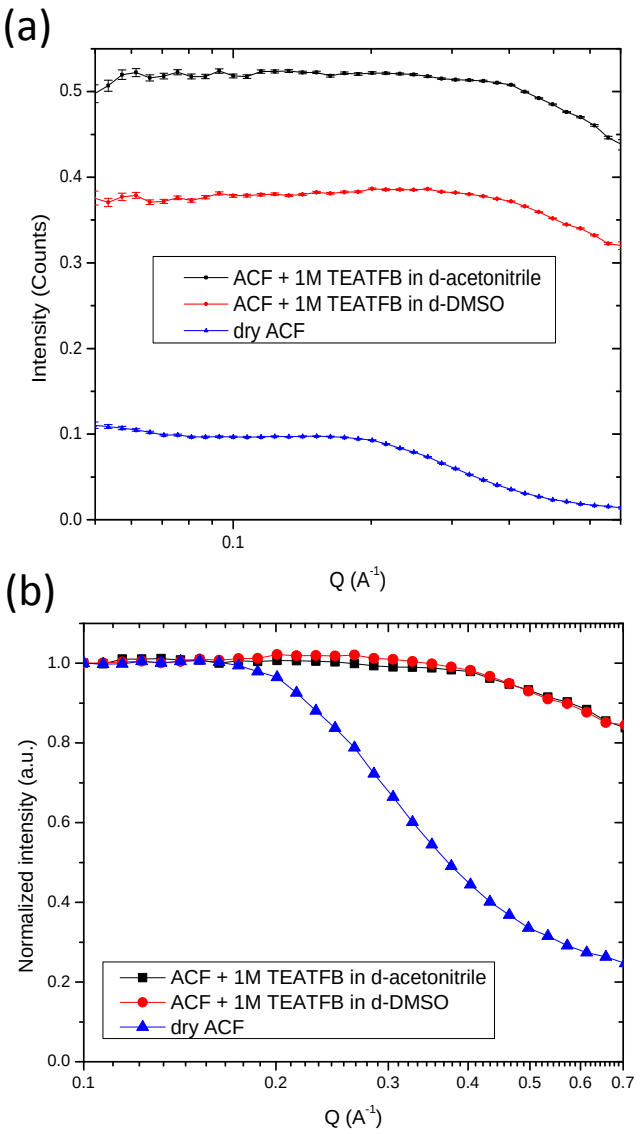

Figure. 5.13 Comparison of neutron scattering experiments performed on dry ACF electrodes vs. ACF electrodes immersed in 1M TEATFB in d-acetonitrile and in 1M TEATFB in d-DMSO electrolytes: (a) SANS profiles, and (B) profiles normalized to 1 to compare wetting.

Comparing the SANS profiles of the dry carbon to that of the carbon in each electrolyte (without an applied potential) confirms the trends stated previously (Fig. 5.13). The scattering intensity profile of the activated carbon in d-acetonitrile solvent is ~25% higher than that of the activated carbon in d-DMSO solvent in all pores. It can thus

be concluded that the d-acetonitrile solvent results in stronger H-containing cation adsorption. This may be due to, for example, a lower carbon-solvent interfacial energy (allowing more ions to fit in the pores) or higher solvation energy combined with faster ion transport in d-AN (so that reduction in the ion concentration in electrolyte caused by ion adsorption in carbon is compensated by ion diffusion from electrolyte outside the pores; as a result the total ion concentration in pores increases). The normalized plots (Fig. 5.13 b) indicate incomplete wetting of ions in the smallest pores in both solvents. Therefore, we can conclude that enhancing of ion adsorption in the smallest pores observed at higher potentials (Fig. 5.12 b, d) is a result of electro-wetting.

5.4.4 Electrochemical Measurements

ACF electrodes cycled using 1M TEATFB in d-acetonitrile solvent show slightly higher capacitance than ACF electrodes cycled using 1M TEATFB in d-DMSO consistent with higher ion sorption observed under no applied potential (Fig. 5.14). In the case of both solvents, the CV profile is fairly rectangular, meaning that most of the energy storage is due to electrostatic interactions between the ions and the electrode surface. Due to the absence of functional groups on the surface of the ACF electrodes, it is the nature of the solvent and its effect on ion electroadsorption which is responsible for the changes between the two voltammograms and between the recorded specific capacitances of the two samples.

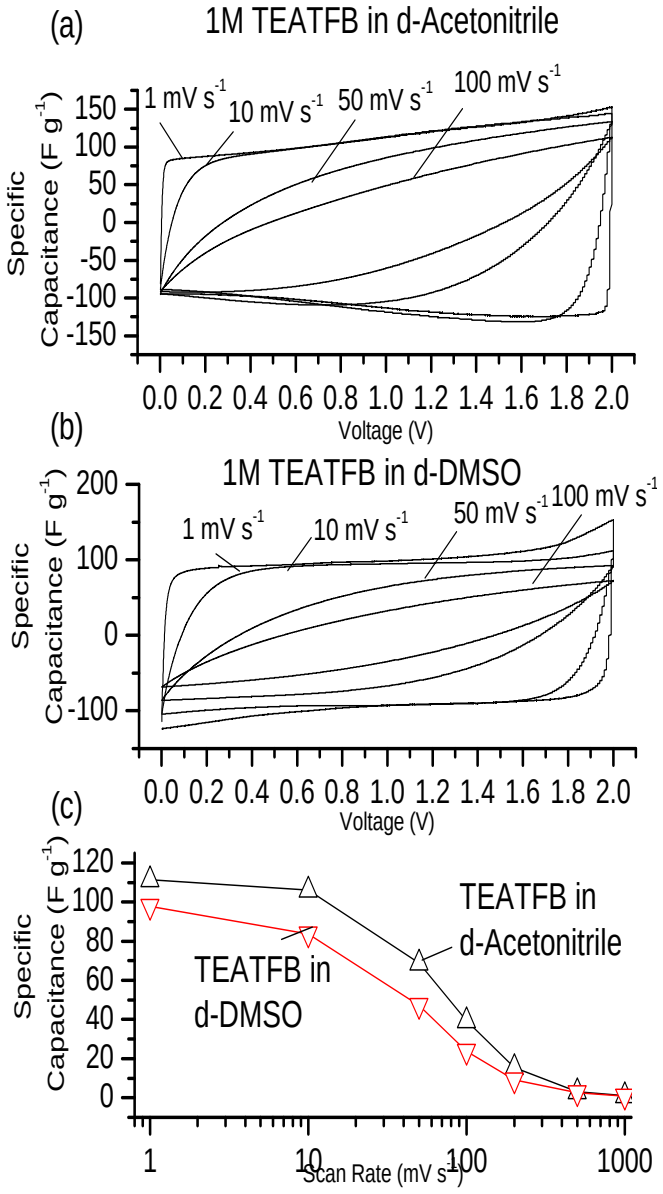

Figure. 5.14 Electrochemical characterization of ACF in symmetric cells: cyclic voltammetry performed at different sweep rates in 1M TEATFB solution in (a) d-acetonitrile and (b) d-DMSO, (c) capacity retention as a function of sweep rate.

5.4.5 Conclusions

SANS was used to study the effect of organic solvent on ion adsorption properties in nanoporous activated carbons. This study confirms that TEATFB ion adsorption is

enhanced in d-AN over d-DMSO solvents. Smaller pores were found to exhibit higher ion storage ability. The higher ion concentration was found to adsorb in carbon pores from d-AN-based electrolyte than from d-DMSO-based electrolyte under no applied potential. It is, therefore, possible, that higher ion solvation energy and the resulting higher ion solubility in d-AN vs. d-DMSO may shift the equilibrium between the adsorbed and solvated ions at a given applied potential and affect specific capacitance. The methodology outlined in this paper can be used to investigate and compare other solvents for use in energy storage applications.

5.5 Effect of Concentration on Ion Electroadsorption in Supercapacitor Electrodes

5.5.1 Motivation

The effect of higher molar concentration of the electrolyte on the energy storage capabilities of a supercapacitor has been to increase capacitance, energy and power densities in selected supercapacitors since higher concentration could be expected to result in higher amount of electro-adsorbed ions. At maximum concentrations of electrolyte ions the limiting factor for the capacitance of the device becomes the electrode material itself [156]. This is because the maximum energy which can be stored in a supercapacitor is dependent on the capacitance of the material, the operating voltage, and the quantity of freely available ions from the electrolyte. Increasing the molar concentration of the electrolyte equates to increasing the number of ions present in the electrolyte solution, and maximizing either this concentration or the molar conductivity of the electrolyte is employed in order to minimize power losses[157] and increase molar conductivity. Indeed, Conway et.al. demonstrated that possessing sub-optimal concentrations of electrolytes will lead to a distortion of the voltammogram and to a

reduction in capacitance[157]. This maximization of electrolyte concentration is also achieved in order to avoid the effect of electrolyte starvation, which occurs when low concentrations of the electrolyte are used and the concentration of ions is too low to access all of the accessible surface area of the electrodes[2, 158-160]. This can lead to adsorption of the ions at the high area locations in the pore system of the electrode, creating potential "bottlenecks" and increasing the internal resistance of the electrode, which has a more pronounced effect on the charge-discharge profile of supercapacitors at high current densities.

It is important to note that the insertion of ions in the smallest sub-nm pores and the resultant distortion of the solvation shell in order to allow these ions to "fit" will be highly dependent on the nature of the solvent, and thus on the carbon-solvent interfacial energy and the wettability of the electrolyte. Although this effect has been acknowledged in the simplest case for EDLCs, the effect of molar concentration on ion electroadsorption in the smallest sub-nm pores has not been fully explored. The SANS technique developed over the course of this work and presented in the previous sections was used to investigate the effect of ion concentration on the ion electroadsorption mechanism.

5.5.2 Discussion of SANS Results

In this study, varying concentrations of an organic electrolyte (0.5M, 1M. And 2M TEATFB in d-acetonitrile solvent) were investigated. These are typical concentrations used in the construction of supercapacitor devices. This electrolyte is typically used for its high conductivity and for the high capacitance it induces in supercapacitors due to its relatively small ion size (size of the solvated cation is 1.3nm, size of the solvated anion is

1.16nm, size of unsolvated cation is 0.67nm, and size of unsolvated anion is 0.48nm)[161]. The same commercially available ACF was used as electrode material for study. Overall it is important to note that the 0.5M sample had a lower intensity (~0.1-0.7 vs. ~0.1-1.1 and ~0.1-2 counts for the 1M and 2M solutions respectively). This trend is in direct correlation with the number of ions present in the solutions as the concentration is increased.

In all three cases (0.5M, 1M, and 2M TEATFB in d-acetonitrile), the application of potential resulted in the behavior expected from the previous studies. Application of a negative potential (-2V) resulted in a higher intensity than higher potentials (0V and 2V, respectively), due to the electroadsorption of hydrogen-containing cations.

To visualize the difference (caused by charging) in the concentration of H-containing cations, the intensity of the (2V) samples was subtracted from the intensity of the (-2V) samples and these results were normalized to compare objectively between the different concentrations (Fig. 5.15). For the 0.5M, 1M, and 2M concentrations, there is an increase in the difference in H-containing cations across the pore range as the pore size is decreased. This effect is most likely due to a combinations of two effects: (i) increased wetting in the pores under applied potential and (ii) since the only source of hydrogen is in the cation (and hydrogen is the element which will have the largest effect on increasing intensity in these measurements), these increases in intensity reveal a higher concentration of ions in the smallest pores and can be attributed to a distortion of the solvent shell surrounding the ions which permits more ions to squeeze into constrained pore volumes than is predicted by the Helmholtz double-layer model, as was predicted in Chmiola et.al ‘s 2006 paper[3].

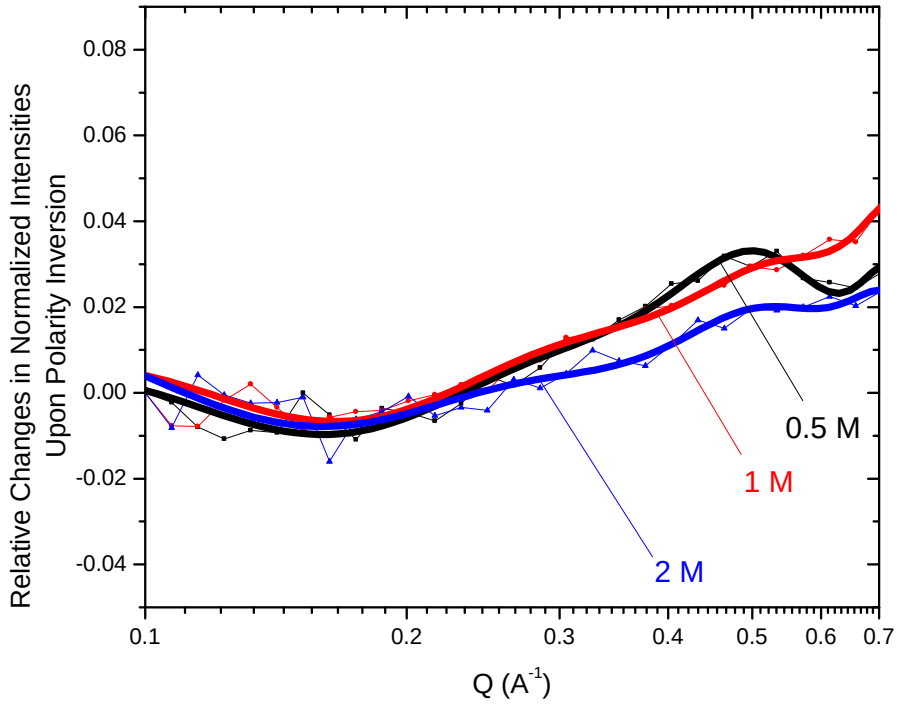

Figure. 5.15 Normalized changes in intensity between (-2V) and (2V) scans vs. Q

CHAPTER 6

PSEUDOCAPACITIVE-CARBON NANOCOMPOSITE ELECTRODES FOR HIGH POWER AND HIGH ENERGY SUPERCAPACITOR APPLICATIONS

6.1 Introduction

As discussed in the introduction section, with the advent of modern electronics, electrical vehicles and smart grid, energy storage and conversion is becoming increasingly important. There is a critical need to develop novel supercapacitor electrodes with improved high-energy and high-power characteristics. The formation of EDLC/pseudocapacitive nanocomposite electrodes may offer unique benefits for such applications. Broadly available transition metal oxides, such as vanadium oxide, offer high ion storage capabilities due to the broad range of their oxidation states, but suffer from high resistivities. CNTs, in contrast, are not capable to store high ion content, but offer high and readily accessible surface area and high electrical conductivity. By exploiting the ability of atomic layer deposition (ALD) to produce uniform coatings of metal oxides on CNT electrodes, we demonstrate an effective way to produce high power supercapacitor electrodes with ultra-high energy capability.

Among various transition metal oxides, vanadium oxides have received relatively modest attention for supercapacitor applications [17, 162-172]. Yet, this material is abundant, relatively inexpensive (~\$12 kg^{-1}) and offers a broad range of oxidation states, which shall offer the broad range of redox reactions suitable for supercapacitor operation. Specific capacitance of vanadium oxide is known to depend on the preparation conditions and its morphology. It also strongly depends on the measurement technique

(measurements in a symmetric two-electrode cell configuration vs. individual electrode measurements in a three-electrode cell configuration). The difference by the factor of 3 or more between such measurements is common if the redox peaks in the positive and negative electrodes of the two-electrode cell do not take place at the same value of the applied voltage. When referenced to the ultimate device performance, the three-electrode measurements will give an over-estimated capacitance value unless the second electrode prepared from a different material can offer identical or higher capacitance. The two-electrode measurements, in contrast, will give an under-estimated performance because the symmetric electrodes are commonly not balanced and not optimized, particularly those that are based on Faradaic reactions [173].

Several types of vanadium oxide-based electrodes have been previously investigated. Pure V_2O_5 with enhanced surface area prepared by co-precipitation and calcinations [168] or via formation of sol-gel [169] or via electrodeposition [172] offer moderately high capacitance (200-260 $F \cdot g^{-1}$) and high resistance in aqueous (KCl) electrolyte when evaluated in a three-electrode configuration. The highest capacitance was reported for vanadium oxide aerogels (960-2000 $F \cdot g^{-1}$) [163-166]. It is important to note, however, that these results were obtained at extremely slow scan rates (0.1mV s^{-1}) on very small samples using a "sticky carbon" method, applicable in a research setting only.

To compensate for the very low electrical conductivity of vanadium oxide, the use of surface-oxidized vanadium nitride nanoparticles was proposed [174]. The produced electrodes, however, demonstrated poor power performance, presumably due to high particle-to-particle resistance. Carbon may offer higher electrical conductivity and higher specific surface area than vanadium nitride. Synthesis of carbon-vanadium oxide

composites via a solid-state reaction process between VO_2 and ordered mesoporous carbons did not allow sufficient control over the composite microstructure at the nano-scale and thus relatively moderate capacitance value (131 $F \cdot g^{-1}$) was achieved [170].

In a recent study, vacuum filtration was used to combine V_2O_5 nanowires and CNTs to form binder-free supercapacitor electrodes. These electrodes, when submerged in organic electrolytes (0.1M LiTFSI), achieved moderate values of capacitance (~60$F \cdot g^{-1}$) and suffered from low power characteristics, due to composite fabrication[175]. By using a different approach which better utilizes the respective strengths of the metal-oxide and carbon materials (such as electrodeposition or vapor deposition routes), electrodes with higher energy and power densities can be fabricated.

Electrodeposition of thin layers of vanadium oxide on the surface of either platinum (Pt) or ultra-thin carbon nanotube (CNT) electrodes resulted in an impressive specific capacitance of 170-900 $F \cdot g^{-1}$ when measured in a three electrode configuration using a Li-ion battery-type electrolyte ($LiClO_4$ salt dissolved in propylene carbonate, PC)[17]. While the obtained results are very promising, some possible limitations of the electrodeposition include the corrosive nature of the deposition electrolyte and limited uniformity of the deposited oxide layer. The lack of uniformity resulted in low capacitance retention at fast scan rates and current densities[17].

Vapor deposition routes may offer an alternative solution for the oxide deposition. Atomic layer deposition (ALD) [176-178], in particular, offers a combination of unique advantages. In ALD, the precursor and other source vapors are pulsed into the chamber one at a time, separated by purging or evacuation periods. Each pulse step commonly deposits a sub-monomolecular layer of the precursor onto the substrate, while the purge

or evacuation step limits the reaction to the surface by removing the excess reaction gases. As such, ALD allows precise, uniform and conformal deposition of oxide coatings on porous substrate surfaces, provided enough time is allocated for the diffusion of the precursor gases into (out of) the porous structure of the substrate during both the pulse and purge periods. Another advantage of ALD is a low synthesis temperature which facilitates deposition of coatings on fabric or fiber substrates for wearable or multifunctional energy storage devices [179-181]. Moreover, even though ALD is expensive in R&D settings these costs become much less important during commercialization, as economies of scale granted by large reactors recoup the high costs of the precursors and increase production speeds. While the use of ALD has been explored for thin film batteries [178] and gas sensing applications [177], it has not been utilized for the fabrication of high energy density supercapacitor electrodes.

Several studies reported the use of thin free-standing CNT films as low capacitance but high-rate electrodes for high-power supercapacitor applications [182-186]. In this work for the first time we conformably deposited vanadium oxide coatings of various thicknesses on the internal surface area of porous CNT electrodes using ALD technique and evaluated the composite performance for use in supercapacitors. We have systematically studied the structural, electrical, and electrochemical properties of the produced nanocomposite electrodes as a function of the coating thickness. The proposed technique can be utilized for the fabrication of both on-chip and wearable supercapacitors and electrochemical sensors. In such composites, CNTs provide high electrical and thermal conductivity while ALD-deposited oxide coating increases the electrode capacitance by more than an order of magnitude.

These fabricated electrodes were then investigated as half-cell supercapacitors for use in organic electrolytes. To improve their power and energy characteristics, post-deposition annealing experiments were used to increase the pore volume and improve the quality of the interface between the carbon substrate and the deposited layer.

6.2 Experimental Details

Multi-walled CNTs were grown via 5 min $FeCl_2$ catalyst-assisted chemical vapor deposition (CVD) process at 820 °C using acetylene precursor [187]. In order to prepare uniform stand-alone CNT electrodes, vertically aligned CNTs were separated from the substrate and boiled at 100°C in a 1:1 mixture of concentrated sulfuric and nitric acid (1 mg of CNT per 1 ml of the solution) under a condenser for 1h. This acid treatment opens the CNT caps and induces defects and multiple carboxylic groups on the CNT surface, which serve as nucleation sites for the subsequent oxide deposition and increase the rate of electron transfer. The CNT-containing solution was then diluted with de-ionized H_2O (DI, 18 MOhm) and vacuum filtered through a grade 2 Whatman filter (Whatman, USA). Ethanol was used to remove the acid residues and stop the oxidation process. The CNT electrodes were then dried overnight in a vacuum oven at 80°C. The acid purification step also allows for the formation of a binder-free, flexible, and, free-standing CNT electrode, since the filtered nanotubes form a three dimensional (3D) porous network of entangled and well-bonded CNTs. Similar processes could be used to deposit well-adhered CNTs on the surface of various fabrics [179]. These electrodes were used as substrates for deposition of vanadium oxide via ALD.

ALD deposition was done in a custom-built ALD system consisting of a quartz tube (heated in a furnace) through which precursor vapors were introduced alternately.

Vanadium tri-n-propoxide oxide (Gelest, Inc, USA) and DI H_2O (18 MOhm) were used as precursors and were heated to ~45 °C and 100 °C, respectively, during the deposition. High purity Ar (99.999 %, Air Gas, USA) was used as both carrier and purging gas (residence and purging periods were 10s and 20s, respectively for the H_2O precursor and for the vanadium precursor). All the precursor gas lines were maintained at 100°C during the deposition process. The pressure of the system was maintained at 4 Torr throughout the deposition. The temperature of the furnace was maintained at 170-190°C.

X-ray diffraction (XRD) experiments using Cu-K_α radiation were performed with a X'Pert PRO Alpha-1 diffractometer (Panalytical, USA) equipped with a monochromator. Scanning electron microscopy (SEM) measurements of the nanowire morphology, and diameter were performed using a LEO 1550 microscope (Carl Zeiss, Germany). ImageJ software was employed for the SEM image analysis to determine the nanowire diameter distributions. Raman experiments were performed on a Raman spectrometer (WITec, Germany) excited using a 514 nm wavelength laser with a 50x objective. The intensity of the laser was 215μW at the sample surface and the laser spot size was ~420nm. Spectra were acquired by accumulating 30x1s spectra.

The mass ratios of CNT and the oxide in the VO_x-CNT composites were estimated using thermogravimmetric analysis (TGA) performed in an oxidizing atmosphere of air by detecting the burning off of the CNT at around 400-600 °C. Such measurements were performed using a Q50 Thermogravimmetric analyzer (TA Instruments, USA). TGA measurements were performed on the samples by heating them from room temperature to 900°C at a 5°C·min^{-1} ramping rate in a Pt pan. Air was flown over the samples at 10 mL·min^{-1}.

Four types of samples were investigated through the course of this study. An uncoated CNT electrode sample was compared with CNT samples coated with vanadium oxide deposited through 100, 300, and 500 ALD cycles. For electrochemical testing, the coated electrodes were split into two near-identical electrodes of ~ 80 μm in average thickness, with each electrode attached to a current collector foil by the "split" side. All electrodes were rectangular and possessed a surface area of 0.25-0.30 cm^2. All electrochemical tests have been performed in fully symmetric two-electrode configuration using beaker-type cells, Au current collectors (Sigma-Aldrich, USA) and 25μm thick GorTex separator (GorTex, USA). We selected 8M LiCl solution (Sigma-Aldrich, USA) as an electrolyte because of vanadium oxide's solubility in other aqueous electrolytes. For example, vanadium oxide will dissolve if cycled in H_2SO_4 electrolyte. Previous experiments[168] have used 2MLiCl to test V2O5 supercapacitor electrodes with relatively high capacitance values (~260 $F \cdot g^{-1}$) and this is why we decided to use this electrolyte.

Electrochemical characterization was performed using galvanostatic (constant current) charge-discharge (C-D) measurements, electrochemical impedance spectroscopy (EIS), and cyclic voltammetry (CV). Cyclic voltammetry was performed using a Solartron 1480A (AMETEK Advanced Measurement Technology, USA) with the potential being swept from -0.6V to 0.6V at scan rates of 5-1000 $mV \cdot s^{-1}$. The integrated-average gravimetric capacitance of each electrode was calculated from the CV data according to:

$$C_{electrode} = 2C_{cell} = \left(\frac{2}{(dU/dt) \cdot m} \right) \cdot \left\{ \int_{-0.6V}^{0.6V} I(U)dU - \int_{0.6V}^{-0.6V} I(U)dU \right\} \cdot \frac{1}{2} \cdot \frac{1}{1.2V}$$

, where *dU/dt* is the scan rate, m is the mass of each electrode in a symmetric cell, and *I(U)* is the total current. The C-D tests were carried out using an Arbin SCTS supercapacitor testing system (Arbin Instruments, TN, USA) between -0.6 V to +0.6 V at charge/discharge current densities between 1000 and 20000 m $A \cdot g^{-1}$, based on the mass of a single electrode. The gravimetric capacitance was deduced from the average slope of the discharge curve according to:

$$C_{electrode} = 2C_{cell} = \left(\frac{2I}{(dU/dt) \cdot m} \right)$$

, where I is the total current, *dU/dt* is the slope of the discharge curve, m is the mass of each electrode in a symmetric cell. EIS measurements were performed on a Gamry Potentiostat from 100KHz to 1mHz at 1 V scanning amplitude. All supercapacitors were tested in the following order to ensure reproducibility and accuracy: CV (at scan rates increasing from 5 to 1000 $mV \cdot s^{-1}$) was followed by C-D (at current densities increasing from 1 to $20A \cdot g^{-1}$) and EIS.

6.3 Results and Discussion

SEM studies (Fig. 6.1) showed very high degree of coating uniformity throughout the electrodes. Even for the largest number of ALD cycles (500 cycles) the CNTs appear to be conformally coated with an oxide layer and no clusters are seen blocking the electrode pores. Since in an ideal case ALD is a surface-limited process, the average coating thickness or the average tube diameter should increase proportionally to the number of the ALD cycles. Software analysis of multiple SEM micrographs confirmed this and showed a linear increase in the average CNT diameter from ~70 nm (for bare CNTs) to

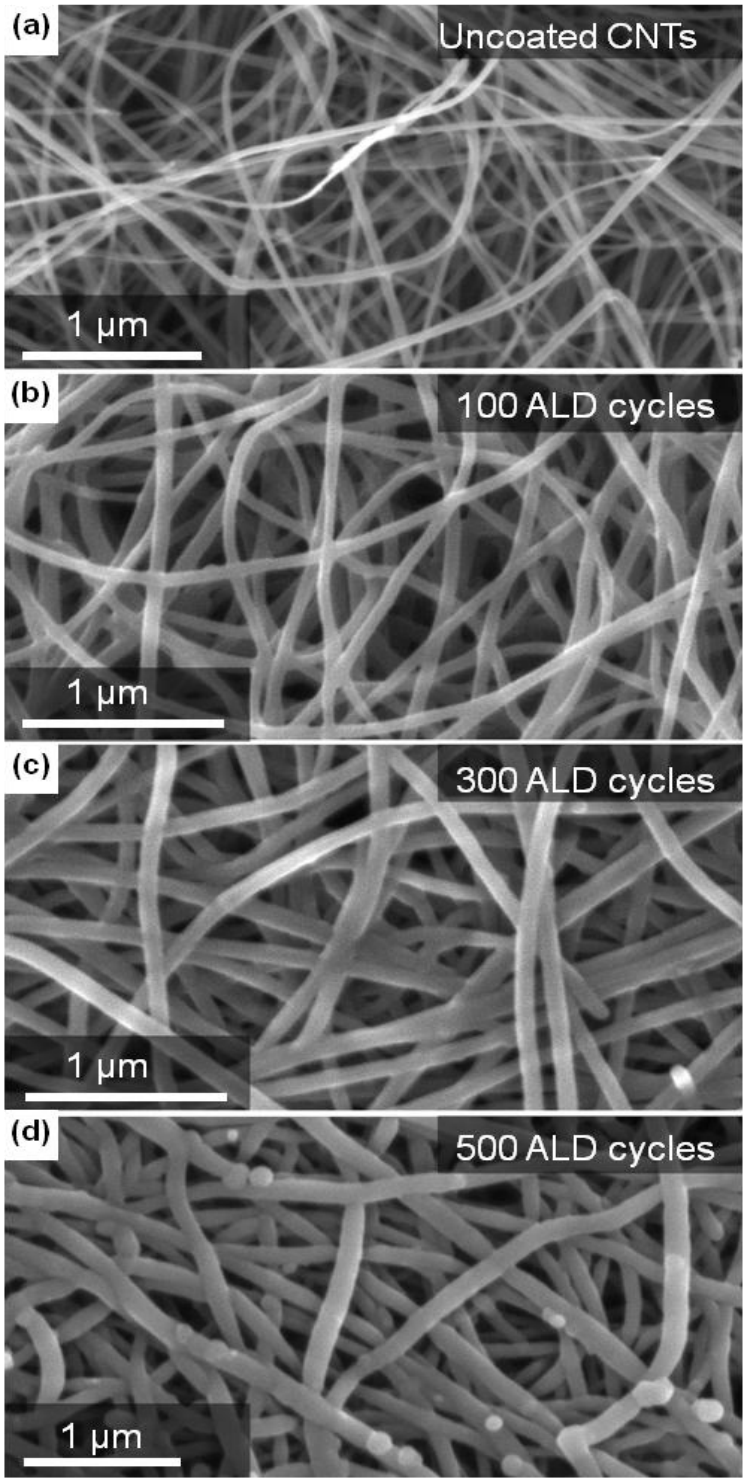

Figure. 6.1 SEM images of (a) uncoated samples, and samples coated with (b) 100 ALD cycles, (c) 300 ALD cycles, and (d) 500 ALD cycles.

~180 nm (after 500 ALD cycles) (Fig. 6.2), suggesting that the time allocated for the diffusion of the precursor gases into the porous structure in each cycle was sufficient for the reaction to be surface kinetics-controlled. The average coating thickness increases by $0.1 nm \cdot cycle^{-1}$.

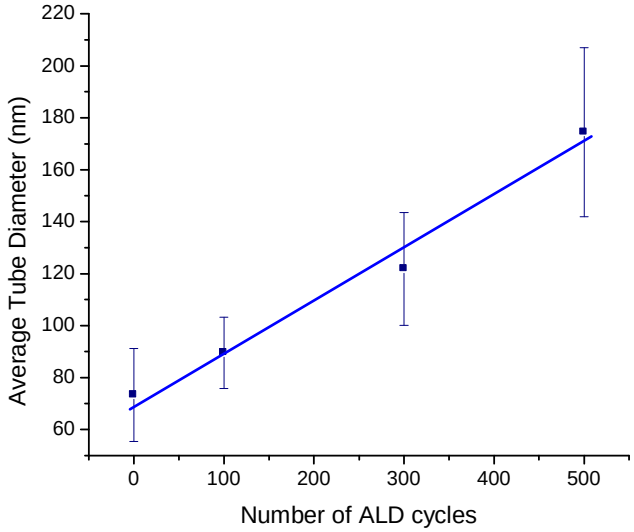

Figure. 6.2 Changes in the average tube diameters with cycle number.

XRD measurements of the as-deposited oxide films showed both amorphous and nano-crystalline features, but did not allow us to unambiguously identify the present phases due to the small peak intensity, large peak width and similarity in the spectral position of the reflections corresponding to different phases (Fig. 6.3a). Vanadium oxide (VO_x) possesses numerous oxidation states, with the most common phases being VO, V_2O_3, VO_2, V_2O_5 and V_6O_{13}. Comparison of the recorded patterns with literature [188-192] suggests the presence of all these phases. The color of the coated electrode is in between green (typical for VO_2) and yellow (typical for V_2O_5).

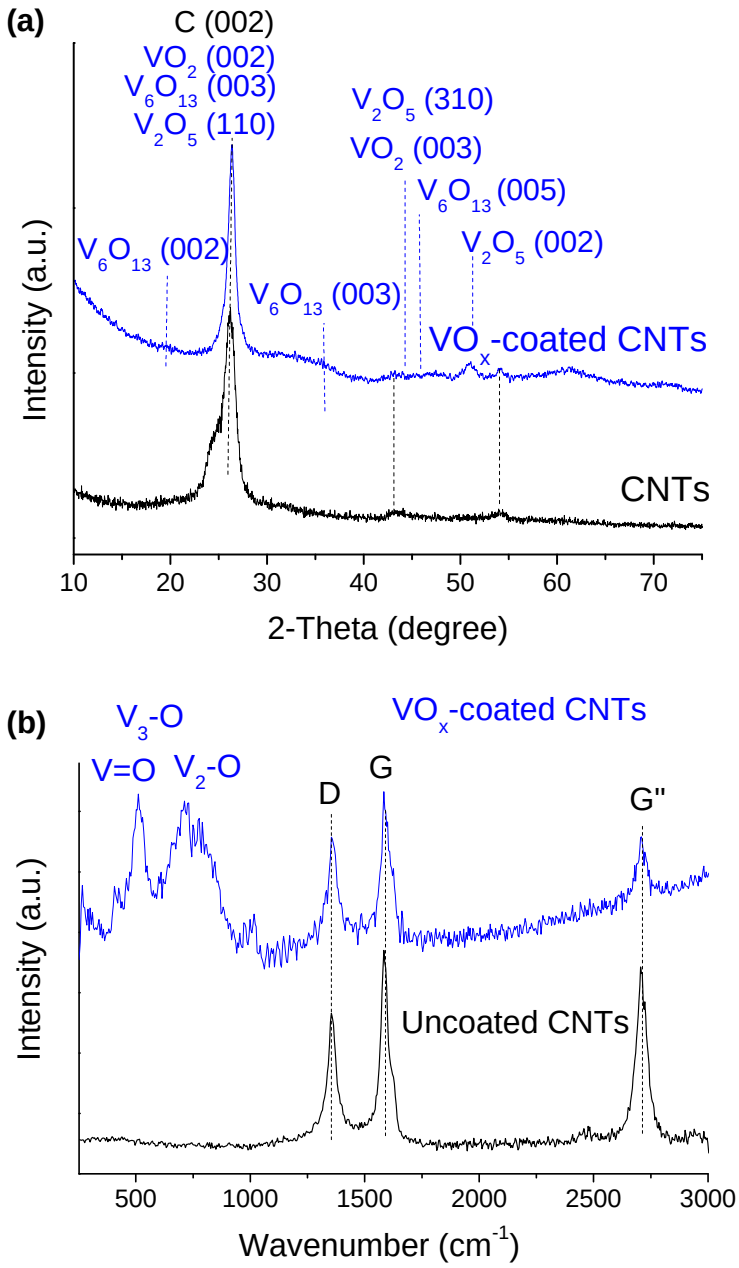

Figure. 6.3 Spectroscopic studies of VO_x-coated and uncoated CNT samples: (a) XRD and (b) Raman spectroscopy.

Raman spectroscopy was also used to characterize the purity and the degree of disorder in the starting CNT electrodes and further verify the presence of different phases in the ALD-deposited VO_x coatings (Fig. 6.3b). Perfect graphite clearly shows only one Raman active mode, the G-band, located at 1582 cm^{-1} and corresponding in-plane vibrations

[193]. Defective graphite, CNTs and disordered carbons show an additional band at ~1360 cm^{-1} (D-band) associated with a double-resonance Raman process [194]. The low value of the ratio of the integrated intensities of D and G bands (I_D/I_G) (in our case ~0.9) and high intensity of the G" band at ~2710 cm^{-1} indicate high CNT purity and low concentration of defects in the inner tubes of the oxidized multi-walled CNTs [193].

The VO_x-coated samples exhibit several additional peaks in the 200-1000 cm^{-1} region, as expected from previous studies [192, 195]. The first two peaks occurring at 267 cm^{-1} and at 406 cm^{-1} are attributed to bending vibrations due to V=O bond. This is supported by the presence of the small peak at 1017 cm^{-1}, which is also indicative of a V=O bond. The peak occurring at 511 cm^{-1} is attributed to a V_3-O (triply coordinated oxygen) bond. Finally, the peak at 712 cm^{-1} is attributed to a V_2-O (doubly coordinated oxygen) bond. It is important to note that V=O bonds are present in VO_2, V_2O_5, and V_2O_3. Triply coordinated V_3-O bonds only appear in the chemical structure of V_2O_5, while doubly coordinated V_2-O bonds are present in the chemical structure of VO_2 and V_2O_3. These findings further suggest the presence of nanocrystalline regions of different vanadium oxide phases.

CV graphs of CNT electrodes before and after coating with VO_x of different thicknesses (Fig. 6.4) reveal a significant impact of the sample preparation conditions on both the shape of the curves and their relative changes with increasing sweep rate. The bare CNT electrode exhibits specific capacitance of ~30 $F \cdot g^{-1}$ (Fig. 6.4a), consistent with previous measurements [14, 182-186]. In spite of the surface oxidation, CNTs do not show evident redox peaks. Furthermore, the capacitance of CNT electrodes show little changes in the range of sweep rates from 5 to 500 $mV \cdot s^{-1}$, which indicates high-power

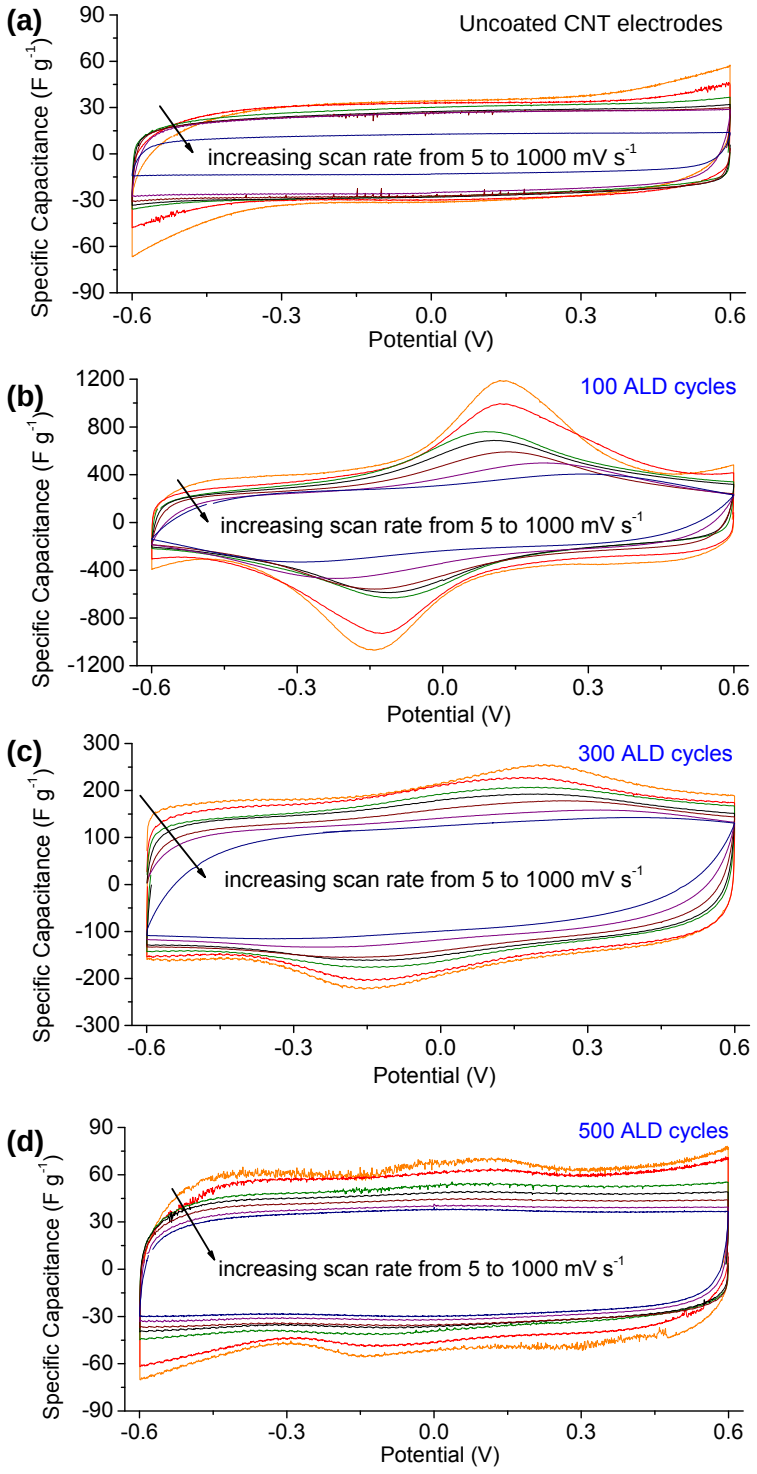

Figure. 6.4 Cyclic voltammograms of CNT electrodes: (a) uncoated, (b) exposed to 100 ALD cycles, (c), 300 cycles and (d) 500 cycles at different scan rates in the range of 5-1000 mV·s^{-1}.

performance capability and is likely due to the high electrical conductivity of CNTs and large interconnected mesopores present in this sample.

After exposure to 100 ALD cycles and coated with ~ 10 nm of VO_x, the symmetric supercapacitor increases its capacitance and energy density by more than an order of magnitude (Fig. 6.4b). Interestingly, we can distinguish two types of pseudo-capacitive behavior in VO_x-coated samples: (i) a broad peak in the central region which is typical for battery-like Faradaic reactions of intercalating compounds and (ii) a nearly rectangular background (~300F·g^{-1}), which is typical for an ideal pseudocapacitor-like materials, including hydrous ruthenium oxide [133]. As expected, the height of the battery-like redox peak diminishes rapidly with increasing sweep rate, while the rectangular background exhibits little change, indicating very high rate of the pseudocapacitive reactions between the deposited VO_x coating and the electrolyte. This, in turn, suggests very good promise of the hydrous vanadium oxide for high energy / high-power supercapacitor applications.

Increasing the VO_x coating thickness by exposing the surface-oxidized CNTs to 300 (Fig. 6.4c) and 500 (Fig. 6.4d) ALD cycles decreases the capacitance value significantly. The rectangular background decreases by two and six times, respectively, while the central battery-like peak disappears almost completely. This behavior can be explained by the contributions of three separate phenomena: (i) by the presence of active redox sites only in the top surface layer of VO_x coatings, (ii) by a limited access of the electrolyte ions to the bulk of the coating, and (iii) by a decrease in the electron transport to the active redox sites due to the increase in thickness of electrically insulative coating. Indeed, all redox reactions require the presence of both ions and electrical carriers

(electrons or holes) near the active site and the increase in the coating thickness likely impedes the transport of both: electrons from the CNT and ions from electrolyte. We further propose that the top layer of the coating unlikely exhibits higher concentration of active sites because ALD processes are known to produce rather uniform structure. At the same time, the interface between CNT and the coating (being a non-coherent interface) may increase the specific volume, concentration of vacancies, nano-sized voids and defects in this region of the coating, and thus may potentially offer higher concentration of active redox sites than both the bulk and the top coating layer. However, while we cannot exclude the possibility that the defects at the carbon-oxide interface favor higher pseudocapacitance, we could not detect significant structural differences between the coatings using the Raman spectroscopy studies.

Fig. 6.5 summarizes results of the CV measurements. While all the coated CNT electrodes offer higher capacitance than bare CNT, the electrodes with the thinnest coating of ~ 10 nm offer the best performance with the specific capacitance of the composite approaching ~530 $F \cdot g^{-1}$ at 5 $mV \cdot s^{-1}$. Even at the ultra-high sweep rate of 1000 $mV \cdot s^{-1}$ the capacitance remains higher than 240 $mV \cdot s^{-1}$, which is unmatched even by the most advanced porous carbon electrodes of comparable thickness [3, 91, 105, 106, 196-199]. Furthermore, the capacitance of the VO_x coating alone approaches 1400 $F \cdot g^{-1}$ at 5 $mV \cdot s^{-1}$. This is one of the highest capacitance values for any metal oxide measured in aqueous electrolytes in a symmetric two-electrode configuration. It exceeds the performance of hydrous manganese oxide and ruthenium oxide [133, 200, 201].

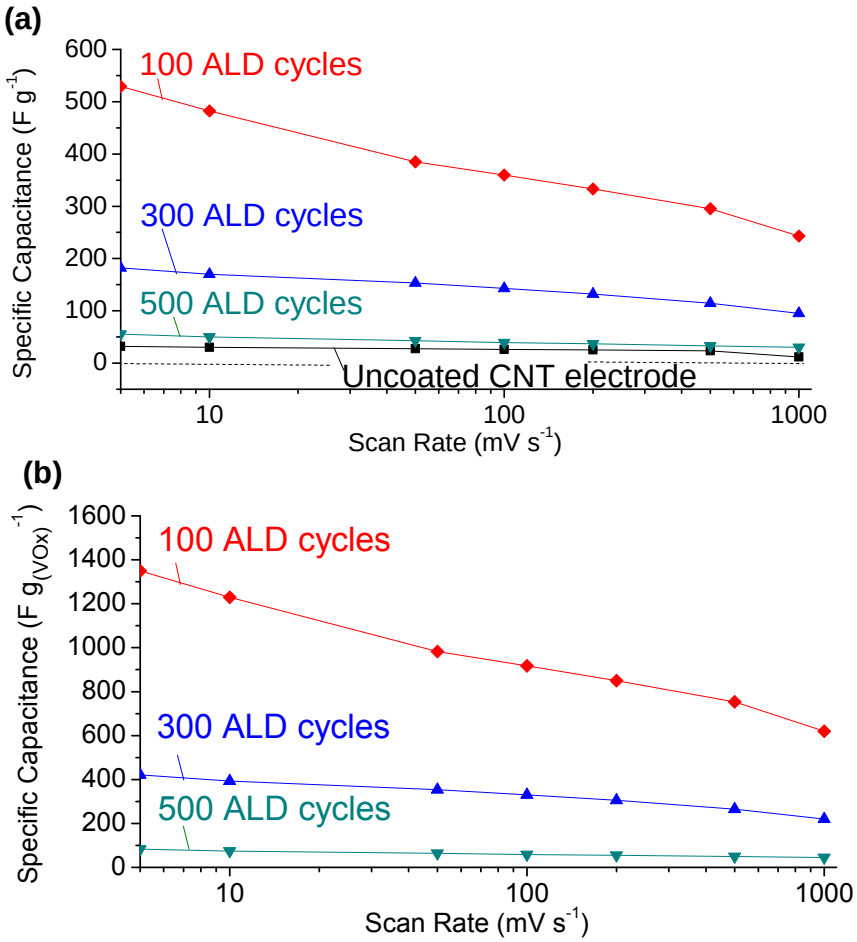

Figure. 6.5 Changes in the specific capacitance of the produced samples for: (a) composite electrode and (b) contribution of VO_x coating.

C-D measurements (Fig. 6.6) reveal similar trends. Except for the sample produced with 100 ALD cycles, the electrodes show relatively linear profiles, characteristic of ideal capacitor behavior. Fig. 6.7a, b shows capacitance retention of the electrodes at increasing current density. Due to the slow reactions at the battery-like redox sites (Fig. 6.4b), the sample produced with 100 ALD cycles shows the lowest power characteristics. Nonetheless, the capacitance of this sample remains above 360 $F \cdot g^{-1}$ even at very high current density of 20 $A \cdot g^{-1}$. The slightly higher capacitance value for this sample obtained from C-D than from CV measurements is an artifact of the capacitance deduction

procedures (see experimental section) designed for samples exhibiting a near-ideal capacitive behavior. The C-D measurements also confirm the extremely low resistance of our electrodes. Even at a very high current density (20 $A \cdot g^{-1}$), the IR drop found at the onset of the discharge curve (Fig. 6.7c) is extremely small, which indicates the low value of the equivalent series resistance (ESR) for the symmetric supercapacitor and confirms the usability of the device for high power operations.

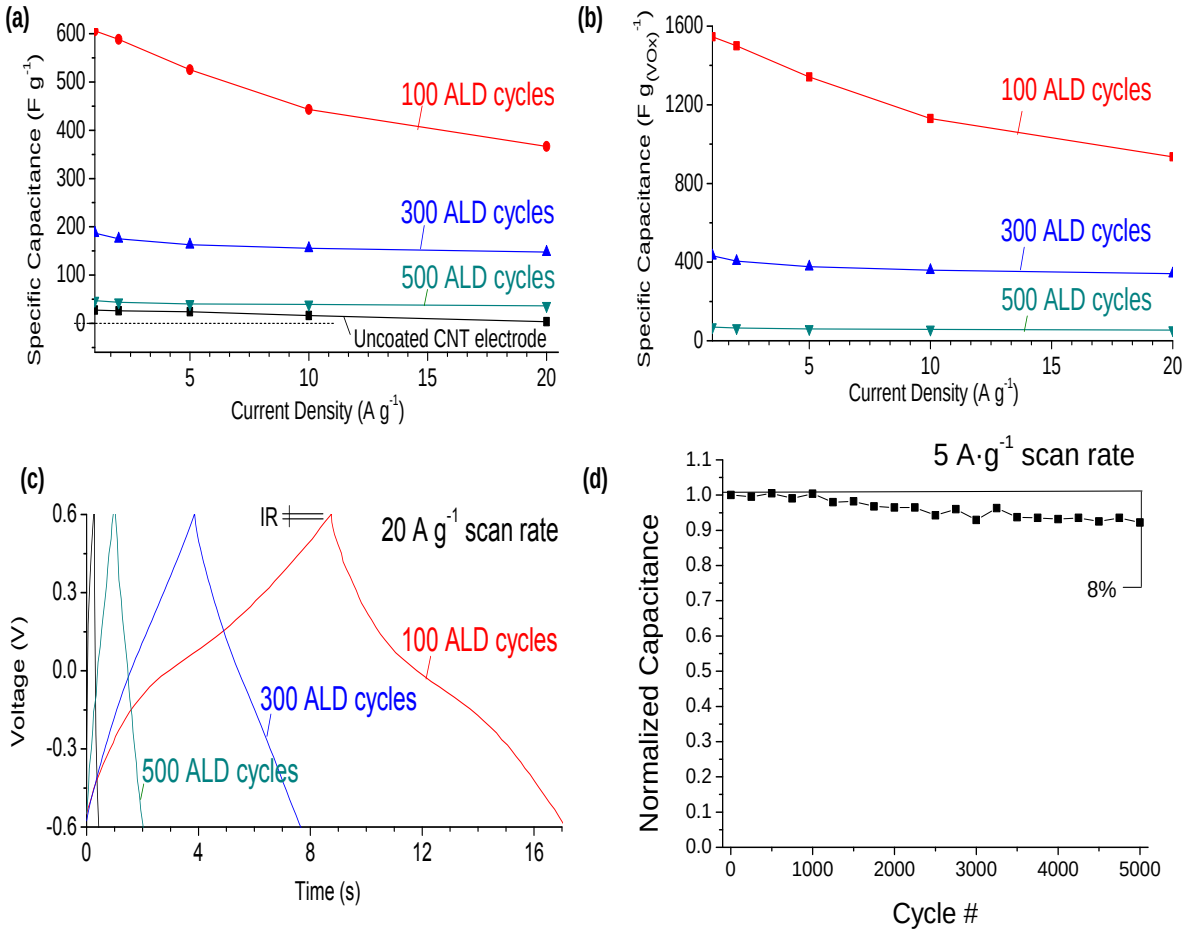

Figure. 6.7 Changes in the specific capacitance of the produced electrode samples for: (a) composite electrode and (b) contribution of VO_x coating as a function of current density. (c) Charge-discharge profiles of the produced electrodes at the current density of 20 $A \cdot g^{-1}$. (d) Evaluation of device life for coated electrode at 5 $A \cdot g^{-1}$ current density.

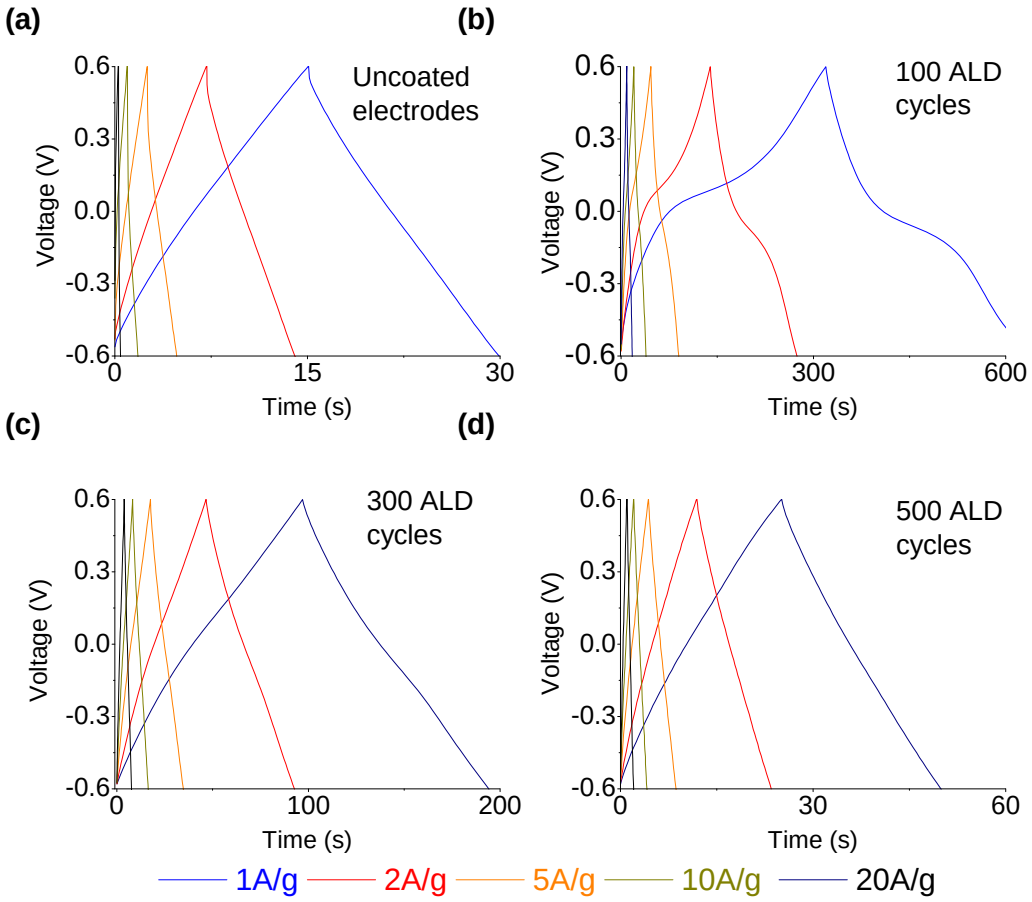

Figure. 6.6 Charge-discharge profiles of the produced samples: (a) uncoated CNT electrode, (b) exposed to 100 ALD cycles, (c) 300 cycles and (d) 500 cycles for current density in the range of 1-20 A·g^{-1}.

The Nyquist plots (Fig. 6.8) extracted from the EIS measurements are typical for supercapacitors. A classical Nyquist plot contains two segments: the 45 degree segment at high frequency and the nearly vertical line at low frequency. The length of the 45 degree segment is related to the resistance faced by the ions during their transport into the core of the porous electrode. The very small length of this segment (~0.1 Ohm·cm^2) indicates rapid ion transport within all of our electrodes. An ESR is another important characteristic of a supercapacitor. It is measured at high frequency where the imaginary component of the complex impedance becomes zero. The contributions to ESR primarily

include the electrical resistance of the electrodes and the electrode-current collector interfaces. As expected from the C-D measurements, the ESR for all the samples is very low, ranging from as little as 0.025-0.4 $\Omega \cdot cm^2$. In comparison, typical porous carbon

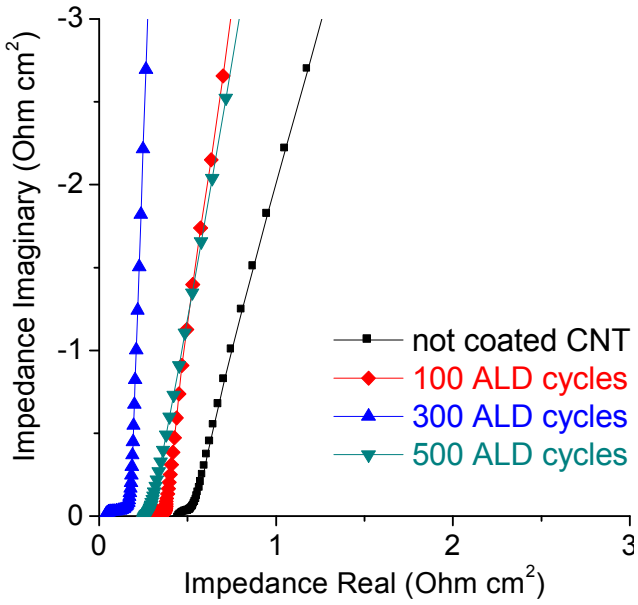

Figure. 6.8 Nyquist plots of the produced electrode

powder – based supercapacitors exhibit ESR of 0.2-1 $\Omega \cdot cm^2$ [3, 14, 91, 196-198, 202-204]. The low values of ESR in our devices are related to the interconnected network of highly conductive CNTs within our binder-free electrodes. Indeed, vanadium oxide coating was deposited after the CNT film preparation and thus it does not interfere with the very good electron transport at the occasional contact points between the individual CNTs. The lower ESR of the coated CNT electrodes was unexpected as the metal-oxide has lower conductivity than the CNTs themselves. We therefore postulate that the observed improvements are related to the lower impedance of the electrode-current collector interface between the gold foil and a more rigid vanadium oxide-reinforced

CNT electrode containing individual CNTs perpendicular to the electrode surface (see experimental details) and providing better electron transport. The very small semi-circles observed at high frequencies are related to the parasitic capacitance at the electrode-current collector interface [12, 205, 206].

6.3.1 Conclusions

ALD allows one to uniformly deposit metal oxides on porous CNT or carbon nanofiber electrodes, thus offering a novel route for the formation of binder-free supercapacitor electrodes with controlled porosity and greatly increased electrical conductivity and specific capacitance. The ability to precisely control the coating thickness and microstructure permits systematic studies of the ion intercalation and diffusion into the bulk of the electrodes. Electrochemical measurements revealed stable performance of the vanadium oxide-coated CNT electrodes with excellent capacitance retention at high current densities or sweep rates. Decreasing the coating thickness to ~10 nm allows one to achieve very high capacitance of the vanadium oxide with values approaching ~1550 $F \cdot g^{-1}$ at the current density of 1 $A \cdot g^{-1}$. Such high capacitance values are unprecedented for supercapacitor electrodes measured in a symmetrical two-electrode configuration in aqueous electrolytes. Our results indicate the importance of the electrode uniformity, precise control over the conformity and thickness of the oxide coatings and a promise of the application of ALD techniques for supercapacitors. Our future efforts will be focused on the application of ALD technique to the deposition of other metal oxides, optimization of oxide layer microstructure, and the use of smaller diameter CNTs are expected to further improve the specific capacitance of the composite electrodes.

6.4 Post deposition Annealing studies

In order to improve the energy density and power density of theses electrodes, the microstructure needs to be optimized to allow for optimal charge transfer between the pseudocapacitive vanadium oxide coating and the underlying EDLC carbon-based substrate. Annealing of these electrodes can achieve this purpose in three ways: (1) by improving the quality of the interface between the carbon and the vanadium oxide coating (thus reducing the internal resistance of the device), (2) by optimizing the vanadium oxide architecture so that only the most effective phase of vanadium oxide is present for energy storage (the materials characterization performed in the previous section identified the presence of multiple phases of vanadium oxide in the deposited layer), and (3) by increasing the internal pore volume accessible to ions in the electrolyte through a reduction in the size of the coated vanadium oxide layer.

6.4.1 Annealing Experiments in Air

Initial post-deposition annealing experiments were performed in air under atmosphere. One of the goals of the annealing treatment was to leave only the V_2O_5 phase present within the deposited layer. Close examination of the Ellingham diagrams developed by Mizuta et.al. and Hanglund et. al. identified heat treatment above 300˚C (and up to 800˚C) as leading to the formation of the V_2O_5. However, the presence of the underlying carbon substrate limited the temperature range to 500-600˚C in air in order to prevent its thermal oxidation (as was determined by previous TGA measurements). As such, two temperatures (400 and 500 ˚C) were initially chosen to investigate the effect of annealing on the developed electrodes by comparing it to the control samples. The annealing was performed in a quartz tube furnace for 2 hours. XRD measurements were

made on the modified electrodes to determine the effect of the treatment on the microstructure and on the phases present in the electrodes. The XRD spectra demonstrate that the temperature treatment at 400˚C reduced the number of VOx phases to V_2O_5, VO_2, and V_2O_3, while the temperature treatment at 500˚C further reduced this number of phases to only V_2O_5 (Fig. 6.9). The FWHM of the exhibited peaks also decreased, indicating an increase in crystallinity of the coated samples after the annealing treatment. As such, the initial goals of improving microstructure and reducing the initial numbers of vanadium oxide phases were achieved.

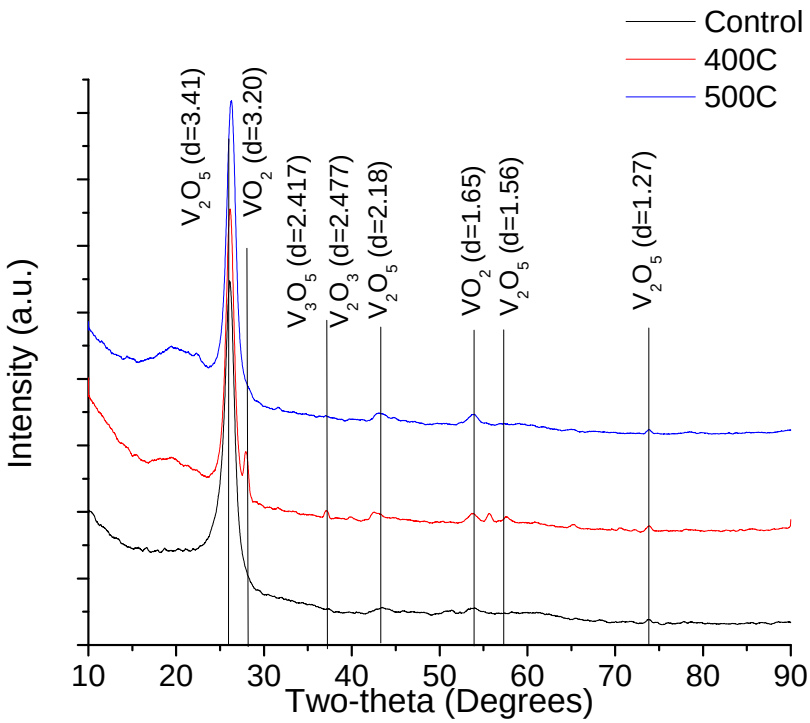

Figure. 6.9 XRD spectra of as-deposited samples, and samples annealed at 400˚C and

In order to see this effect on the energy storage capabilities of these electrodes, half cells were constructed in coin cells (fabricated by using lithium foil as a counter electrode in a 1M $LiPF_6$ in propylene carbonate solvent organic electrolyte solution). The

motivation behind this construction was to determine how the electrodes would perform in more complex systems favored for higher energy applications. Because of their nature, the capacity retention of these devices was limited by the rate of Li plating onto and dissolution from the Li foil. Electrochemical measurements (cyclic voltammetry and charge-discharge) were conducted to test the energy storage capabilities of these devices. As can be seen from the results (Fig. 6.10), the optimal temperature for the annealing experiments (in order to maximize the energy storage properties) was around 400˚C, leading to a maximum capacitance of over 546 $F \cdot g^{-1}$ (as opposed to 495 $F \cdot g^{-1}$ and 157 $F \cdot g^{-1}$ for the control and 500˚C samples, respectively).

The capacitance retention at higher current densities was also improved in the cases of the 400˚C annealed sample, possibly due to the improvement in the quality of the interface between carbon and vanadium oxide. It is also remarkable that the capacity achieved with the 400˚C sample closely approached the maximum theoretical capacity for vanadium oxide of 294mAh g^{-1} [207] at a value of nearly 230mAh g^{-1} (based on the total composite mass of the electrode).

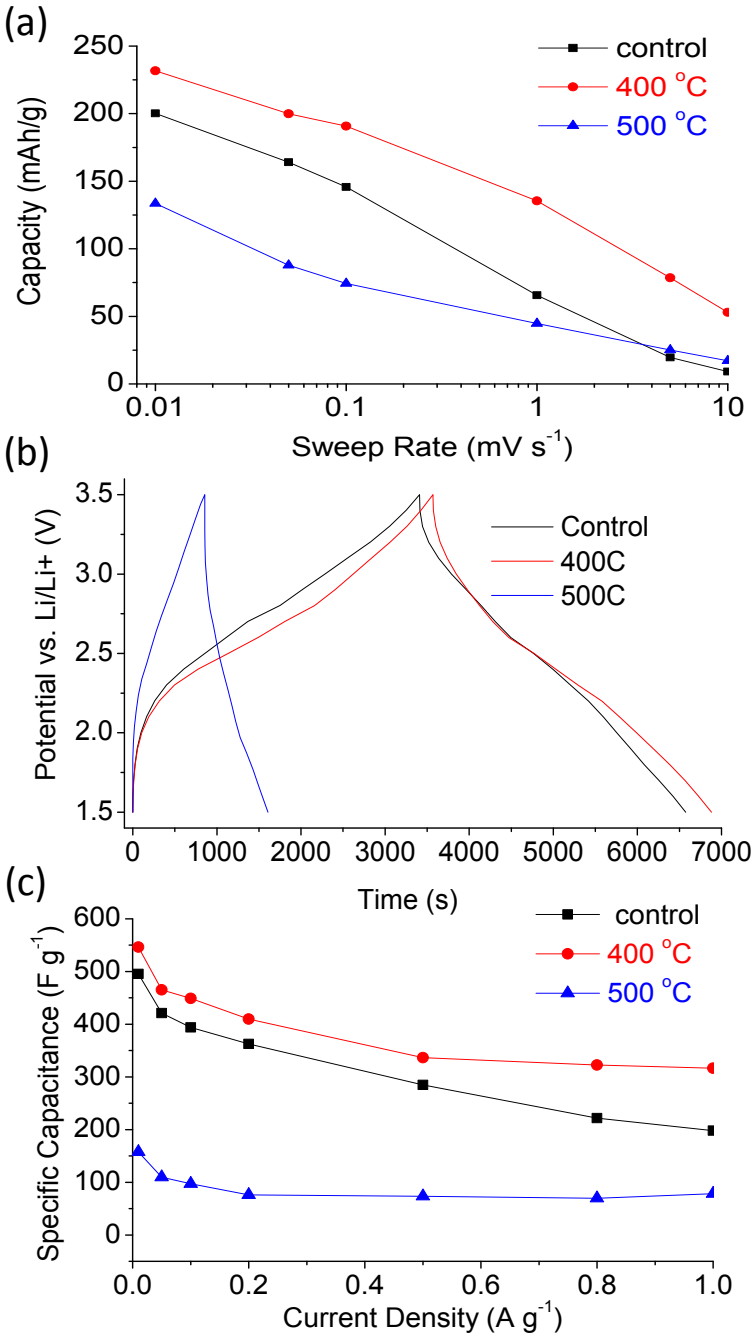

Figure. 6.10 Electrochemical characterization of as-deposited samples, and samples annealed at 400˚C and 500˚C in air: (a) capacity vs. scan rate generated from CV measurements, (b) CD profiles, and (c) capacitance vs. scan rate obtained from CV measurements.

6.4.2 Annealing Experiments in Argon

In spite of these promising results, the annealing treatment in air offered one large disadvantage. Even though the temperatures selected were lower than that at which carbon decomposes in air, the resulting samples became mechanically very fragile, making assembly of the devices very difficult and time consuming, and unable to be used in any other setting than in a research laboratory. As such, additional post-deposition annealing experiments were performed to continue improving the microstructure and the energy storage properties of these electrodes. In this case, the annealing experiments were performed at 400 °C in an Ar atmosphere for 2 hours. SEM measurements revealed an improvement in the quality of the interface through a reduction in the size of the hydrous layer, which resulted in an increase in accessible internal pore volume to the electrolyte and higher capacity and capacitance (Fig. 6.11).

Electrochemical characterization was performed through assembly of coin cell half cells with the electrodes using Li foil as a counter electrode. The electrolyte used in this case was 1M $LiClO_4$ in propylene carbonate solvent (and was based on its favorable performance in recent reports with vanadium oxide based electrodes). The shape of the CVs changed from one with a rectangular nature and numerous broad faradaic peaks (corresponding to the numerous vanadium oxide phases present in the control sample) to one with four very large sharp oxidation and reduction peaks, corresponding to the presence of only two vanadium oxide phases in the annealed electrode, and confirms the XRD measurements performed previously (Fig. 6.11). Once again, the specific capacity of these annealed electrodes increased dramatically to reach close to the maximum theoretical capacity of V_2O_5.

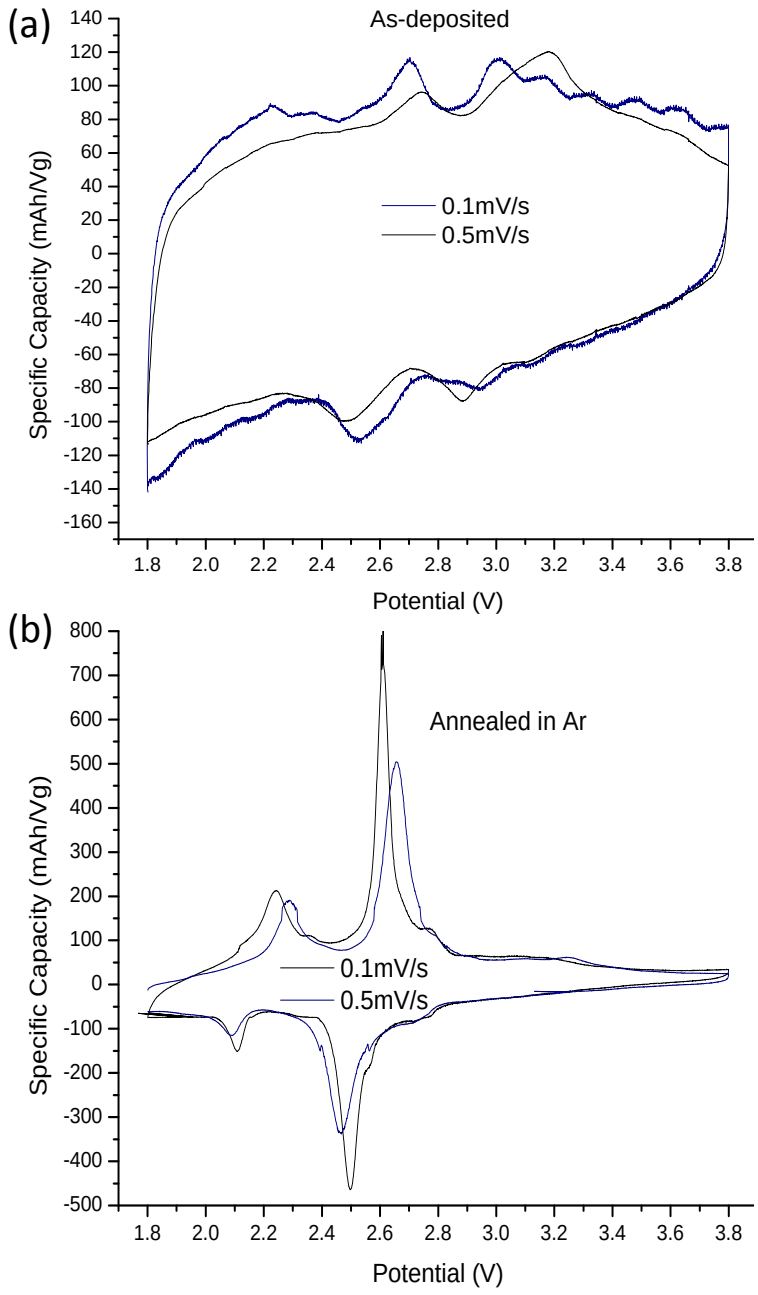

Figure. 6.11 Electrochemical characterization of (a) as-deposited samples, and (b) samples annealed at 400˚C in Ar.

6.5 Atomic Layer Deposition of Vanadium Oxide onto Aluminum Nanowire substrates

In order to demonstrate the versatility of the ALD technique, electrodes were also produced by the uniform ALD coating of VO_x on Aluminum nanowires(Al NW) (Fig. 6.12) and were evaluated for supercapacitor applications. In our view the 1D geometry of nanostructured NWs may offer some unique advantages, including higher thermal and electrical conductivity and higher power density of the NW-based energy storage devices[187]. In an ideal case of perfectly straight and aligned NWs (Fig. 6.12a), the pores between them would allow for the shortest ion transport distance within the electrode, thus contributing to minimizing the charging or discharging time. In fact, in our group's prior studies on pure carbon supercapacitors it was demonstrated that changing the pores within individual porous carbon particles from tortuous to straight can reduce the charging time by three orders of magnitude[106]. When nanopores are not straight but relatively large (> 2 nm), very high rate performance can still be achieved[14, 208].

SEM and TEM measurements (Fig. 6.12 b and c) demonstrated uniform coatings of ~50nm deposited conformally onto the Al NW substrate. The electrochemical measurements show that the electrochemically active VO_x offers some of the highest capacitance ever demonstrated in organic electrolytes[162-166, 171, 209-211] (Fig. 6.12e f), but suffers from very low electrical conductivity. The use of lightweight highly conductive Al NW (Fig. 6.12a) overcomes this key limitation. At a very slow slew rate of 0.01 $mV \cdot s^{-1}$ the specific (gravimetric) capacitance of the 50 nm coating approaches 964 $F \cdot g^{-1}$, but it drops to 836 $F \cdot g^{-1}$ and further to 483 $F \cdot g^{-1}$ at 0.1 and 1 $mV \cdot s^{-1}$, respectively (Fig. 6.12 f). The obtained values are moderately high as compared to 620-2150 $F \cdot g^{-1}$ reported in aerogels and xerogels when measured with a "sticky carbon" technique

needed to overcome their low electrical conductivity during measurements [165]. In spite of the relatively large oxide thickness, gravimetric capacitance advantage over activated carbon used in commercial devices can be maintained even at high sweep rates (Fig. 6.9c) and even if the mass of Al is taken into account. Indeed, assuming a density of 3.3 $g \cdot cc^{-1}$ for VO_x and 2.7 $g \cdot cc^{-1}$ for Al, we can easily calculate that the relative weight of Al in a core-shell NW (Fig. 6.13a) composed of a 45 nm diameter Al core and a 50 nm VO_x shell is only 8 wt. %. This is a typical contribution of either a binder or conductive carbon additives in commercial activated carbon – based supercapacitors. The key advantage of the proposed technology over conventionally used porous carbons, however, is significantly higher density and thus volumetric capacitance. Indeed, assuming the true density of the discussed core-shell NW to be 3.2 $g \cdot cc^{-1}$ and the remaining electrode porosity to be 30-50 vol. % , the volumetric capacity of the NW electrode reaches 1390-1950 $F \cdot cc^{-3}$, which is 10-100 times higher than the volumetric capacitance of various porous carbon electrodes [14, 106, 199, 208, 212-215]. This demonstrates the high potential of the Al NW technology for supercapacitor and other energy storage applications. It is expected that maintaining the same core-shell ratio and decreasing the shell thickness to below 10 nm while optimizing the VO_x microstructure will increase both the rate capability and the overall capacitance of the supercapacitor electrodes. Similar techniques of the Al NW growth and ALD oxide deposition could be applicable for the fabrication of electrolytic and regular capacitors as well as electrodes for regular and 3D Li-ion batteries.

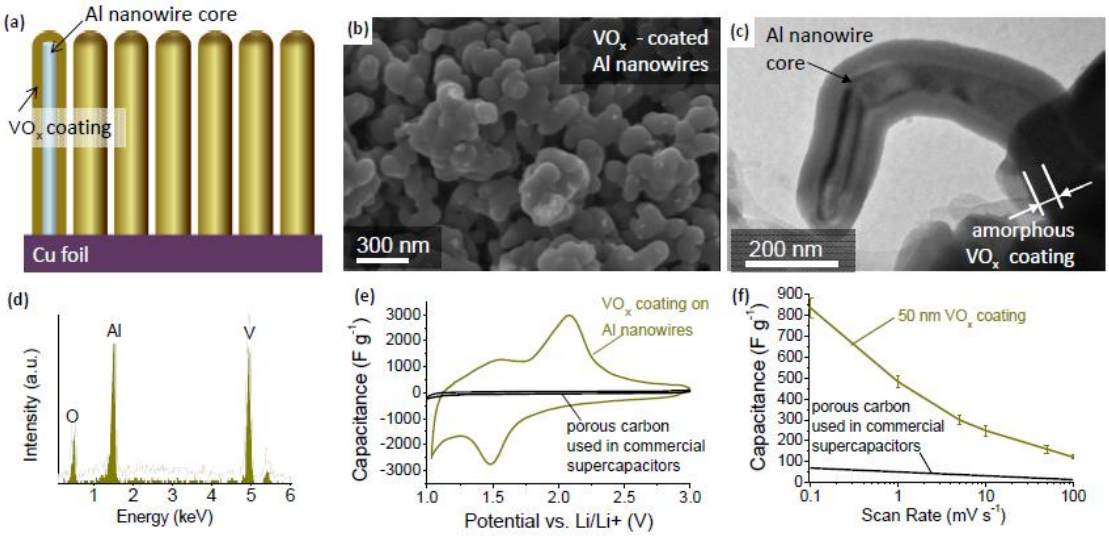

Figure. 6.13 Al nanowire-based supercapacitor: (a) simplified schematic of the electrode; (b) SEM and (c) TEM micrographs of
VOx-coated Al nanowires; (d) EDS spectrum of VOx-coated Al nanowires; (e) cyclic voltammetry recorded at 0.1 mV·s^{-1} for VOxcoated Al nanowire electrode in comparison to that of porous carbon (capacitance is normalized by the active mass); (f)
average capacitance as a function of a slew rate for 50 nm VOx coatings in comparison to that of activated carbon.

Chapter 7

CONCLUSION

Through the course of this study, two new methodologies have been utilized to further the understanding and performance of supercapacitor devices and the advancement of the field. Experimentally, several factors that affect the performance of supercapacitors were elucidated, including but not limited to electrolyte wetting in the smallest pores, electrowetting, ion electroadsorption as a function of pore size, the impact of microstructure, pore volume, coating thickness and the interface between pseudocapacitive material and carbon substrate in nanocomposites, to name a few.

Small angle neutron scattering (SANS) has been used for the first time to quantitatively and qualitatively evaluate the mechanisms of ion electroadsorption in microporous carbons. This investigation was carried out in selected aqueous and organic electrolytes, confirming some of the theories that have been recently discussed in the scientific community. The influence of poor wetting on the penetration of ion in the smallest pores of porous carbons was for the first time proven experimentally, and this will help to dispel some of the uncertainty and controversy which has recently been floating in the supercapacitor community. Moreover, SANS was proven to be a reliable tool to determine the limiting pore size for ion electroadsorption. Finally, the ability of this methodology to evaluate the impact of pore wall–ion interaction on ion adsorption at an open circuit is believed to be unique. The penetration of ions in the smallest (sub-nanometer pores) is becoming increasingly used to achieve EDLC supercapacitors with increased values of capacitance and high power characteristics. Due to the importance of ion electroadsorption in many other fields, the methodology may become adopted by

other researchers and used to further understand the remaining questions underlying the functioning of supercapacitor electrodes. It is my hope that the proposed methodology will be used in the research community to continue performing systematic studies of different carbon/electrolyte combinations in order to elucidate the exact role of many factors on double-layer capacitance. Such studies can begin by using this technique to determine the effect of the solvent's dielectric constant on ion penetration and electrochemical performance, on investigating ions of different sizes in the same solvent to determine its effect on ion concentration throughout the pore volume of various nanomaterials, to systematically investigate different ion/solvent chemistries and the impact of their solvation energy on ion penetration in the smallest sub-nm pores, and on the effect of temperature or pressure on ion penetration and on supercapacitor device performance. These are just a few of the many factors whose impact may affect device performance and ion penetration and are just a starting point for the types of experiments this new methodology will allow scientists to perform.

In another research thrust, the first use of ALD for supercapacitor devices was carried out, and investigated in order to construct supercapacitor electrodes with high energy and power densities. This relatively novel method permitted the low-temperature construction of a binder-free supercapacitor electrode with controlled porosity and with increased conductivity. Thanks to the superior uniformity, smoothness and conformity of the coated material offered by an ALD technique, supercapacitor devices with some of the highest reported energy and power densities were constructed. Due to the precise control that ALD offers, the impact of coating thickness on the performance of nanocomposite electrodes was elucidated, with an optimal coating thickness of ~10nm in the case of

vanadium oxide onto CNTs revealed. Smaller coating thickness would reduce the mass of vanadium oxide and diminish energy storage of a composite, while larger thickness would reduce capacitance utilization. Because a significant portion of the research in the supercapacitor field has focused on creating nanocomposites of carbon and pseudocapacitive materials, the conducted research should be of great benefit to the community. These results were then used to optimize the microstructure of the fabricated electrodes via a post-deposition annealing step. The ALD technique was also used to coat Al nanowire substrates to demonstrate a versatility in the application of this technique. The VO_x coated Al nanowire electrodes with 30-50% of the pore volume available for electrolyte access show volumetric capacitance of 1390-1950 F cc^{-1}, which exceeds the volumetric capacitance of porous carbons and many carbon-metal oxide composites by more than an order of magnitude.

It is my hope that the ALD technique will continue to be used in the supercapacitor research community to create high power high density supercapacitors and perform systematic studies evaluating structure-property relationships in various metal oxide-based nanocomposites. I also hope that the improved performance characteristics achieved by annealing will inspire other scientists to optimize metal oxide-carbon nanocomposite electrodes using post-deposition treatment of their electrodes.

The studies performed over the course of this dissertation may aid in the continuing development of electrodes for energy storage devices help other researchers to fill the remaining gaps in knowledge in a critical niche of high power energy storage devices for an increasingly technological and energy-dependent world.

REFERENCES

1. Jensen, K.F. and W. Kern, *Thin Film Processes*. 1991, New York: J. L. Vossen and W. Kern, Academic Press.
2. Conway, B.E., *Electrochemical Supercapacitors: Scientific Fundamentals and Technological Applications*. 1999, New York: Kluwer Academic/Plenum Publishers.
3. Chmiola, J., et al., *Anomalous increase in carbon capacitance at pore size below 1 nm.* Science, 2006. **313**: p. 1760-1763.
4. Shi, H., *Activated carbons and double layer capacitance.* Electrochim. Acta., 1996. **41**(10): p. 1633.
5. Armand, M., et al., *Ionic-liquid materials for the electrochemical challenges of the future.* Nature Materials, 2009. **8**: p. 621-629.
6. De Levie, R., *The influence of surface roughness of solid electrodes on electrochemical measurements.* Electrochimica Acta, 1965. **10**(2): p. 113-130.
7. Arulepp, A., et al., *Influence of the Solvent Properties on the Characteristics of a Double Layer Capacitor.* J. Power Sources, 2004. **133**(2): p. 320-328.
8. de Levie, R., *On porous electrodes in electrolyte solutions: I. Capacitance effects.* Electrochimica Acta, 1963. **8**(10): p. 751-780.
9. Yamaguchi, I., et al., *Preparation of epitaxial V2O3 films on C-, A- and R-planes of α-Al2O3 substrates by coating-pyrolysis process.* Thin Solid Films, 2000. **366**(294).
10. Cocciantelli, J.M., et al., *Crystal chemistry of electrochemically inserted LixV2O5.* Journal of Power Sources, 1991. **34**(2): p. 103-111.
11. Jow, T.R. and J.P. Zheng, *Electrochemical capacitors using hydrous ruthenium oxide and hydrogen inserted ruthenium oxide.* Journal of the Electrochemical Society, 1998. **145**(1): p. 49-52.
12. Taberna, P.L., P. Simon, and J.F. Fauvarque, *Electrochemical characteristics and impedance spectroscopy studies of carbon-carbon supercapacitors.* Journal of the Electrochemical Society, 2003. **150**(3): p. A292-A300.
13. Chae, J.H., K.C. Ng, and G.Z. Chen, *Nanostructured Materials for Construction of Asymmetrical Supercapacitors.* Proceedings of the Institution of Mechanical Engineers, Part A, Journal of Power and Energy, 2010. **1**(1).
14. Portet, C., G. Yushin, and Y. Gogotsi, *Electrochemical performance of carbon onions, nanodiamonds, carbon black and multiwalled nanotubes in electrical double layer capacitors.* Carbon, 2007. **45**(13): p. 2511-2518.
15. Armstrong, R.D., et al., *An impedance method for the characterization of porous carbons.* Journal of Applied Electrochemistry, 1971. **1**(3): p. 179-183.
16. Kötz, R., M. Hahn, and R. Gallay, *Temperature behavior and impedance fundamentals of supercapacitors.* Journal of Power Sources, 2006. **154**(2): p. 550-555.
17. Kim, I.H., et al., *Synthesis and electrochemical characterization of vanadium oxide on carbon nanotube film substrate for pseudocapacitor applications.* Journal of the Electrochemical Society, 2006. **153**(6): p. A989-A996.

18. Sharma, R.K., et al., *Carbon-supported, nano-structured, manganese oxide composite electrode for electrochemical supercapacitor.* Journal of Power Sources, 2007. **173**(2): p. 1024-1028.
19. Borchardt, L., et al., *Interaction of electrolyte molecules with carbon materials of well-defined porosity: characterization by solid-state NMR spectroscopy.* Physical Chemistry Chemical Physics, 2013. **15**(36): p. 15177-15184.
20. Pell, W.G. and B.E. Conway, *Quantitative modeling of factors determining Ragone plots for batteries and electrochemical capacitors.* Journal of Power Sources, 1996. **63**: p. 255-266.
21. Simon, P. and Y. Gogotsi, *Materials for electrochemical capacitors.* Nature Materials, 2008. **7**: p. 845-853.
22. Pasquier, A.D., et al., *A comparative study of Li-ion battery, supercapcitor, and nonaqueous asymmetric hybrid devices for automotive applications.* Journal of Power Sources, 2002. **115**: p. 117-178.
23. Scherson, D. and A. Palencsar, *Batteries and Electrochemical Capacitors.* The Electrochemical Society Interface, 2006. **15**(1): p. 17-22.
24. Pitcher, G., *If the cap fits… How supercapacitors can help solve problems in portable products.* New Electronics, 2006. **Portable Products Special Report** p. 25-26.
25. Balducci, A., et al., *Ionic Liquids for hybrid supercapacitors.* Electrochemistry Communications, 2004. **6**: p. 566-570.
26. Abruna, H., Y. Kiya, and J. Henderson, *Batteries and electrochemical capacitors.* Physics Today, 2008. **61**(2): p. 43-50.
27. Deyang Qu, H.S., *Studies of activated carbons in double-layer capacitors.* Journal of Power Sources, 1998. **74**: p. 99-107.
28. Innovative research and products, I., *Ultracapacitors for stationary, industrial, consumer, and transport energy storage – An industry, technology, and market analysis.* Report Code: ET-111, 2010: p. 1-171.
29. Hollenkamp, A.G.P.a.A.F., *Carbon properties and their role in supercapacitors.* Journal of Power Sources, 2006. **157**: p. 11-27.
30. Kasap, S.O., *Principles of Electronic Materials and Devices*. 3rd ed. 2006: McGraw Hill.
31. J. Chmiola, G.Y., R. Dash, Y. Gogotsi, *Effect of Pore Size and surface area of carbide-derived carbons on specific capacitance.* Journal of Power Sources, 2006. **158**: p. 765-772.
32. Jiang, J. and A. Kucernak, *Electrochemical Supercapacitor material based on manganese preparation and characterization.* Electrochimica Acta, 2002. **47**: p. 2381-2386.
33. Chang, C.H.a.K., *Cyclic voltammetric deposition of hydrous ruthenium oxide for electrochemical capacitors: effect of codepositing iridium oxide.* Electrochimica Acta, 2000. **45**: p. 2685-2696.
34. Thomberg, T., A. Janes, and E. Lust, *Energy and power performance of vanadium carbide derived carbon electrode materials for supercapacitors.* Journal of Electroanalytical Chemistry, 2009. **630**: p. 55-62.
35. Chen, W., T. Wen, and H. Teng, *Polyaniline-deposited porous carbon electrode for supercapacitor.* Electrochimica Acta, 2003. **48**: p. 641-649.

36. Zhou, Y., et al., *Electrochemical capacitance of well-coated single walled carbon nanotube with polyaniline composites.* Electrochimica Acta, 2004. **49**: p. 257-262.
37. Rudge, A., et al., *Conductive polymers as active materials in electrochemical capacitors.* Journal of Power Sources, 1994. **47**: p. 89-107.
38. J. Park, O.P., *Hybrid electrochemical capacitors based on polyaniline and activated carbon electrodes.* Journal of Power Sources, 2002. **111**: p. 185-190.
39. Goodenough, H.L.a.J.B., *Supercapacitor behavior with KCl Electrolyte.* Journal of Solid State Chemistry, 1999. **144**: p. 220-223.
40. H. Groult, K.L.V., A. Mantoux, L. Perrigaud and P. Doppelt, *Study of the Li+ insertion into V2O5 films deposited by CVD onto various substrates.* Journal of Power Sources, 2007. **174**: p. 312-320.
41. Saliger, R., et al., *High surface area carbon arerogels for supercapcitors.* Journal of Non-crystalline solids, 1998. **225**: p. 81-85.
42. Choi, D., G. Blomgren, and P. Kumta, *Fast and reversible surface redox reaction in nanocrystalline nitride supercapacitors.* Advanced Materials, 2006. **18**: p. 1178-1182.
43. Wang, X.-f., *Hydrous Ruthenium Oxide with High Rate Pseudo-Capacitance Prepared by a New Sol-Gel Process.* Chin. J. Chem. Phys., 2006. **19**.
44. B. Park, C.D.L., H.S. Park, K. Jung, O. Joo, *Performance of supercapacitor with electrodeposited ruthenium oxide film electrodes - Effect of film thickness.* Journal of Power Sources, 2004. **134**(1): p. 148-152.
45. Subramanian, V., H. Zu, and B. Wei, *Nanostructured MnO2: Hydrothermal synthesis and electrochemical properties as a supercapacitor electrode material.* Journal of Power Sources, 2006. **159**: p. 361-364.
46. Fischer, A., et al., *Incorporation of homogeneous nanoscale MnO2 within ultraporous carbon structures via self-limiting electroless deposition: Implictions for electrochemical capacitors.* Nano Letters, 2007. **7**(2): p. 281-286.
47. Taberna, P.L., et al., *High rate capabilities Fe3O4-based Cu nano-architectured electrodes for Li-ion battery applications.* Nature Materials, 2006. **5**: p. 567-573.
48. Wu, N.-L., *Nanocrystalline oxide supercapacitors.* Materials Chemistry and Physics, 2002. **75**: p. 6-11.
49. Kim, I., et al., *Synthesis and Electrochemical Characterization of Vanadium Oxide on Carbon Nanotube Film Substrate for Pseudocapacitor applications.* Journal of the Electrochemical Society, 2006. **153**(6): p. A989-A996.
50. K. Le Van, H.G., A. Mantoux, L. Perrigaud, F. Lantelme, R. Lindstrom, R. Badour-Hadjean, S. Zanna, and D. Lincot, *Amorphous vanadium oxide films synthesised by ALCVD for lithium rechargeable batteries.* Journal of Power Sources, 2006. **160**: p. 592-601.
51. Jurewicz., K., et al., *Capacitance properties of ordered porous carbon materials prepared by a templating procedure.* Journal of Physics and Chemistry of Solids, 2004. **65**: p. 287-293.
52. Field, M.N. and I.P. Parkin, *Atmospheric pressure chemical vapour deposition of vanadium(V) oxide films on glass substrates from reactions of VOCl3 and VCl4 with water* Journal of Materials Chemistry, 2000. **10**(8): p. 1863-1866.

53. Manning, T.D. and I.P. Parkin, *Vanadium(IV) oxide thin films on glass and silicon from the atmospheric pressure chemical vapour deposition reaction of VOCl3 and water.* Polyhedron, 2004. **23**(18): p. 3087-3095.
54. J.S. Sakamoto, B.D., *Vanadium Oxide-Carbon Nanotube Composite Electrodes for use in secondary Lithium batteries.* Journal of the Electrochemical Society, 2002. **149**(1): p. A26-A30.
55. R. Lopez, et al., *Synthesis and characterization of size controlled vanadium-oxide nanocrystals in a fused silica matrix.* Journal of Applied Physics, 2002. **92**(7): p. 4031-4036.
56. Anderson, J.S. and A.S. Khan, *Phase Equilibria in the Vanadium Oxygen system.* Journal of the Less-Common Metals, 1970. **22**: p. 209-218.
57. Enjalbert, R. and J. Galy, *A refinement of the structure of V_2O_5.* Acta crystallographica. Section C, Crystal structure communications, 1986. **42**(11): p. 1467-1469.
58. Ritala, M. and M. Leskela, *Handbook of Thin Materials* ed. H.S. Nalwa. Vol. 1: Deposition and processing of thin films. 2002: Academic Press.
59. Ohring, M., *The Materials Science of Thin Films: Deposition and Structure*. 2nd ed. 2002, London: Academic Press.
60. Markov, I., *Crystal Growth for Beginners: Fundamentals of Nucleation, Crystal Growth, and Epitaxy*. 1995, Singapore: World Scientific.
61. Maier, J., *Nanoionics: ion transport and electrochemical storage in confined systems.* Nature Materials, 2005. **4**: p. 805-815.
62. Choy, K.L., *Chemical Vapour Deposition of Coatings.* Progress in Materials Science, 2003. **48**: p. 57-170.
63. Huang, C., et al., *Pseudocapacitive Characteristics of Vanadium Oxide Deposits with a Three-Dimensional Porous Structure.* Journal of the Electrochemical Society, 2009. **156**(8): p. A667-A671.
64. Balducci, A., F. Soavi, and M. Mastragostino, *The use of ionic liquids as solvent-free green electrolytes for hybrid supercapacitors.* Applied Physics A, 2006. **82**: p. 627-632.
65. Sato, T., G. Masuda, and K. Takagi, *Electrochemical properties of novel ionic liquids for electric double layer capacitor applications.* Electrochimica Acta, 2004. **49**: p. 3603-3611.
66. Tsuda, T. and C. Hussey, *Electrochemical Applications of room-temperature Ionic liquids.* The Electrochemical Society Interface, 2007. **Spring**: p. 42-49.
67. Pandolfo, A.G. and A.F. Hollenkamp, *Carbon properties and their role in supercapacitors.* Journal of Power Sources, 2006. **157**: p. 11-27.
68. Qu, D., *Studies of the activated carbons used in double-layer capacitors.* Journal of Power Sources, 2002. **109**: p. 403-411.
69. Lust, E., A. JÃ¤nes, and M. Arulepp, *Influence of solvent nature on the electrochemical parameters of electrical double layer capacitors.* Journal of Electroanalytical Chemistry, 2004. **562**(1): p. 33-42.
70. JÃ¤nes, A., et al., *Influence of solvent nature on the electrochemical characteristics of nanoporous carbon|1 M (C2H5)3CH3NBF4 electrolyte solution interface.* Surface Science, 2004. **560**(1â€“3): p. 145-157.

71. Arulepp, M., et al., *Influence of the solvent properties on the characteristics of a double layer capacitor.* Journal of Power Sources, 2004. **133**(2): p. 320-328.
72. Janes, A. and E. Lust, *Electrochemical Characteristics of Nanoporous Carbide-derived Carbon materials in various nonaqueous electrolyte solutions.* Journal of the Electrochemical Society, 2006. **153**(1): p. A113-A116.
73. Tamai, H., et al., *Mesoporous activated carbon as electrode for electric double layer capacitor.* Journal of Materials Science, 2005. **40**(14): p. 3703-3707.
74. Bispo-Fonseca, I., et al., *Possible improvements in making carbon electrodes for organic supercapacitors.* Journal of Power Sources, 1999. **79**(2): p. 238-241.
75. Gallagher, K.G., G. Yushin, and T.F. Fuller, *The Role of Nanostructure in the Electrochemical Oxidation of Model-Carbon Materials in Acidic Environments.* Journal of the Electrochemical Society. **157**(6): p. B820-B830.
76. Qu, D.Y., *Studies of the activated carbons used in double-layer supercapacitors.* Journal of Power Sources, 2002. **109**(2): p. 403-411.
77. Wei, Y.Z., et al., *A novel electrode material for electric double-layer capacitors.* Journal of Power Sources, 2005. **141**(2): p. 386-391.
78. Zhang, K., et al., *Surfactant-intercalated, chemically reduced graphene oxide for high performance supercapacitor electrodes.* Journal of Materials Chemistry, 2011. **21**(20): p. 7302-7307.
79. Fic, K., G. Lota, and E. Frackowiak, *Effect of surfactants on capacitance properties of carbon electrodes.* Electrochimica Acta, 2012. **60**(0): p. 206-212.
80. Frumkin, A., S. Reichstein, and R. Kulvarskaja, *Ion adsorption in aqueous surfaces.* Kolloid-Zeitschrift, 1926. **40**(1): p. 9-11.
81. Frumkin, A., *Affectation of the adsorption of neutral molecules by means of electrical field.* Zeitschrift Fur Physik, 1926. **35**(10): p. 792-802.
82. Conway, B.E., E. Gileadi, and M. Dzieciuch, *Deterination of real surface areas and Temkin isotherm parameters from analysis of adsorption pseudocapacity curves.* Journal of the Electrochemical Society, 1963. **110**(3): p. C68-C68.
83. Gu, W. and G. Yushin, *Review of Nanostructured Carbon Materials for Electrochemical Capacitor Applications: Advantages and Limitations of Activated Carbon, Carbide-Derived Carbon, Zeolite-Templated Carbon, Carbon Aerogels, Carbon Nanotubes, Onion-like Carbon and Graphene* WIREs: Energy, 2013.
84. Zheng, J.P., *Ruthenium oxide-carbon composite electrodes for electrochemical capacitors.* Electrochemical and Solid State Letters, 1999. **2**(8): p. 359-361.
85. Conway, B.E., *Transition from supercapacitor to battery behavior in electrochemical energy storage.* Journal of the Electrochemical Society, 1991. **138**(6): p. 1539-1548.
86. Chmiola, J., et al., *Anomalous Increase in Carbon Capacitance at Pore Sizes less than 1 nanometer.* Science, 2006. **313**: p. 1760- 1763.
87. Salitra, G., et al., *Carbon electrodes for double-layer capacitors - I. Relations between ion and pore dimensions.* Journal of the Electrochemical Society, 2000. **147**(7): p. 2486-2493.
88. Raymundo-Pinero, E., et al., *Relationship between the nanoporous texture of activated carbons and their capacitance properties in different electrolytes.* Carbon, 2006. **44**(12): p. 2498-2507.

89. Feng, G., et al., *Ion Distribution in Electrified Micropores and Its Role in the Anomalous Enhancement of Capacitance.* Acs Nano, 2010. **4**(4): p. 2382-2390.
90. Huang, J.S., B.G. Sumpter, and V. Meunier, *Theoretical model for nanoporous carbon supercapacitors.* Angewandte Chemie-International Edition, 2008. **47**(3): p. 520-524.
91. Chmiola, J., et al., *Effect of pore size and surface area of carbide derived carbons on specific capacitance.* Journal of Power Sources, 2006. **158**(1): p. 765-772.
92. Huang, J., B. Sumpter, and V. Meunier, *A Universal Model for nanoporous carbon supercapacitors applicable to diverse pore regimes, carbon materials, and electrolytes.* Chemistry: A European journal, 2008. **14**: p. 6614-6626.
93. Kim, S.J., S.W. Hwang, and S.H. Hyun, *Preparation of carbon aerogel electrodes for supercapacitor and their electrochemical characteristics.* Journal of Materials Science, 2005. **40**(3): p. 725-731.
94. Hwang, S.W. and S.H. Hyun, *Capacitance control of carbon aerogel electrodes.* Journal of Non-Crystalline Solids, 2004. **347**(1-3): p. 238-245.
95. Pandolfo, A.G. and A.F. Hollenkamp, *Carbon properties and their role in supercapacitors.* Journal of Power Sources, 2006. **157**(1): p. 11-27.
96. Fic, K., et al., *Novel insight into neutral medium as electrolyte for high-voltage supercapacitors.* Energy & Environmental Science. **5**(2): p. 5842-5850.
97. Demarconnay, L., E. Raymundo-PiÃ±ero, and F. BÃ©guin, *A symmetric carbon/carbon supercapacitor operating at 1.6 V by using a neutral aqueous solution.* Electrochemistry Communications. **12**(10): p. 1275-1278.
98. Bichat, M.P., E. Raymundo-PiÃ±ero, and F. BÃ©guin, *High voltage supercapacitor built with seaweed carbons in neutral aqueous electrolyte.* Carbon. **48**(15): p. 4351-4361.
99. Brunauer, S., P. Emmett, and E. Teller, *Adsorption of Gases in Multimolecular Layers.* J. of Am. Chem. Soc., 1938. **60**: p. 309–319.
100. Ravikovitch, P.I., et al., *Unified approach to pore size characterization of microporous carbonaceous materials from N-2, Ar, and CO2 adsorption isotherms.* Langmuir, 2000. **16**(5): p. 2311-2320.
101. Centeno, T.A., O. Sereda, and F. Stoeckli, *Capacitance in carbon pores of 0.7 to 15 nm: a regular pattern.* Physical Chemistry Chemical Physics, 2011. **13**(27): p. 12403-12406.
102. Sanchez-Gonzalez, J., F. Stoeckli, and T.A. Centeno, *The role of the electric conductivity of carbons in the electrochemical capacitor performance.* Journal of Electroanalytical Chemistry, 2011. **657**(1â€“2): p. 176-180.
103. Centeno, T.A. and F. Stoeckli, *The volumetric capacitance of microporous carbons in organic electrolyte.* Electrochemistry Communications, 2012. **16**(1): p. 34-36.
104. Centeno, T.A. and F. Stoeckli, *Surface-related capacitance of microporous carbons in aqueous and organic electrolytes.* Electrochimica Acta, 2011. **56**(21): p. 7334-7339.
105. Korenblit, Y., et al., *In-Situ Studies of Ion Transport in Microporous Supercapacitor Electrodes at Ultra-Low Temperatures.* Advanced Functional Materials, 2012(DOI: 10.1002/adfm.201102573).

106. Kajdos, A., et al., *Tailoring the Pore Alignment for Rapid Ion Transport in Microporous Carbons.* J. Am. Chem. Soc., 2010. **132**(10): p. 3252.
107. Fic, K., et al., *Novel insight into neutral medium as electrolyte for high-voltage supercapacitors.* Energy & Environmental Science, 2012. **5**(2): p. 5842-5850.
108. Demarconnay, L., E. Raymundo-PiÃ±ero, and F. BÃ©guin, *A symmetric carbon/carbon supercapacitor operating at 1.6 V by using a neutral aqueous solution.* Electrochemistry Communications, 2010. **12**(10): p. 1275-1278.
109. Bichat, M.P., E. Raymundo-PiÃ±ero, and F. Beguin, *High voltage supercapacitor built with seaweed carbons in neutral aqueous electrolyte.* Carbon, 2010. **48**(15): p. 4351-4361.
110. Gamby, J., et al., *Studies and characterizations of various activated carbons used for carbon/carbon supercapacitors.* Journal of Power Sources, 2001. **101**: p. 109-116.
111. Shi, H., *Activated Carbons and Double Layer Capacitance.* Electrochimica Acta, 1996. **41**(10): p. 1633-1639.
112. C. Portet, Z.Y., Y. Korenblit, R. Mokaya, and G. Yushin, *Electrical Double-Layer Capacitance of Zeolite-Templated Carbon in Organic Electrolyte.* Journal of the Electrochemical Society, 2009. **156**(1): p. A1-A6.
113. Kajdos, A., et al., *Tailoring the Pore Alignment for Rapid Ion Transport in Microporous Carbons.* Journal of the American Chemical Society, 2010.
114. Fuertes, A.B., et al., *Templated Mesoporous carbons for supercapacitor application.* Electrochimica Acta, 2005. **50**: p. 2799-2805.
115. Aida Espinola, P.M.M., Milton Roedel Salles, Ailton Ribeiro Pinto, *Electrical properties of carbons—resistance of powder materials.* Carbon, 1986. **24**(3): p. 337-341.
116. Gooding, J., *Nanostructuring electrodes with carbon nanotubes: A review on electrochemistry and applications for sensing.* Electrochimica Acta, 2005. **50**: p. 3049-3060.
117. Liu, J., et al., *Fullerene Pipes.* Science, 1998. **280**: p. 1253-1256.
118. J.H. Chen, W.Z.L., D.Z. Wang, S.X. Yang, J.G. Yen, Z.F. Ren, *Electrochemical characterization of carbon nanotubes as electrode in electrochemical double-layer capacitors.* Carbon, 2002. **40**: p. 1193-1197.
119. Nugent, J.M., et al., *Fast Electron Transfer kinetics on multiwalled carbon nanotube microbundle electrodes.* Nano Letters, 2001. **1**(2): p. 87-91.
120. Britto, P.J., et al., *Carbon nanotube electrode for oxidation of dopamine.* Bioelectrochemistry and bioenergetics, 1996. **41**: p. 121-125.
121. Kuznetsov, V.L., et al., *Onion-like carbon from ultra-disperse diamond.* Chemical Physics Letters, 1994. **222**(4): p. 343-348.
122. Zheng, J., et al., *Carbon with an Onion-Like Structure Obtained by Chlorinating Titanium Carbide.* J. Mater. Chem., 2000. **10**: p. 1039-1041.
123. Bushueva, E.G., et al., *Double layer supercapacitor properties of onion-like carbon materials.* Physica Status Solidi B-Basic Solid State Physics, 2008. **245**(10): p. 2296-2299.
124. Giorgi, L., et al., *Influence of the PTFE content in the diffusion layer of low-Pt loading electrodes for polymer electrolyte fuel cells.* Electrochimica Acta, 1998. **40**(24): p. 3675-3680.

125. Yoshida, A., I. Tanahashi, and A. Nishino, *Effect of concentration of surface acidic functional groups on electric double-layer properties of activated carbon-fibers.* Carbon, 1989. **28**(5): p. 611-615.
126. Stoller, M.D. and R.S. Ruoff, *Best Practice Methods for determining and electrode material's performance for ultracapacitors.* Energy and Environmental Science, 2010. **3**: p. 1294-1301.
127. Hammouda, B., *Probing Nanoscale Structures - The SANS toolbox*. 2010, Gaithersburg, MD: National Institute of Standards and Technology.
128. King, S.M., *Small Angle Neutron Scattering.* 1995.
129. Cohaut, N., et al., *The porous network in carbon aerogels investigated by small angle neutron scattering.* Carbon, 2007. **45**(6): p. 1185-1192.
130. Chabot, G., *Answer to question #1094 Submitted to 'Ask the Experts'*. Health Physics Society, http://hps.org/publicinformation/ate/q1094.html.
131. McIntyre, N.S., et al., *Chemical information from XPS---applications to the analysis of electrode surfaces.* Journal of Vacuum Science and Technology, 1981. **18**(3): p. 714-721.
132. Janes, A., et al., *Electrochemical characteristics of nanoporous carbide-derived carbon materials in non-aqueous electrolyte solutions.* Electrochemistry Communications, 2004. **6**(3): p. 313-318.
133. Zheng, J.P., P.J. Cygan, and T.R. Jow, *Hydrous ruthenium oxide as an electrode material for electrochemical capacitors.* Journal of the Electrochemical Society, 1995. **142**(8): p. 2699-2703.
134. Miller, J.R. and P. Simon, *Materials science - Electrochemical capacitors for energy management.* Science, 2008. **321**(5889): p. 651-652.
135. Choi, N.S., et al., *Challenges Facing Lithium Batteries and Electrical Double-Layer Capacitors.* Angewandte Chemie-International Edition, 2012. **51**(40): p. 9994-10024.
136. Oren, Y., *Capacitive delonization (CDI) for desalination and water treatment - past, present and future (a review).* Desalination, 2008. **228**(1-3): p. 10-29.
137. Fedorov, M.V., N. Georgi, and A.A. Kornyshev, *Double layer in ionic liquids: The nature of the camel shape of capacitance.* Electrochemistry Communications. **12**(2): p. 296-299.
138. Foroughi, J., et al., *Torsional Carbon Nanotube Artificial Muscles.* Science, 2011. **334**(6055): p. 494-497.
139. Arulepp, M., et al., *Influence of the solvent properties on the characteristics of a double layer capacitor.* Journal of Power Sources, 2004. **133**(2): p. 320-328.
140. Kotz, R., M. Hahn, and R. Gallay, *Temperature behavior and impedance fundamentals of supercapacitors.* Journal of Power Sources, 2006. **154**(2): p. 550-555.
141. Huang, J.S., B.G. Sumpter, and V. Meunier, *A universal model for nanoporous carbon supercapacitors applicable to diverse pore regimes, carbon materials, and electrolytes.* Chemistry-a European Journal, 2008. **14**(22): p. 6614-6626.
142. Boukhalfa, S., K. Evanoff, and G. Yushin, *Atomic layer deposition of vanadium oxide on carbon nanotubes for high-power supercapacitor electrodes.* Energy & Environmental Science, 2012. **5**(5): p. 6872-6879.

143. Evanoff, K., et al., *Towards Ultrathick Battery Electrodes: Aligned Carbon Nanotube - Enabled Architecture.* Advanced Materials, 2012. **24**(4): p. 533-+.
144. Benson, J., et al., *Chemical Vapor Deposition of Aluminum Nanowires on Metal Substrates for Electrical Energy Storage Applications.* Acs Nano, 2012. **6**(1): p. 118-125.
145. Yang, L., et al., *Molecular Simulation of Electric Double-Layer Capacitors Based on Carbon Nanotube Forests.* Journal of the American Chemical Society, 2009. **131**(34): p. 12373-12376.
146. Merlet, C., et al., *On the Molecular Origin of Supercapacitance in Nanoporous Carbon Electrodes.* Nature Materials, 2012. **DOI:10.1038/nman3260**.
147. Levi, M.D., et al., *Application of a quartz-crystal microbalance to measure ionic fluxes in microporous carbons for energy storage.* Nature Materials, 2009. **8**(11): p. 872-875.
148. Melnichenko, Y.B. and G.D. Wignall, *Small-angle neutron scattering in materials science: Recent practical applications (vol 102, art no 021101, 2007).* Journal of Applied Physics, 2008. **103**(3).
149. He, L., et al., *Small-angle neutron scattering characterization of the structure of nanoporous carbons for energy-related applications.* Microporous and Mesoporous Materials. **149**(1): p. 46-54.
150. Scheiner, S. and M. Cuma, *Relative Sstability of Hydrogen and Deuterium Bonds.* Journal of the American Chemical Society, 1996. **118**(6): p. 1511-1521.
151. Millero, F.J., R. Dexter, and E. Hoff, *Density and Viscosity of Deuterium Oxide Solutions from 5-70 C.* Journal of Chemical and Engineering Data, 1971. **16**(1): p. 85-87.
152. Yang, R.T., *Adsorbents: Fundamentals and Applications*. 2003, Hoboken, NJ, USA: Wiley & Sons, Inc.
153. Fedorov, M.V., N. Georgi, and A.A. Kornyshev, *Double layer in ionic liquids: The nature of the camel shape of capacitance.* Electrochemistry Communications, 2010. **12**(2): p. 296-299.
154. Kiyohara, K., T. Sugino, and K. Asaka, *Electrolytes in porous electrodes: Effects of the pore size and the dielectric constant of the medium.* Journal of Chemical Physics, 2010. **132**(14).
155. Kondrat, S., et al., *A superionic state in nano-porous double-layer capacitors: insights from Monte Carlo simulations.* Physical Chemistry Chemical Physics, 2011. **13**(23): p. 11359-11366.
156. Zheng, J.P. and T.R. Jow, *The Effect of Salt Concentration in Electrolytes on the Maximum Energy Storage for Double Layer Capacitors.* Journal of the Electrochemical Society, 1997. **144**(7): p. 2417-2420.
157. Conway, B.E. and W.G. Pell, *Power limitations of supercapacitor operation associated with resistance and capacitance distribution in porous electrode devices.* Journal of Power Sources, 2002. **105**(2): p. 169-81.
158. Lust, E., A. Janes, and M. Arulepp, *Influence of Electrolyte Characteristics on the Electrochemical Parameters of Electrical Double Layer Capacitors.* J. Solid State Chem., 2004. **8**(7): p. 488-496.
159. Pell, W.G., B.E. Conway, and N. Marincic, *Analysis of non-uniform charge/discharge and rate effects in porous carbon capacitors containing sub-*

optimal electrolyte concentrations. Journal of Electroanalytical Chemistry, 2000. **491**(1â€“2): p. 9-21.
160. Lust, E., et al., *Electrochemical properties of nanoporous carbon electrodes in various nonaqueous electrolytes.* Journal of Solid State Electrochemistry, 2003. **7**(2): p. 91-105.
161. Chmiola, J., et al., *Desolvation of Ions in Subnanometer Pores and Its Effect on Capacitance and Double-Layer Theory.* Angewandte Chemie, 2008. **120**(18): p. 3440-3443.
162. Sun, D., et al., *The relationship between nanoscale structure and electrochemical properties of vanadium oxide nanorolls.* Advanced Functional Materials, 2004. **14**(12): p. 1197-1204.
163. Sudant, G., et al., *Synthesis and electrochemical properties of vanadium oxide aerogels prepared by a freeze-drying process.* Journal of the Electrochemical Society, 2004. **151**(5): p. A666-A671.
164. Dong, W., J. Sakamoto, and B. Dunn, *Electrochemical properties of vanadium oxide aerogels and aerogel nanocomposites.* Journal of Sol-Gel Science and Technology, 2003. **26**(1-3): p. 641-644.
165. Dong, W., D.R. Rolison, and B. Dunn, *Electrochemical properties of high surface area vanadium oxide aerogels.* Electrochemical and Solid State Letters, 2000. **3**(10): p. 457-459.
166. Rolison, D.R. and B. Dunn, *Electrically conductive oxide aerogels: new materials in electrochemistry.* Journal of Materials Chemistry, 2001. **11**(4): p. 963-980.
167. Wang, B., et al., *Synthesis of nanosized vanadium pentoxide/carbon composites by spray pyrolysis for electrochemical capacitor application.* Electrochimica Acta, 2009. **54**(5): p. 1420-1425.
168. Lao, Z.J., et al., *Synthesis of vanadium pentoxide powders with enhanced surface-area for electrochemical capacitors.* Journal of Power Sources, 2006. **162**(2): p. 1451-1454.
169. Reddy, R.N. and R.G. Reddy, *Porous structured vanadium oxide electrode material for electrochemical capacitors.* Journal of Power Sources, 2006. **156**(2): p. 700-704.
170. Hu, L., et al., *Synthesis and Characterization of VO(2)/Mesoporous Carbon Composites for Hybrid Capacitors.* Journal of Wuhan University of Technology-Materials Science Edition, 2010. **25**(4): p. 574-578.
171. Chen, Z., et al., *High-Performance Supercapacitors Based on Intertwined CNT/V2O5 Nanowire Nanocomposites.* Advanced Materials, 2011. **23**(6): p. 791-+.
172. Huang, C.-M., et al., *Pseudocapacitive Characteristics of Vanadium Oxide Deposits with a Three-Dimensional Porous Structure.* Journal of the Electrochemical Society, 2009. **156**(8): p. A667-A671.
173. Khomenko, V., E. Frackowiak, and F. Beguin, *Determination of the specific capacitance of conducting polymer/nanotubes composite electrodes using different cell configurations.* Electrochimica Acta, 2005. **50**(12): p. 2499-2506.
174. Choi, D., G.E. Blomgren, and P.N. Kumta, *Fast and reversible surface redox reaction in nanocrystalline vanadium nitride supercapacitors.* Advanced Materials, 2006. **18**(9): p. 1178-+.

175. Perera, S.D., et al., *Vanadium Oxide Nanowire–Carbon Nanotube Binder-Free Flexible Electrodes for Supercapacitors.* Advanced Energy Materials. **1**(5): p. 936-945.
176. Jung, Y.S., et al., *Ultrathin Direct Atomic Layer Deposition on Composite Electrodes for Highly Durable and Safe Li-Ion Batteries.* Advanced Materials, 2010. **22**(19): p. 2172-+.
177. Willinger, M.-G., et al., *Vanadium Oxide Sensing Layer Grown on Carbon Nanotubes by a New Atomic Layer Deposition Process.* Nano Letters, 2008. **8**(12): p. 4201-4204.
178. Le Van, K., et al., *Amorphous vanadium oxide films synthesised by ALCVD for lithium rechargeable batteries.* Journal of Power Sources, 2006. **160**(1): p. 592-601.
179. Jost, K., et al., *Carbon coated textiles for flexible energy storage.* Energy & Environmental Science, 2011. **4**(12): p. 5060-5067.
180. Bae, J., et al., *Fiber Supercapacitors Made of Nanowire-Fiber Hybrid Structures for Wearable/Flexible Energy Storage.* Angewandte Chemie-International Edition, 2011. **50**(7): p. 1683-1687.
181. Hu, L., et al., *Symmetrical MnO(2)-Carbon Nanotube-Textile Nanostructures for Wearable Pseudocapacitors with High Mass Loading.* Acs Nano, 2011. **5**(11): p. 8904-8913.
182. Zhang, M., et al., *Strong, transparent, multifunctional, carbon nanotube sheets.* Science, 2005. **309**(5738): p. 1215-1219.
183. Barisci, J.N., G.G. Wallace, and R.H. Baughman, *Electrochemical studies of single-wall carbon nanotubes in aqueous solutions.* Journal of Electroanalytical Chemistry, 2000. **488**(2): p. 92-98.
184. Lota, G., K. Fic, and E. Frackowiak, *Carbon nanotubes and their composites in electrochemical applications.* Energy & Environmental Science, 2011. **4**(5): p. 1592-1605.
185. Zheng, G., et al., *Paper supercapacitors by a solvent-free drawing method.* Energy & Environmental Science, 2011. **4**(9): p. 3368-3373.
186. Niu, Z., et al., *Compact-designed supercapacitors using free-standing single-walled carbon nanotube films.* Energy & Environmental Science, 2011. **4**(4): p. 1440-1446.
187. Evanoff, K., et al., *Toward Ultra-Thick Battery Electrodes: Aligned Carbon Nanotube - Enabled Architecture.* Advanced Materials, 2011: p. DOI: adma.201103044.
188. Whittaker, L., J.M. Velazquez, and S. Banerjee, *A VO-seeded approach for the growth of star-shaped VO(2) and V(2)O(5) nanocrystals: facile synthesis, structural characterization, and elucidation of electronic structure.* Crystengcomm, 2011. **13**(17): p. 5328-5336.
189. Qi, J., et al., *Synthesis and characterization of V(2)O(3) microcrystal particles controlled by thermodynamic parameters.* Materials Science-Poland, 2010. **28**(2): p. 535-543.
190. Nguyen, T.-D. and T.-O. Do, *Solvo-Hydrothermal Approach for the Shape-Selective Synthesis of Vanadium Oxide Nanocrystals and Their Characterization.* Langmuir, 2009. **25**(9): p. 5322-5332.

191. Anderson, J.S. and S. Khan, *Phase Equilibria in Vanadium-Oxygen System.* Journal of the Less-Common Metals, 1970. **22**(2): p. 209-&.
192. Wang, X.J., et al., *XRD and Raman study of vanadium oxide thin films deposited on fused silica substrates by RF magnetron sputtering.* Applied Surface Science, 2001. **177**(1-2): p. 8-14.
193. Tan, P., S. Dimovski, and Y. Gogotsi, *Raman Scattering of Non-Planar Graphite: Arched Edges, Polyhedral Crystals, Whiskers and Cones.* Phil. Trans. R. Soc. Lond. A, 2004. **362**: p. 2289-2310.
194. Thomsen, C. and S. Reich, *Doable resonant Raman scattering in graphite.* Phys. Rev. Lett., 2000. **85**(24): p. 5214-5217.
195. Lee, S.H., et al., *Raman spectroscopic studies of amorphous vanadium oxide thin films.* Solid State Ionics, 2003. **165**(1-4): p. 111-116.
196. Wei, L., et al., *Hydrothermal Carbonisation of Abundant Renewable Natural Organic Chemicals for High-Performance Supercapacitor Electrodes.* Advanced Energy Materials, 2011. **1**: p. 356-361.
197. Wei, L., et al., *Polypyrrole-derived Activated Carbons for High-performance Electrical Double-layer Capacitors with Ionic Liquid Electrolyte.* Advanced Functional Materials, 2011(DOI: 10.1002/adfm.201101866).
198. Rose, M., et al., *Hierarchical Micro- and Mesoporous Carbide-Derived Carbon as High Performance Electrode Material in Supercapacitors*, in *Small*. 2011. p. 1108-1117.
199. Korenblit, Y., et al., *High-Rate Electrochemical Capacitors Based on Ordered Mesoporous Silicon Carbide-Derived Carbon.* Acs Nano, 2010. **4**(3): p. 1337-1344.
200. Zheng, J.P. and T.R. Jow, *A new charge storage mechanism for electrochemical capacitors.* Journal of the Electrochemical Society, 1995. **142**(1): p. L6-L8.
201. Fischer, A.E., et al., *Incorporation of homogeneous, nanoscale MnO2 within ultraporous carbon structures via self-limiting electroless deposition: Implications for electrochemical capacitors.* Nano Letters, 2007. **7**(2): p. 281-286.
202. Wei, L. and G. Yushin, *Electrical Double Layer Capacitors with Sucrose Derived Carbon Electrodes in Ionic Liquid Electrolytes* Power Sources, 2011. **196** (8): p. 4072 - 4079.
203. Kovalenko, I., D. Bucknall, and G. Yushin, *Detonation Nanodiamond and Onion-like Carbon - Embedded Polyaniline for Supercapacitors.* Advanced Functional Materials, 2010: p. DOI: 10.1002/adfm.201000906.
204. Portet, C., G. Yushin, and Y. Gogotsi, *Effect of Carbon Particle Size on Electrochemical Performance of EDLC* J. Electrochem. Soc, 2008. **155 (7)**: p. A531-A536.
205. Portet, C., et al., *Modification of Al current collector/active material interface for power improvement of electrochemical capacitor electrodes.* Journal of the Electrochemical Society, 2006. **153**(4): p. A649-A653.
206. Portet, C., et al., *Modification of Al current collector surface by sol-gel deposit for carbon-carbon supercapacitor applications.* Electrochimica Acta, 2004. **49**(6): p. 905-912.

207. Wang, S., et al., *Porous monodisperse V2O5 microspheres as cathode materials for lithium-ion batteries.* Journal of Materials Chemistry, 2011. **21**(17): p. 6365-6369.
208. Pech, D., et al., *Ultrahigh-power micrometre-sized supercapacitors based on onion-like carbon.* Nature Nanotechnology, 2010. **5**(9): p. 651-654.
209. Sakamoto, J.S. and B. Dunn, *Vanadium oxide-carbon nanotube composite electrodes for use in secondary lithium batteries.* Journal of the Electrochemical Society, 2002. **149**(1): p. A26-A30.
210. Shembel, E., et al., *Synthesis, investigation and practical application in lithium batteries of some compounds based on vanadium oxides.* Journal of Power Sources, 1999. **80**(1-2): p. 90-97.
211. Shembel, E., et al., *Interrelation between structural and electrochemical properties of the cathode based on vanadium oxide for rechargeable batteries.* Journal of Power Sources, 1999. **81**: p. 480-486.
212. Chmiola, J., et al., *Monolithic Carbide-Derived Carbon Films for Micro-Supercapacitors.* Science, 2010. **328**(5977): p. 480-483.
213. Li, J., Q.M. Yang, and I. Zhitomirsky, *Composite Electrodes for Electrochemical Supercapacitors.* Nanoscale Research Letters, 2010. **5**(3): p. 512-517.
214. Li, J. and I. Zhitomirsky, *Cathodic electrophoretic deposition of manganese dioxide films.* Colloids and Surfaces a-Physicochemical and Engineering Aspects, 2009. **348**(1-3): p. 248-253.
215. Hulicova-Jurcakova, D., et al., *Combined Effect of Nitrogen- and Oxygen-Containing Functional Groups of Microporous Activated Carbon on its Electrochemical Performance in Supercapacitors.* Advanced Functional Materials, 2009. **19**(3): p. 438-447.

VITA

SOFIANE BOUKHALFA

Sofiane Boukhalfa was born in Hamamat, Algeria. He grew up in Algeria, France, Taiwan, and the United States. He received a B.S. in Materials Science and Engineering from the University of Illinois at Urbana-Champaign in 2009 before coming to Georgia Tech to pursue a doctorate in Materials Science and engineering.